CHALMERS

Improving the Performance of Strongly Coupled Antennas Using a Compensating Transmission Line Network

JANNE LEIVO AND TIN VUKUSIC

Department of Signals and Systems
Chalmers University of Technology
Göteborg, Sweden, 2009

EX091/2009

Improving the Performance of Strongly Coupled Antennas Using a Compensating Transmission Line Network

Master thesis at the Department of Signals and Systems, Chalmers University of Technology, Gothenburg, Sweden.
Performed at Ericsson AB, Antenna Research Center, Gothenburg, Sweden.

Janne Leivo

Tin Vukusic

Mats Viberg	Examiner, Chalmers University of Technology
Anders Derneryd	Supervisor, Ericsson AB
Anders Stjernman	Supervisor, Ericsson AB

Abstract

In MIMO systems the capacity of a wireless link in a rich scattering environment is increased by using multiple antennas on both transmitter and receiver sites. It is desirable to receive different uncorrelated replicas of the signal, but for closely spaced antennas the channel responses will be correlated. Moreover the strong mutual coupling reduces the antenna efficiency. In this thesis the performance of two 0.08 wavelengths separated monopole antennas in the 700 MHz band is evaluated and improved by connecting a compensating network to the antenna ports. It is shown through measurements that the network improves the efficiency with 0.9 dB, diversity gain with 1.3 dB and reduces the envelope correlation coefficient from 0.59 to 0.20. The simulated 2 x 2 MIMO Shannon capacity is increased with 17 %. Finally the concept is implemented into a dual-antenna mock up with the size of a mobile phone.

Acknowledgements

First we wish to thank Ericsson and specially Antenna Research Center for this great opportunity. Furthermore we want to thank our supervisors Anders Derneryd and Anders Stjernman for their excellent guidance and encouragement. They were always there and willing to help us and assist, always with calm and patience.

Special thanks go to Lars Manholm for his assistance with layouts and practical issues, and Jonas Fridén and Patrik Persson for the help with Matlab. We are very grateful to Lars Torstensson and Håkan Karlsson for their help and patience with Bluetest measurements.

In addition, we would like to thank Sony Ericsson Mobile Communications at Lund for the opportunity to use their anechoic chamber for the measurements

Contents

1 Introduction

There is a constant demand for higher bit-rates in wireless communication systems. In multipath environments this can be achieved by using multiple transmitting and receiving antennas, which is known as multiple-input multiple-output (MIMO) technology. Today this is a very hot research topic in both the communication and antenna community [1].

The performance of a single antenna communication system in a multi-path environment is severely decreased by multi-path fading. In MIMO systems the capacity of the system is increased by exploiting the effects of the fading. The main idea behind MIMO is to add a spatial dimension and use spatial multiplexing. The multiple transmit antennas are used to send independent data streams and in a rich enough scattering environment the data streams can be separated at the receiver by the use of multiple receiving antennas [2].

For a $M \times N$ MIMO system the capacity can be increased by $k = \min(M, N)$ compared to a single-input single-output system (SISO) [1]. This is under the assumption that the received signals are uncorrelated, which isn't the case for very closely spaced antennas. Close spacing of the antennas will also result in some energy being coupled to the nearby antennas, reducing the antenna efficiency and thereby degrading the performance even more. In base stations these problems aren't an issue due to available space, but in e.g. mobile phones the space is very limited. Hence, designing an antenna array with low antenna correlation and high efficiency for small hand-held devices can be a real challenge, especially for lower frequencies.

The object of this thesis is to evaluate and improve the performance of closely spaced antennas in a scattering environment. An antenna array with two closely spaced monopole antennas for the 750 MHz to 800 MHz band is designed and constructed. To improve the performance, three compensating transmission line networks, which decrease the antenna correlation and increase the efficiencies, are designed and connected to the antenna ports. Simulations and measurements in a reverberation chamber and anechoic chamber, with and without compensation networks, are performed. Efficiency, correlation, Shannon capacity and diversity gain are evaluated. Finally a theoretical study is made where the concept is implemented into a mobile phone of modern size.

1.1 Earlier Work

Theoretical studies on the mutual couplings effects on MIMO performance for closely spaced antennas are made in [3]. It is shown that mutual coupling between two closely spaced dipoles reduces the correlation, but due to reduced efficiency the Shannon capacity is nearly unchanged compared to the case without coupling. It is also shown that a decoupling network can completely eliminate the coupling while at the same time match the antennas to zero reflection, but this is only achieved for a single frequency. There is still a good improvement in the capacity for very narrowband systems (2%) with a separation as close as 0.03 λ.

A network consisting of transmission lines and a shunt reactive component for the 2.4 GHz band is proposed in [4]. It is shown that low coupling and good matching can be obtained for two printed monopoles on a 45 mm x 22 mm ground plane. Another easier approach is presented [5], where just a single metal strip is connected between two 2 GHz PIFA antennas resulting in reduced correlation and higher efficiency. This concept is also applied to two microstrip patch antennas in the 5 GHz frequency band, but the antenna spacing is relatively large (0.4 λ) [6]. In [7] a slot is etched on the ground plane between two PIFA elements to reduce the current flow and thereby reduce the coupling.

1.2 Thesis layout

Theory and definitions that the reader should be familiar with will be introduced in chapter 2. In chapter 3 the monopole array is designed through computer simulations. Measurements of S-parameters and radiation patterns are also presented. In the next chapter the three stripline networks are designed by optimizing the lengths and widths of the transmission lines for minimum correlation and maximum efficiency at the antenna ports. Measurements and simulations of the performance metrics, with and without compensation networks, are presented in chapter 5. Finally in chapter 6 the same concept is implemented into a dual antenna mock-up.

2 Background theory

Some theory and definitions required in the analysis of multiple antennas for MIMO systems are introduced and discussed in this chapter.

2.1 MIMO

In a Multiple-Input-Multiple-Output (MIMO) system multiple transmit and receive antennas are used to increase the capacity. MIMO systems exploit the added spatial dimension which is provided by the multi-path fading. For a MIMO system with M transmitting antennas and N receiving antennas the capacity can be increased by $k = \min(M, N)$ [1]. The increase in the capacity is called spatial multiplexing gain and by the use of diversity schemes at the receiver and coherent combining of the received signals, spatial diversity gain and array gain can also be achieved. These three gains are explained below.

Array Gain: When using multiple receiving antennas the SNR at the receiver is increased by coherently combining the received signals on the different antennas. The increase in the SNR is referred to as the array gain.

Diversity Gain: Diversity schemes exploit the effects of multi-path fading. The main idea is that every receiving antenna receives the transmitted signal through different uncorrelated channels. The probability of having dips on all the antennas at the same time is much lower than having a dip on a single antenna. There are three different diversity techniques; spatial diversity, pattern diversity and polarization diversity [8]. In spatial diversity the antennas are spaced apart so that the received signals have experienced different fading. Pattern diversity uses different patterns on the antennas so that every antenna receives a different set of multipath waves. In polarization diversity, different polarizations are used on the antennas. If some smart combing scheme is used together with any of the above techniques the average received SNR can be increased significantly. Often a combination of the different diversity techniques is employed.

Spatial Multiplexing gain: The spatial dimension provided by the fading channel can be used to send parallel independent data streams. Every receiving antenna transmits an independent data stream. The MIMO channel can be modeled with a channel matrix

$$\mathbf{H} = \begin{bmatrix} h_{11} & h_{12} & \cdots & h_{1M} \\ h_{21} & & & \vdots \\ \vdots & & & \vdots \\ h_{N1} & \cdots & \cdots & h_{NM} \end{bmatrix} \tag{2.1}$$

where h_{ij} is the complex antenna and channel gain between transmit antenna port i and receiver antenna port j. They are usually modeled as complex Gaussian random variables, i.e., the amplitudes are Rayleigh distributed and the corresponding powers are exponentially distributed. If $\mathbf{x}$ is the $M \times 1$ transmitted data vector and $\mathbf{n}$ is the complex Gaussian noise vector, then the received vector $\mathbf{y}$ is equal to

$$\mathbf{y} = \mathbf{H}\mathbf{x} + \mathbf{n} \tag{2.2}$$

By the use of multiple receiver antennas the data streams can be separated at the receiver. First the channel matrix is estimated with training symbols. Then the M transmitted data streams are estimated in the same way as M unknowns are resolved from a linear system of M equations [9]. If the number of receiving antennas is equal or higher than the number of transmit antennas and the equations are independent, then the system of equations can be solved. Having Independent equations is equivalent to having uncorrelated channels. The maximum number of data streams is equal to the minimum number of transmit or receive antennas. Hence, the spatial multiplexing gain increases the capacity by $k = \min(M, N)$.

2.2 Mutual coupling and scattering parameters

When multiple antennas are electrically close to each other some of the energy intended for a specific antenna will be radiated to other antennas. This happens in both transmitting and receiving mode and is called mutual coupling. The closer the antennas are the stronger the coupling is. In MIMO systems it's desirable to have uncorrelated signals on the antennas. At first one might think that coupling will increase the correlation between the antennas, but in [3] and [10] it is shown that the correlation between the far-field patterns is reduced by coupling in some environments.

When one antenna is transmitting, a part of the energy may be radiated to other antennas and set up currents in them. Some of the energy that the antennas pick up will be rescattered back out in the air and to other antennas, while some energy will travel towards the generator. If one antenna that picks up the energy is also excited by its own generator, the rescattered energy will be added to its own generated energy and alter the phase and amplitude of the excited wave. This means that the radiation pattern from every antenna will not only depend on the waves radiated on its own but also on the mutual coupling between other antennas [11]. The radiation pattern for one antenna, when all the other antennas are terminated with their port impedances, is usually called the embedded element pattern [12]. In receiving mode it's the same principle. Some energy received at one antenna will be rescattered to another antenna and interfere with the intended incident wave. Thus, the correlation between the received signals at the antenna ports will change. Another consequence of the mutual coupling is reduced radiation efficiency [12].

The mutual coupling between the antenna ports can be described with either scattering parameters or antenna port impedances. When using impedances the impedance matrix $[\mathbf{Z}]$ relates the voltages and currents of N antenna ports as

$$\begin{bmatrix} V_1 \\ V_2 \\ \vdots \\ V_N \end{bmatrix} = \begin{bmatrix} Z_{11} & Z_{12} & \cdots & Z_{1N} \\ Z_{21} & & & \vdots \\ \vdots & & & \vdots \\ Z_{N1} & \cdots & \cdots & Z_{NN} \end{bmatrix} \begin{bmatrix} I_1 \\ I_2 \\ \vdots \\ I_N \end{bmatrix} \tag{2.3}$$

The scattering matrix relates the voltage waves incident on the ports to those reflected on the ports as

$$\begin{bmatrix} V^-_1 \\ V^-_2 \\ \vdots \\ V^-_N \end{bmatrix} = \begin{bmatrix} S_{11} & S_{12} & \cdots & S_{1N} \\ S_{21} & & & \vdots \\ \vdots & & & \vdots \\ S_{N1} & \cdots & \cdots & S_{NN} \end{bmatrix} \begin{bmatrix} V^+_1 \\ V^+_2 \\ \vdots \\ V^+_N \end{bmatrix} \tag{2.4}$$

where $\left[\mathbf{V}^-\right]$ contains the reflected waves and $\left[\mathbf{V}^+\right]$ the incident waves. The relationship between (2.3) and (2.4) is given by $V_i^+ + V_i^- = V_i$ and $V_i^+ - V_i^- = Z_0 I_i$, where Z_0 is the characteristic impedance. When working with reflected and transmitted waves the S-parameters are much more convenient and will be the preferred method for this thesis. Another advantage is that they can be directly measured with a network analyzer.

2.3 Antenna efficiency

The antenna efficiency, defined as the ratio of the power radiated by the antenna to the power fed to the network of the antenna, of a lossless antenna j is given by the S-parameters as [12]

$$\eta_j = 1 - \sum_{i=1}^{N} \left| S_{ij} \right|^2 \tag{2.5}$$

The efficiency of antenna j is maximized when all S_{ij} are equal to zero. This should be pretty obvious as the condition implies that there are no reflections or leakages to other antennas. If the antenna is lossy, i.e., the radiation efficiency is less than 100 %, then this should also be included in (2.5).

2.4 Shannon capacity

The Shannon capacity is the theoretical upper bound on the data rate that can be achieved with an arbitrarily small error probability. In a SISO system corrupted by Additive White Gaussian Noise (AWGN) the Shannon capacity is

$$C = \log_2(1+\gamma) \text{ bps/Hz} \tag{2.6}$$

where γ is the signal-to-noise ratio (SNR) at the receiver. If we instead consider a $M \times N$ MIMO system with a complex Gaussian channel matrix $\mathbf{H}$, uniform power allocation to each transmitting antenna and AWGN at the receiver, the Shannon capacity is modified to [13]

$$C = \log_2 \det(\mathbf{I}_N + \frac{\gamma \cdot \mathbf{H}\mathbf{H}^*}{M}) \text{ bps/Hz} \tag{2.7}$$

where $\mathbf{I}_N$ is the identity matrix of size N, $\mathbf{H}$ is the $M \times N$ channel matrix with embedded element patterns included, * is the complex conjugate and γ is the SNR at every receiving antenna. It is also possible to express the capacity in terms of the eigenvalues λ_i of $\mathbf{H}\mathbf{H}^*$ as [14]

$$C = \sum_{i=1}^{\min(M,N)} \log_2 (1 + \lambda_i \cdot \gamma / M) \tag{2.8}$$

When the channel is known at the transmitter the capacity can be increased by allocating more power to channels with higher gains λ_i. A method that maximizes the capacity is called water filling. If the power transmitted through channel i is P_i, then the capacity obtained with water filling is [14]

$$C = \sum_{i=1}^{\min(M,N)} \log_2 \left(1 + \frac{P_i}{\sigma^2} \lambda_i \right) \tag{2.9}$$

where σ^2 is the receiver noise power. For a fading channel the capacity will vary and to get a good figure of merit the capacity should be averaged over the distribution function of the channel.

2.5 Antenna diversity

In antenna diversity different radiation patterns are used on the receiving antennas to receive the data through different channels. The techniques used for this was already mentioned in chapter 2.1. Here they will be explained a little bit more.

Space diversity: Diversity is obtained by separating antennas with identical radiation patterns**.** When moving an antenna relative to a reference point, its power pattern will be the same but the phase of the pattern will change. If the distance between two antennas is d and the first antennas radiation pattern is denoted with $\mathbf{F_1}$, then the second antenna's radiation pattern is given by [15]

$$\mathbf{F_2} = \mathbf{F_1} e^{(-j\mathbf{k}\bullet\mathbf{d})} \tag{2.10}$$

where $k = 2\pi / \lambda$ is the wavenumber. When the incident waves cover large angles even a small phase change can have a large impact on the correlation between the patterns. In the case of a uniform 3D Rayleigh environment, omnidirectional antennas and neglecting the coupling, the real correlation coefficient between the received signals is [15]

$$\rho(d) = \sin(kd)/d \tag{2.11}$$

A plot of the correlation between two received signals is shown in Fig. 2.1. High diversity is usually obtained if the magnitude of the correlation is below 0.7 [16]. It can be seen that the magnitude of the correlation coefficient is below 0.7 for $d > 0.23\lambda$. If mutual coupling is included, the antennas can be placed even closer [15].

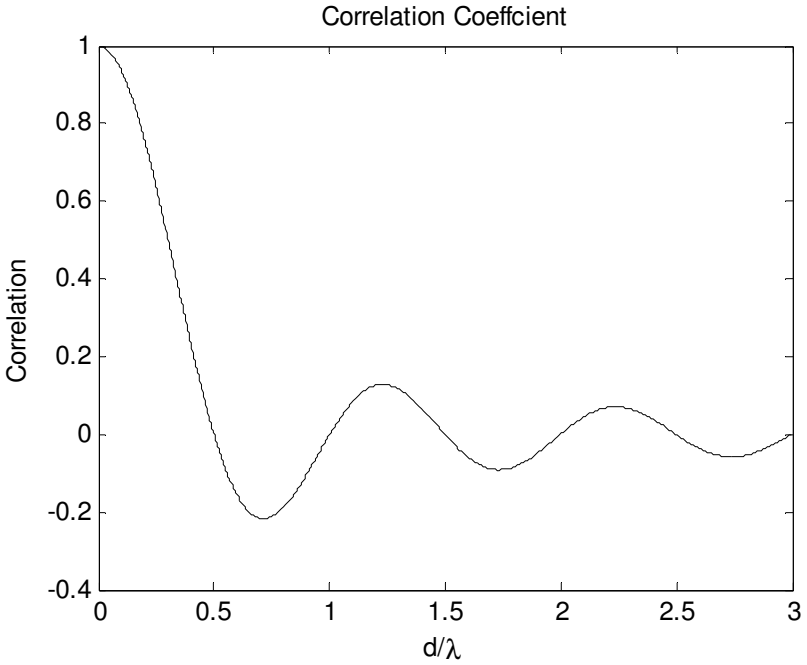

Fig. 2.1 Correlation coefficient between two received signals for two uncoupled antennas separated a distance d.

Pattern diversity: Different patterns can be used on the antennas to reduce the correlation. In the case of zero overlap between the patterns, every antenna will receive a different set of incoming waves.

Aside from using different isolated element patterns, identical isolated patterns can also be used in the case of mutual coupling, which will change the radiation patterns in a way that they will not be identical anymore. This is the reason why mutual coupling can reduce the correlation.

Polarization diversity: Diversity can be achieved by using two different polarizations (e.g. vertical and horizontal). In a uniform rich scattering environment the powers of the receiving waves are equally distributed to both polarizations and the probability that there is a simultaneous dip on the differently polarized antennas is low [14].

2.5.1 Maximal-ratio combining

There are different methods for combing the different branches, but only one scheme will be used in this thesis, called Maximal-Ratio Combining (MRC). MRC maximizes the average SNR at the combined output, which is

$$r = \sum_{i=1}^{M} a_i r_i \tag{2.12}$$

where M is the number of branches, r_i is the received signal at branch i and $a^2{}_i = r_i^2 / \sigma^2$, where σ^2 is the noise power in each branch [14]. The resulting SNR is

$$\gamma = \sum_{i=1}^{M} r_i^2 / \sigma^2 \tag{2.13}$$

The probability that the received SNR in a Rayleigh fading channel is below a given threshold γ_0 is [14]

$$\Pr(\gamma < \gamma_0) = 1 - e^{(-\gamma_0 / \bar{\gamma})} \sum_{k=1}^{M} \frac{(-\gamma_0 / \bar{\gamma})^{k-1}}{(k-1)!} \tag{2.14}$$

where $\bar{\gamma}$ is the average SNR in each branch. In Fig. 2.2 the outage probability is plotted for one and two antennas.

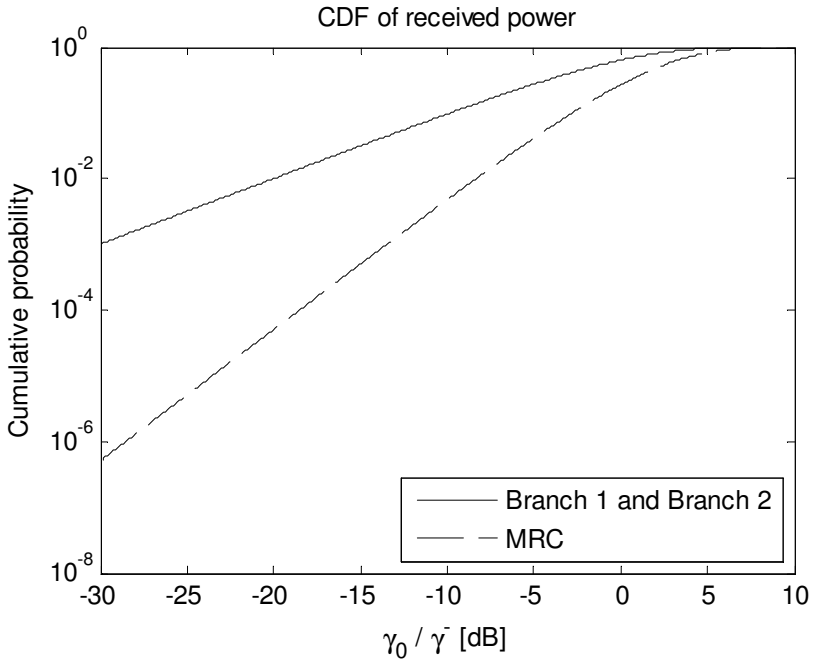

Fig. 2.2 CDF of the received power for two uncorrelated branches.

2.5.2 Diversity gain

The diversity gain is defined as the difference in the SNR, corresponding to a certain outage probability (usually 1 %), between the combined signals and the best single element. The effective diversity gains is the difference in the SNR compared to the same antenna but with 100 % antenna efficiency. The theoretical diversity gain at 1% level that can be achieved with two receiving antennas and MRC in a Rayleigh fading channel is calculated from (2.14) to about 11.7 dB. Obviously the diversity gain will be higher with a lower correlation coefficient, but when going below the usually considered acceptable value of 0.7 the diversity gain is not very sensitive to the correlation coefficient [16].

2.6 Signal correlation

The complex correlation, with mutual coupling included, between two signals can be found by calculating the complex correlation coefficient between the induced voltages on the antenna ports. This will require a statistical approach. Another approach is to use far-field functions of the two ports. The relationship is given by [12]

$$\rho = \frac{\iint_{4\pi} \mathbf{F}_n \cdot \mathbf{F}_m^{*} \, d\Omega}{\sqrt{\iint_{4\pi} |\mathbf{F}_n|^2 \, d\Omega \cdot \iint_{4\pi} |\mathbf{F}_m|^2 \, d\Omega}} \tag{2.15}$$

where $\mathbf{F}_n$ and $\mathbf{F}_m$ are the embedded far-field functions on port n and port m, respectively. It is also possible to express the correlation coefficient in terms of the S-parameters as [17]

$$\rho = \frac{-\sum_{i=1}^{N} S_{in} S^{*}_{im}}{\sqrt{(1-\sum_{i=1}^{N} |S_{in}|^2)(1-\sum_{i=1}^{N} |S_{im}|^2)}} \tag{2.16}$$

This expression is valid for a lossless system with an arbitrary number of ports and antennas under the assumption that the environment is uniform. When working with powers it may be more convenient to use the envelope correlation which is defined as $\rho_e = |\rho|^2$.

3 Antenna design

In this chapter a two-element array is designed and the performance in terms of S-parameters, efficiency and correlation is evaluated. The dimensions of the elements are obtained from an optimization of a single antenna.

3.1 Single monopole antenna

The first priority during the antenna system design was simplicity, i.e. design an antenna system that could be easily constructed and also easily modeled and analyzed.

An antenna that fits both of the criteria's above is the monopole antenna, which consists of an electric conductor above a ground plane. If the ground plane is of infinite size, the far field pattern above the ground plane can be found by the use of image theory. The monopole and the ground plane can be replaced with a dipole antenna, which is one of the simplest antennas from a theoretical point of view, of twice the length. Theory of dipole antennas can then be used to analyze the monopole antenna. In practice the ground plane will always be of finite size and this will affect the properties of the antenna. A monopole antenna can be very easily constructed by the use of e.g. a metal plate and a wire connected to it.

A circular metal plate was used as a ground plane. This choice was motivated by the fact that when using only one antenna centered on a circular ground plane the radiation pattern will not vary with the azimuth angle. Hence, a three-dimensional geometry can be modeled in two dimensions, resulting in a simpler model and less computations during simulations. In Fig. 3.1 the conductor and the ground plane is placed in a Cartesian coordinate system, where the spherical angles are defined through a vector $\mathbf{r}$.

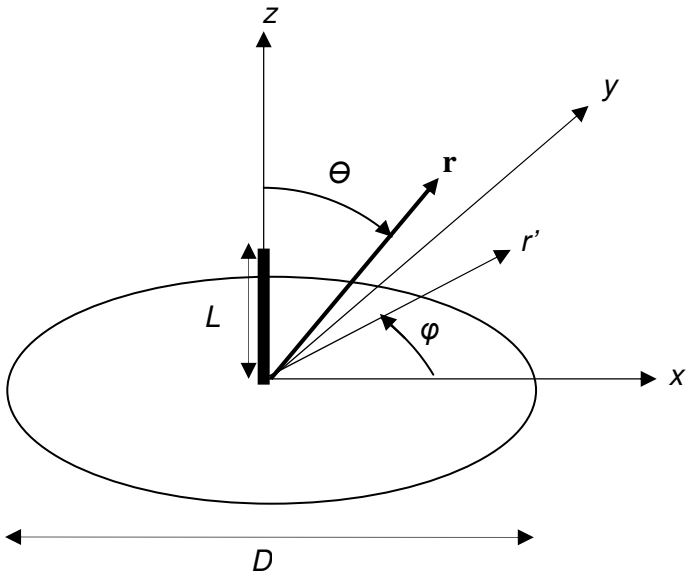

Fig. 3.1 Monopole antenna with length *L* on a circular ground plane with diameter *d*. The azimuth angle is denoted with φ, the inclination angle is denoted with Θ and r' is the projection of r into the xy-plane.

As an electric conductor a brass rod with a diameter of 3 mm was chosen. The brass rod was soldered to a SMA-contact which was fastened to the ground plane with metal screws. To feed the antenna a 50 Ω coaxial cable is connected to the SMA-contact. See Fig. 3.2 for a cross section drawing of the antenna.

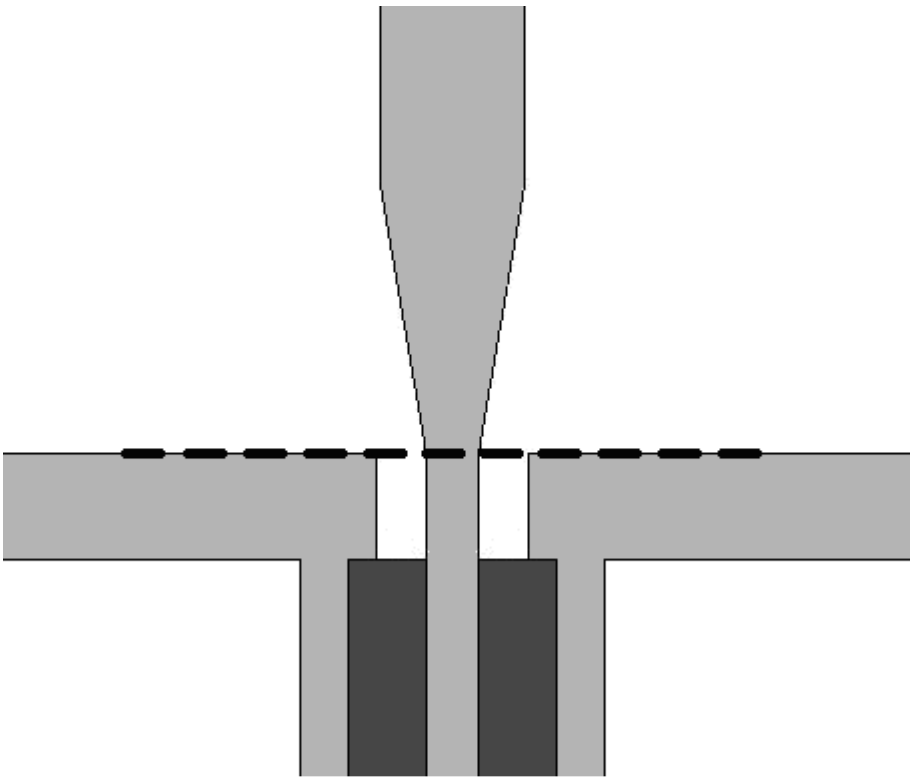

Fig. 3.2 Cross section drawing of the antenna with ground plane, SMA contact and coaxial cable. The dashed bold line is the reference plane of the S-parameters. Light grey area denotes conductors and the darker grey Teflon.

3.1.1 Ground plane size

The size of the ground plane will mainly affect the radiation pattern of the antenna, and to a lesser degree the antenna impedance [18]. A far-field radiation pattern for a quarter wavelength monopole for different ground plane diameters was simulated in the finite element analysis and solver software Comsol. The maximum diameter was 0.8 m, which was set by the size of the reverberation chamber to be used. The far-field radiation pattern in partial realized gain[1] g_r for different ground plane diameters is plotted in Fig. 3.3. The diameter was chosen to $D = 0.7$ m, because it gives low back-scattering and a constant pattern above the ground plane.

[1] IEEE Std 145-1993, ”IEEE Standard Definitions of Terms for Antennas”: Realized gain, partial. The partial gain of an antenna for a given polarization reduced by the losses due to mismatch of the antenna input impedance to a specified impedance.

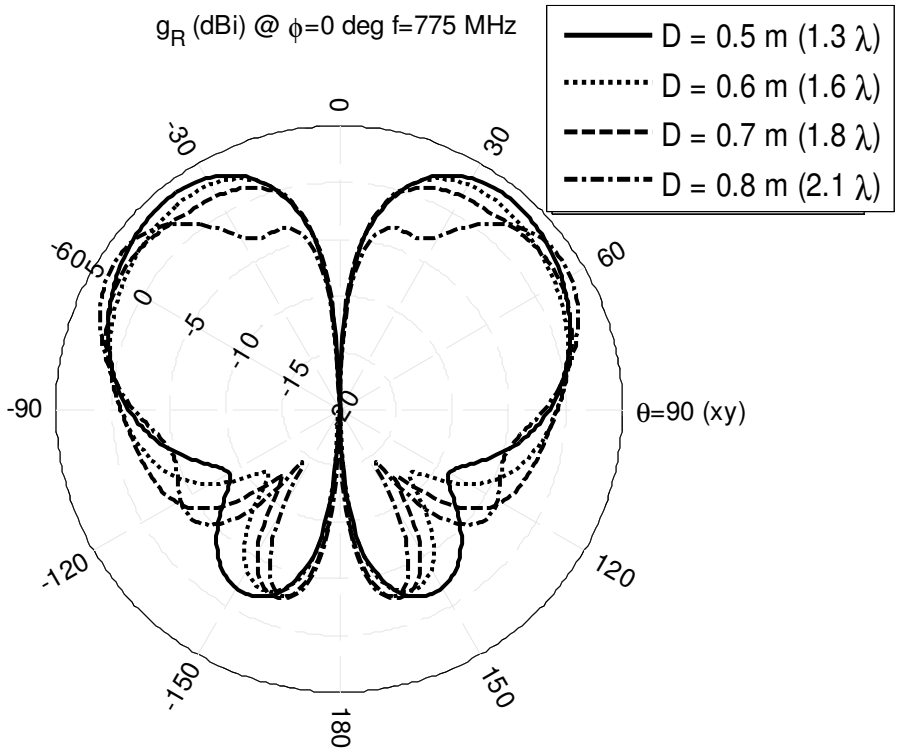

Fig. 3.3 The far-field radiation pattern in g_r at ϕ = 0 for a $\lambda/4$ - monopole for different ground plane diameters D. The thickness of the ground plane is 2 mm.

3.1.2 Optimization of radiated power

The length of the antenna was optimized for maximum radiated power. This is equivalent to minimizing the reflection at the antenna port, i.e. impedance match the antenna to the transmission line. Because a lossless transmission line has resistive characteristic impedance it's desirable to have antenna impedance with zero reactance to achieve best matching. The most commonly used length on the monopole antenna is $L = \lambda/4$ that gives antenna impedance equals to $Z_a = 36.5 + j21.5\Omega$ [19]. Depending on the radius of the conductor, the reactance will be zero if the length is reduced to about $L = 0.23\lambda$ to 0.24λ [19]. Simulations and measurements for different antenna lengths were made. The reflection coefficient S_{11} at the antenna port was simulated in the finite element solver softwares HFSS and Comsol. A monopole antenna, on a circular ground plane with $D = 0.7$ m, connected to a 50 Ω coaxial transmission line was modeled. The measurement of S_{11} was done with HP 8850 network analyzer.

Magnitude of S_{11} for both simulations and measurements are plotted in Fig. 3.4 . The results from HFSS and the results from measurements follow the same characteristic, but differ in magnitude. In Comsol, the resonant frequency is slightly shifted. It can be seen that the optimal length is $L = 0.233\lambda$, which is the length that was chosen. The magnitude of S_{11} for the optimal length is plotted in Fig. 3.5. As expected the resonance frequency is around 775 MHz.

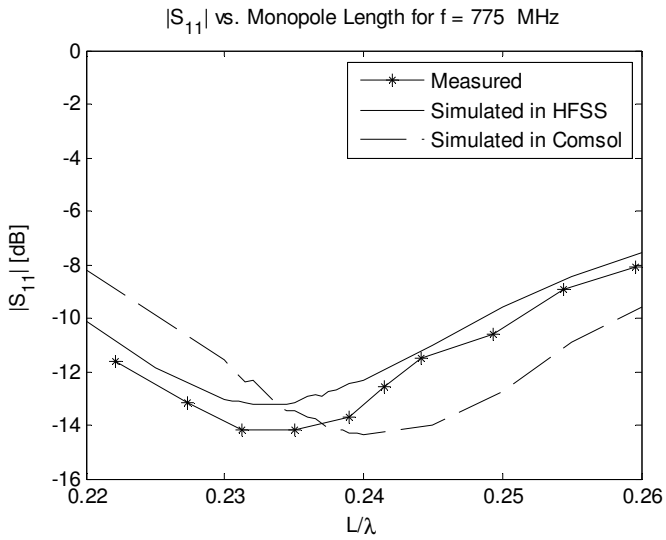

Fig. 3.4 Magnitude of S_{11} for varying monopole length. Ground plane diameter d = 0.7 m (1.8λ) and thickness a = 2 mm.

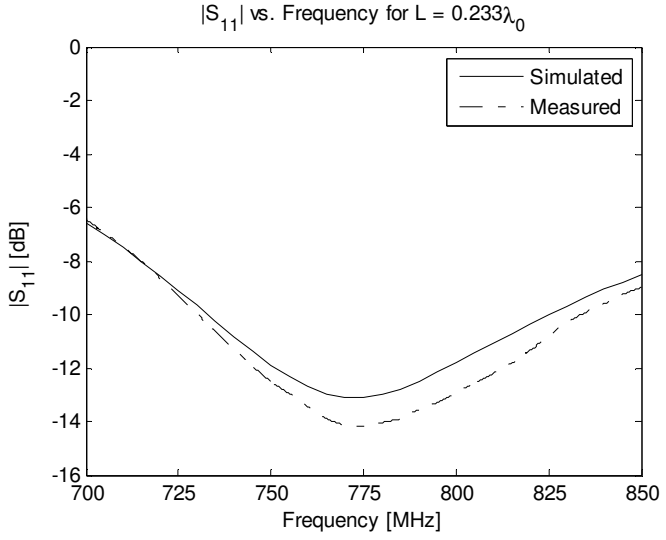

Fig. 3.5 Magnitude of S_{11} for optimized monopole length. Simulation was performed in HFSS.

3.1.3 Radiation pattern

The far-field radiation pattern in partial realized gain for the designed antenna has also been simulated in HFSS and measured in an anechoic chamber. Three different patterns are shown in Fig. 3.6. The shapes of the measured and simulated patterns are very similar. As expected, most of the power is radiated into the upper hemisphere and the antenna is omnidirectional in the ϕ-planes.

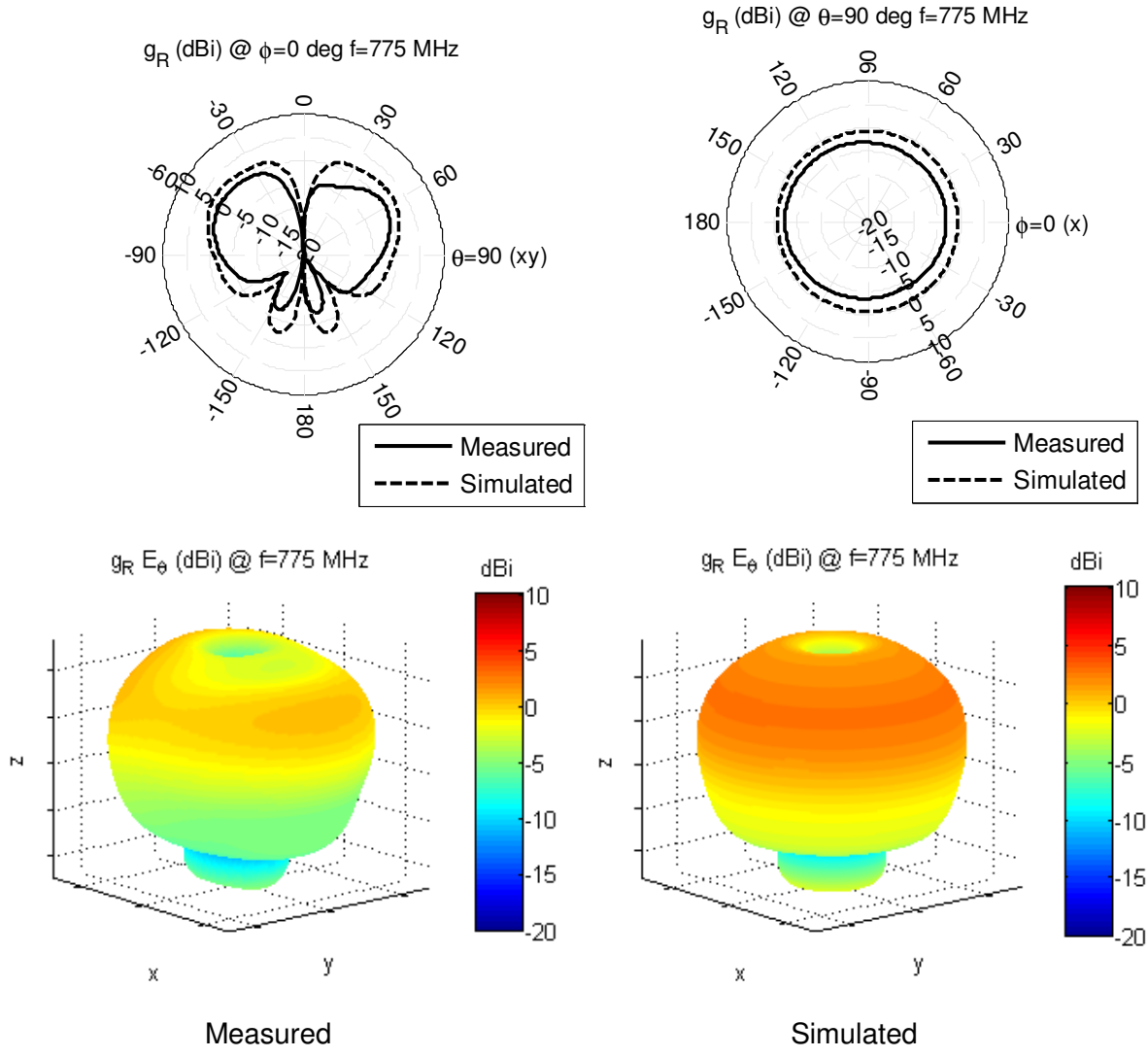

Fig. 3.6 Measured and simulated radiation pattern in partial realized gain g_r for the monopole antenna.

3.2 Dual monopole antenna

The antenna array consists of two identical monopoles mounted on the same ground plane and at equal distances from the center. A setup is seen Fig. 3.7. The size of the ground plane and the length of the antennas are the same as for the single antenna. The antennas can be mounted on three different distances from the center of the ground plane. Thus, three different separations between the antennas are possible, 30 mm (0.08λ), 100 mm (0.26λ) and 400 mm (1.03λ).

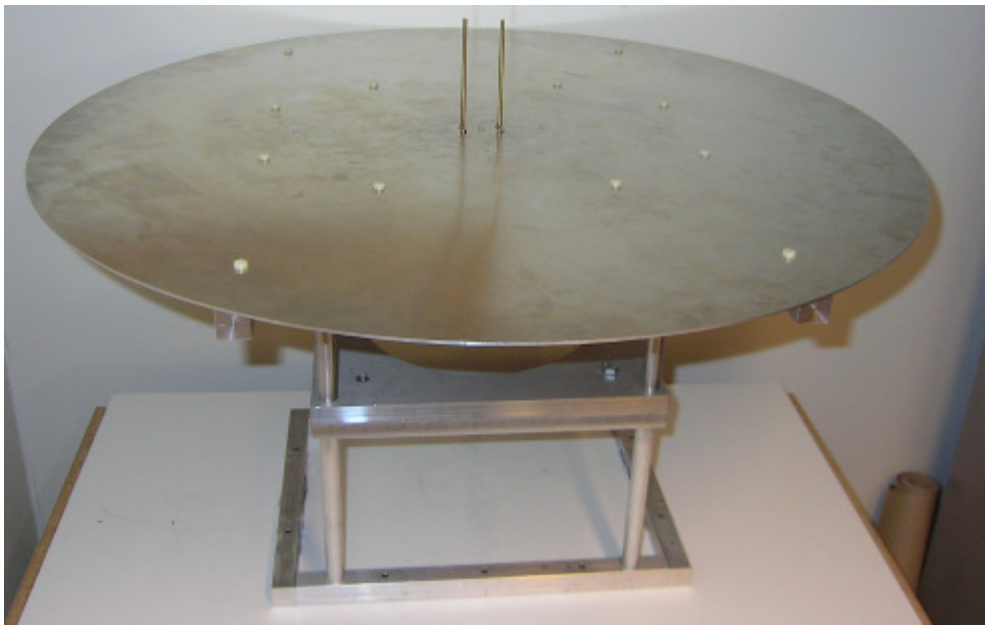

Fig. 3.7 The antenna array with antenna separation of 30 mm.

Due to the symmetry of the antenna array the system is symmetric, i.e., $S_{11} = S_{22}$, and reciprocal , i.e., $S_{21} = S_{12}$. Simulated and measured reflection (S_{11}) and coupling (S_{21}) are shown in Fig. 3.8 and Fig. 3.9. The measured return loss for the two smallest separations is lower than for the single antenna at the center of the ground plane, which is a consequence of the mutual coupling between the antennas. It can also be seen that the resonant frequency has been slightly shifted. For the separation of 1.03 λ the return loss is higher than for the single antenna. Most likely this is due to the antenna's new location on the ground plane, and not the mutual coupling which can be considered negligible. As expected the mutual coupling is decreasing with increasing separation.

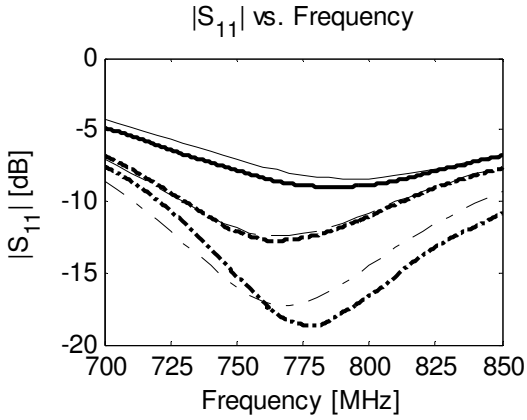

Fig. 3.8 Magnitude of S_{11} for different separations

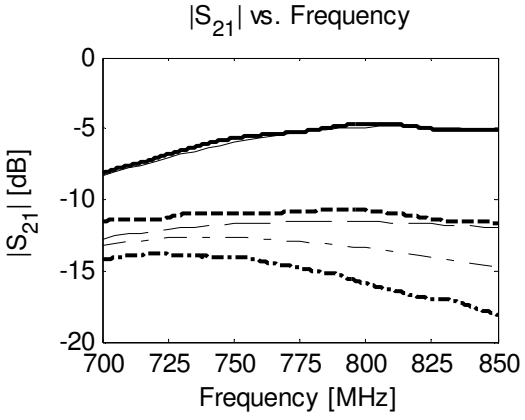

Fig. 3.9 Magnitude of S_{21} for different separations.

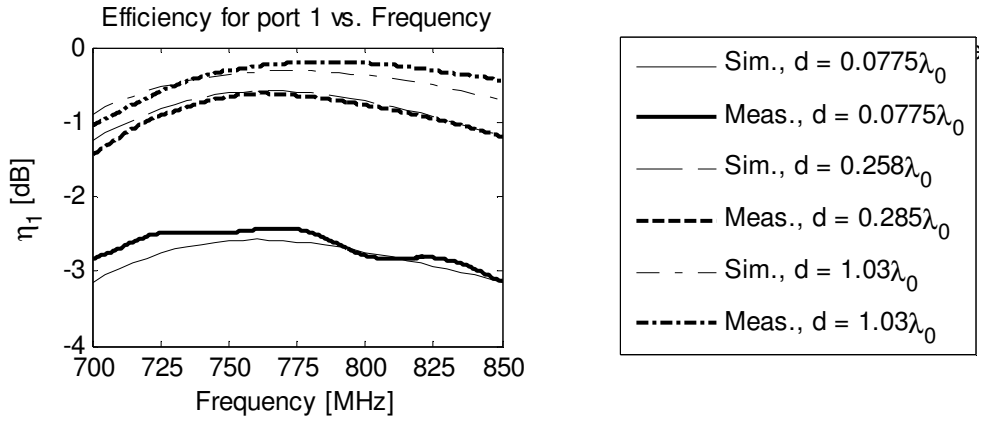

Fig. 3.10 Antenna efficiency at port 1 for different separations.

Under the assumption that the antenna is lossless the antenna efficiency can be calculated from the S-parameters according to (2.5). Calculated efficiencies from both the measured and simulated parameters are shown in Fig. 3.10. For a separation of 0.08 λ the measured mean efficiency over 750 MHz to 800 MHz is -2.56 dB. Increasing the distance from 0.08 λ to 0.26 λ gives about 2 dB higher efficiency. This is primarily due to the lower coupling.

The envelope correlation, which has been calculated with (2.16), is shown in Fig. 3.11. As mentioned earlier, high diversity is usually obtained for envelope correlations below 0.5. The envelope correlation is above 0.5 for the smallest separation, but already for the second distance the envelope correlation is below 0.08 for all frequencies. For the largest distance the correlation is very small and in practice negligible. Comparing with the theory for the uncoupled antennas, it can be seen that the correlation is lower, which is expected.

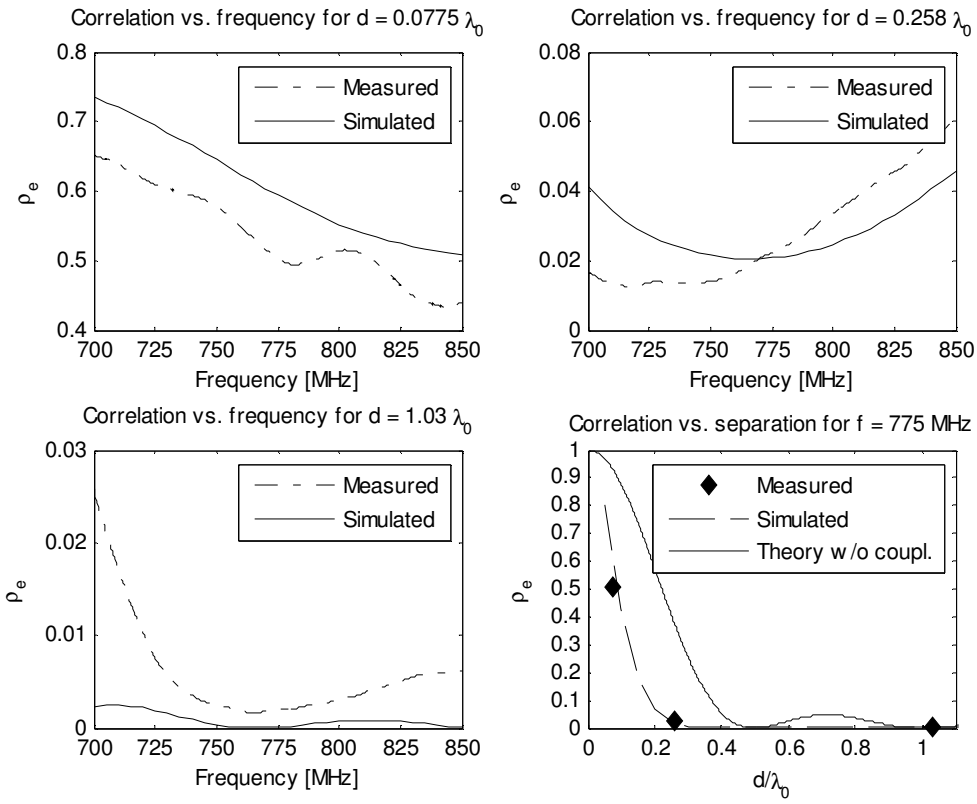

Fig. 3.11 Envelope correlation vs. frequency for all separations and correlation at the center frequency vs. separation.

3.2.1 Radiation pattern

Measured and HFSS simulated embedded far-field radiation patterns for antenna 1 when separated 0.08 λ from antenna 2 are shown in Fig. 3.12. Due to the mutual coupling the pattern has been modified. It can be seen that the pattern is no longer symmetrical about the yz-plane or constant in the ϕ-plane. The radiation pattern for antenna 2 is the same but mirrored about the yz-plane. Radiation patterns for the two larger separations will not be presented here, because the low mutual coupling doesn't have any noticeable effect on the radiation patterns.

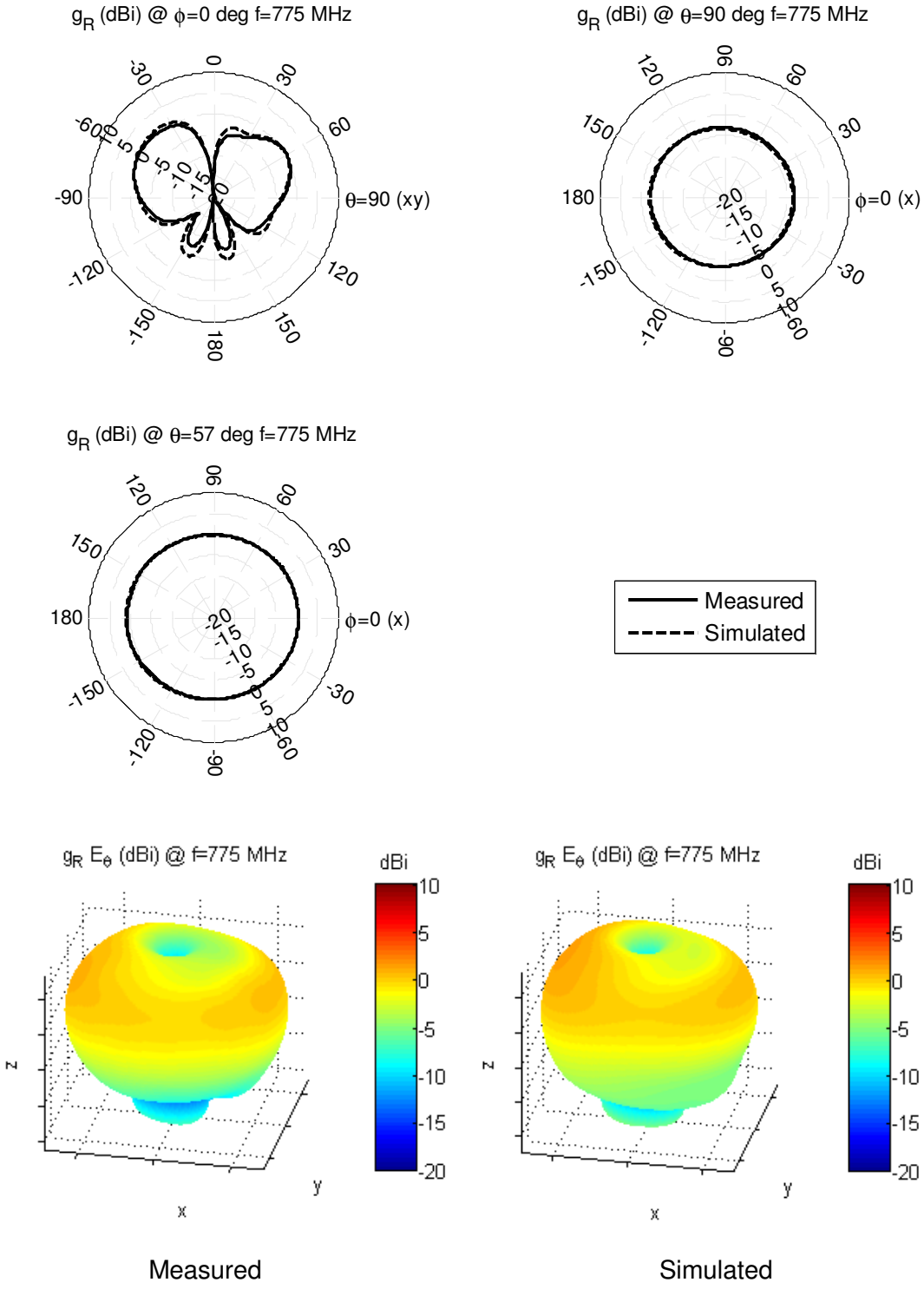

Fig. 3.12 Embedded radiation patterns in partial realized gain g_R for antenna 1 at the center frequency 775 MHz. The solid lines are measurements and the dashed lines are simulations. $\theta = 57^\circ$ cut contains the direction of the maximum gain.

3.3 Summary and conclusion

Optimization of a single antenna was done for the antenna array. Good matching was still obtained and the resonant frequency was only slightly shifted when placed in the array environment. For an antenna separation of 0.0775 λ the mutual coupling reduces the antenna efficiency significantly. On average the efficiency is reduced from close to 0 dB to –2.56 dB. Also the correlation envelope is above 0.5, which is usually considered as the upper bound for achieving good diversity. For the other two separations acceptable performance in terms of efficiency and correlation are still obtained. Hence, we come to the conclusion that a compensation network is only needed for a separation of 0.0775λ and from now on this is the only distance that will be tackled.

4 Compensating networks

4.1 Introduction

A number of different layouts were tested and optimized but only three passive networks were chosen and are presented in this chapter, each one with a certain advantage. The neglected ones usually did not have a physically realizable geometry in the chosen technology, which stopped further investigation. After optimization, layouts were generated and further simulations were carried out in Momentum, using method of moments. All the figures presented in chapters about the network design contain antennas and the designed network together, forming a new 2-port.

4.1.1 Technology and substrate

For the realization of the compensation networks stripline technology was selected due to its electromagnetic shielding properties. On the downside, possible solutions using lumped components were early discarded due to practical inconvenience. Using lumped components would reduce the physical size considerably and higher order resonance matching circuits could be realized. Common problem with parasitics that follow with higher frequencies, when dealing with lumped components, would also be avoided due to frequency band of interest being bellow 1 GHz. Substrate used for this project is Neltec 9300 and its properties can be viewed in Table 4-1. Properties are measured at 10 GHz which contributes to a small error between simulated and measured scattering parameters. Substrate cross-section, with corresponding quantities, is presented in Fig. 4.1.

Neltec 9300	
Permittivity, ε_r	3.0±0.04
Loss tangent, tanδ	0.0023
Ground plane spacing, B	1.6 mm
Conductor thickness, T	34 µm

Table 4-1 Substrate properties.

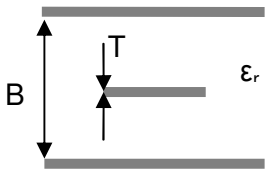

Fig. 4.1 Substrate cross-section.

4.1.2 S-parameters and matching

Contrary to what was stated earlier in chapter 3, where reference plane was defined at the upper ground plane surface in order to compare simulation and measurement results, reference plane will from now on be located at the SMA interface at the ground plane. S-parameters are measured using HP 85107A network analyzer.

Reflection and coupling for 2 x 1 antenna array, separated 30 mm and with no network connected, are depicted in Fig. 4.2 and Fig. 4.3 respectively, both measured and simulated in Ansoft HFSS. Both ports must be matched simultaneously due to 2-port MIMO system not being unilateral, which is caused by the strong coupling between the antennas and reciprocity due to the physical symmetry along the y-axis. Hence direct matching for both reflection and coupling over the frequency band is quite strenuous, if not impossible, insisting on simplicity and physical size at the same time. Instead of matching to reduce mismatch and coupling losses a different approach was applied early: directly matching for high antenna efficiency and low envelope correlation. The goal changed from matching for coupling and reflection to less than -10 dB for 750 – 800 MHz to obtain radiation efficiency higher than -1.55 dB (70 %) and signal envelope correlation lower than 0.3 for same frequency range. During the optimization process no considerations to the ohmic losses have been taken. Correlation and efficiency without any network are presented in Fig. 4.4 and Fig. 4.5 respectively.

4.1.3 Optimization

Optimization of the networks is performed in RF and microwave software Agilent ADS using built-in optimization tool. SMA-connectors at the ports connecting the compensation network to the antennas were modeled and included in the optimization process. Four hundred iterations were performed using the default optimization type and goals according to Table 4-2. Equal weights have been used on both goals.

Expression	Min	Max	Frequency Range
$\rho_e = \dfrac{\left\lvert S_{11}^* S_{12} + S_{21}^* S_{22} \right\rvert^2}{(1-\lvert S_{11}\rvert^2 - \lvert S_{21}\rvert^2)(1-\lvert S_{12}\rvert^2 - \lvert S_{22}\rvert^2)}$	-	0	750 – 800 MHz
$\eta_1 = 1-\lvert S_{11}\rvert^2 - \lvert S_{21}\rvert^2$	1	-	750 – 800 MHz

Table 4-2 Optimization goals.

4.1.4 Dimensions

For those networks containing parallel sections of striplines, length of these is kept constant in order to enable easier mounting to the antennas. The idea is to keep 30 mm between the inner conductors of SMA-connectors due to antenna spacing being equal in length. Hence the length of each parallel stripline is simply *30 – W*, where *W* is the width of the series line to which the parallel piece is connected.

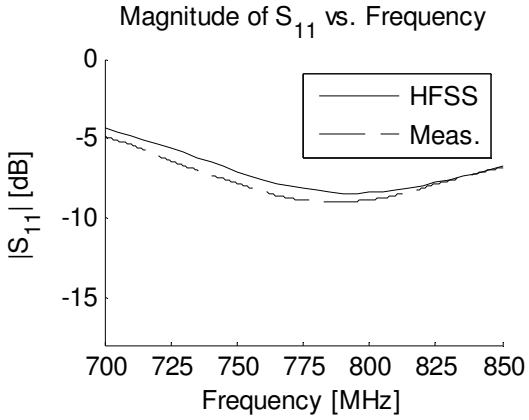

Fig. 4.2 Simulated and measured reflection.

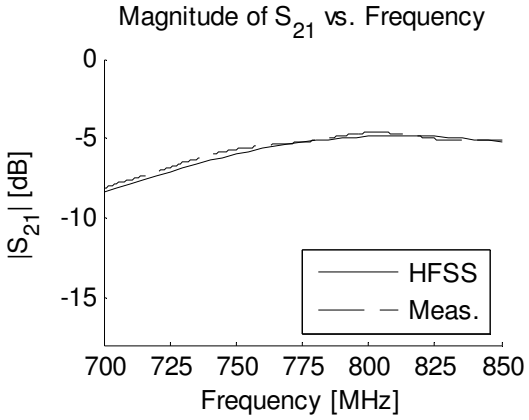

Fig. 4.3 Simulated and measured coupling.

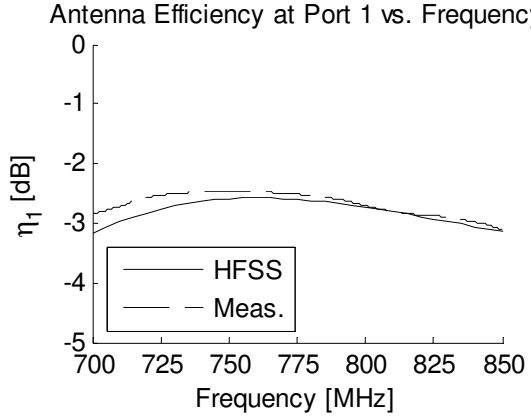

Fig. 4.4 Simulated and measured efficiency.

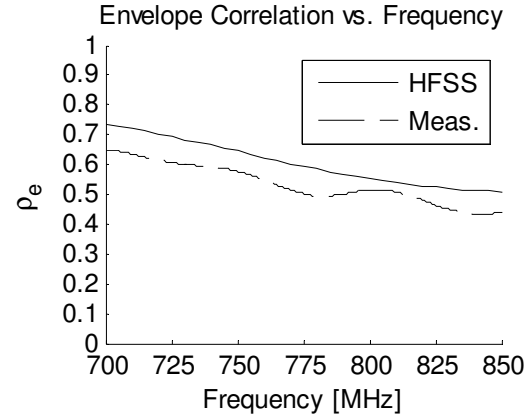

Fig. 4.5 Simulated and measured envelope correlation.

4.2 Network design

4.2.1 Network 1: Impedance Transformer

The first network presented is chosen due to its geometric simplicity and size, as can be viewed in Fig. 4.6. It consists of two single pieces of stripline connected together and works as an impedance transformer. Width and length of the line marked as 1 are used as parameters in the optimization while the second line is just a 50 Ohm line used for SMA-connectors.

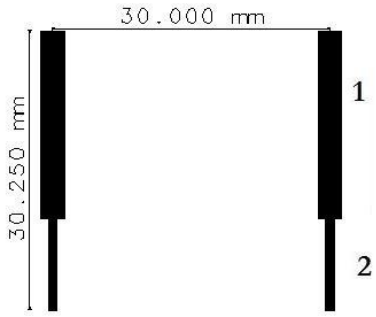

Fig. 4.6 Layout with outlined physical size of the network. Numbering corresponds to different sections of stripline with different length and width, for more detailed information check Table 4-3.

Physical dimensions of the lines in the compensation network are presented in Table 4-3. Performance of the network is very limited due to only two degrees of freedom when optimizing and the strong coupling between the monopoles. As can be concluded from Fig. 4.7 and Fig. 4.8, a first order resonance with bandwidth of approximately 50 MHz is achieved for power reflection less than 10 %. Coupling on the other hand has increased by 1-2 dB in the same frequency band.

	Param.	**Value**	**Optim.**
1: Single stripline			
	Width	2.57 mm (25.5 Ω)	Yes
	Length	20.25 mm (32.6º)	Yes
2: Single stripline			
	Width	0.95 mm (50.0 Ω)	No
	Length	10.00 mm (16.1º)	No

Table 4-3 Optimization results for the impedance transformer.

Fig. 4.10 shows the S-parameter based envelope correlation with the compensating network proposed. As one can conclude the curve is under the goal value of 0.3 for frequencies higher than 750 MHz. Antenna efficiency, Fig. 4.9, on the other hand could not be optimized for the desired goal, which is understandable considering network having only two degrees of freedom and being simply an impedance transformer.

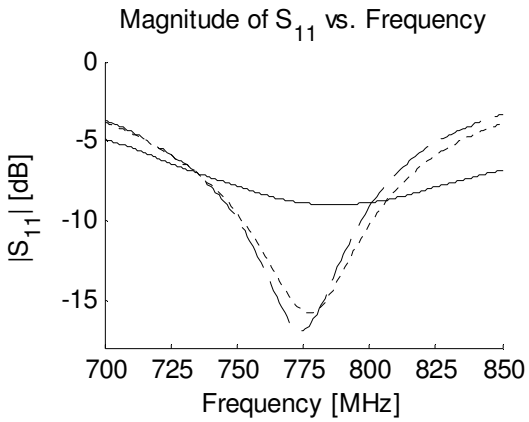

Fig. 4.7 Reflection with and without compensating network.

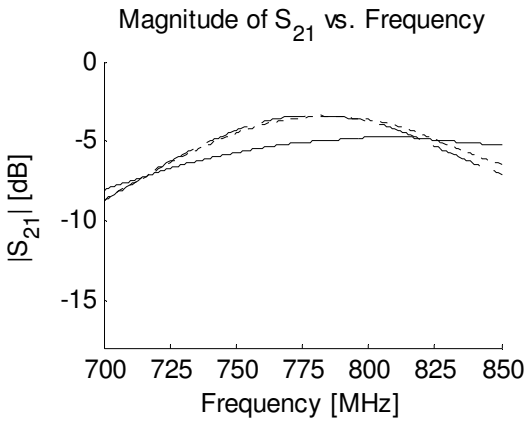

Fig. 4.8 Coupling with and without compensating network.

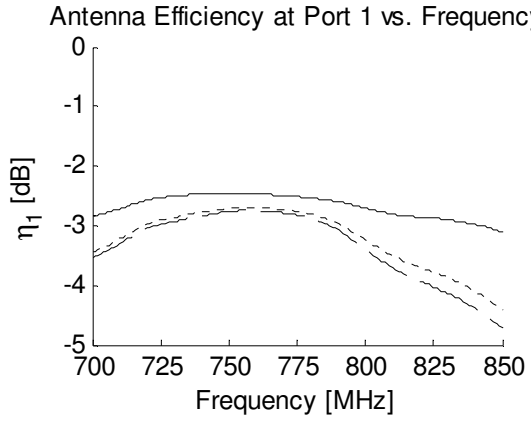

Fig. 4.9 Antenna efficiency at port 1 with and without compensating network.

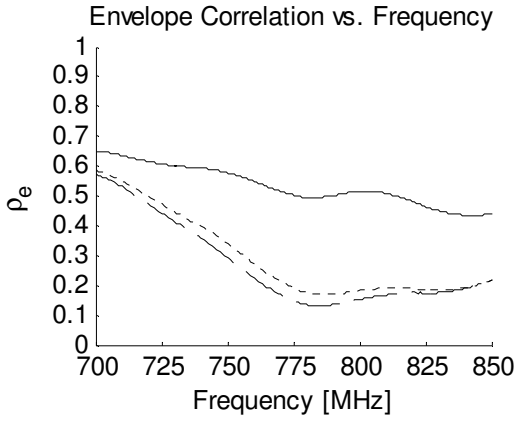

Fig. 4.10 Envelope correlation with and without compensating network.

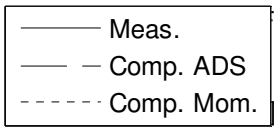

4.2.2 Network 2: Impedance Transformer with Coupled Lines

Next step was to design a physically small network that at the same time fulfilled the design requirements. The idea was to try to incorporate coupled lines of some kind in order to reduce the effects of coupling. Due to practical inconvenience when dealing with striplines, broadband properties of a Lange coupler-like structure were not pursued. A number of different approaches were under a trial, using both one and two parallel pieces of coupled lines, but unfortunately neither one provided acceptable results. Instead a series coupled line, see Fig. 4.11, together with a single parallel stripline, working as an impedance transformer, were selected. Curved lines were used to achieve 30 mm port separation in order to avoid parasitics that often come with corners.

Line marked as 1 is a half a centimeter long 50 ohm line for easier mounting due to curved nature of the first impedance transformer. Width of the curved line, denoted as 2, is a part of the optimization. Its length on the other hand is indirectly optimized through the width and separation of the coupled lines.

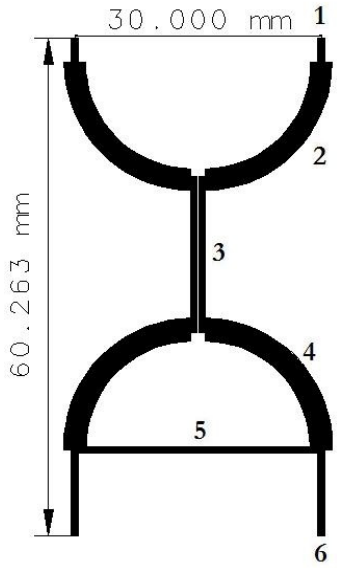

Fig. 4.11 Layout with outlined physical size of the network. Numbering corresponds to different sections of stripline with different lengths and widths, for more information check Table 4-4.

What was noted during the simulations was that the separation between the coupled lines contributed to a negligible difference in performance when bellow a certain value. For that reason the separation distance was kept constant at one quarter of a stripline width. Length and width of the lines are optimization parameters, marked as 3. Line 4 has the same characteristic as line 2 except for the different width. The fifth stripline is optimized only for width in order to keep port separation at 30 mm. Optimization values can be viewed in Table 4-4.

	Param.	Value	Optim.
1: Single stripline			
	Width	0.95 mm (50.0 Ω)	No
	Length	5.00 mm (8.1º)	No
2: Single curved stripline			
	Width	2.61 mm (25.2 Ω)	Yes
	Length	22.21 mm (35.8º)	No
3: Coupled lines			
	Width	0.76 mm	Yes
	Length	17.43 mm	Yes
	Separation	0.19 mm	No
4: Single curved stripline			
	Width	2.78 mm (24.84 Ω)	Yes
	Length	22.21 mm (35.8º)	No
5: Single stripline			
	Width	0.79 mm (58.3 Ω)	Yes
	Length	27.22 mm (43.9º)	No
6: Single stripline			
	Width	0.95 mm (50.0 Ω)	No
	Length	10.00 mm (16.1º)	No

Table 4-4 Optimization results for the impedance transformer with coupled lines.

Reflection and coupling are depicted in Fig. 4.12 and Fig. 4.13 respectively. Return loss is 10 dB at 760 – 790 MHz and 8.3 – 9.3 dB at the desired frequency band. Coupling is also reduced to between -6 and -7 dB for the same band. Goals for the correlation are reached to bellow 0.3, see Fig. 4.15. Antenna efficiency is shown in Fig. 4.14: -1.5 dB is reached at 757 – 793 MHz while at 750 – 800 MHz at around -1.9 dB.

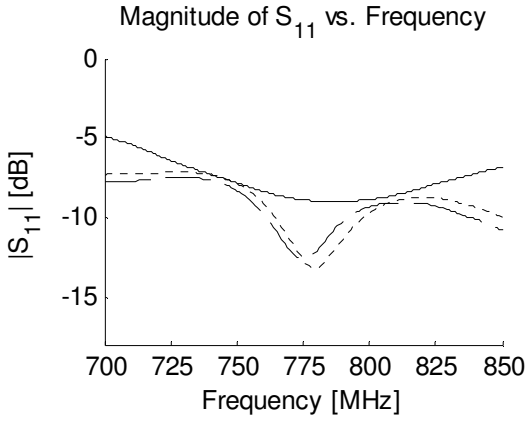

Fig. 4.12 Reflection with and without compensating network.

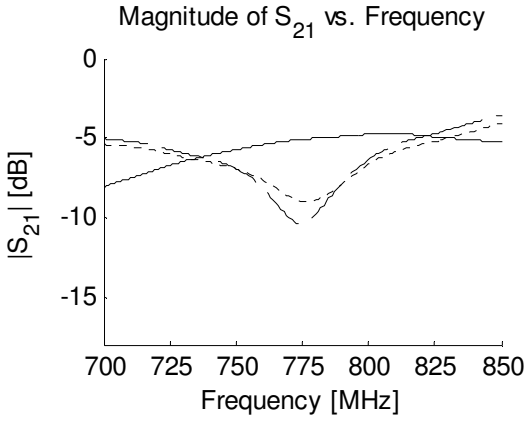

Fig. 4.13 Coupling with and without compensating network.

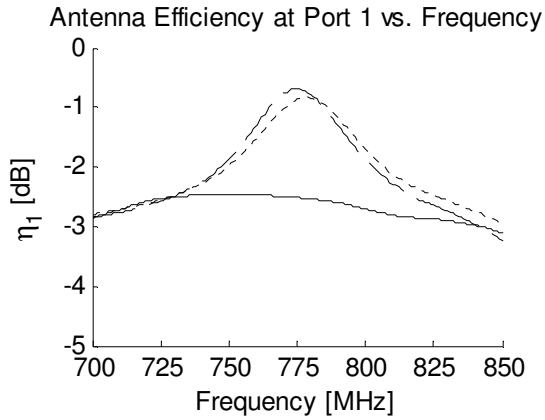

Fig. 4.14 Antenna efficiency at port 1 with and without compensating network.

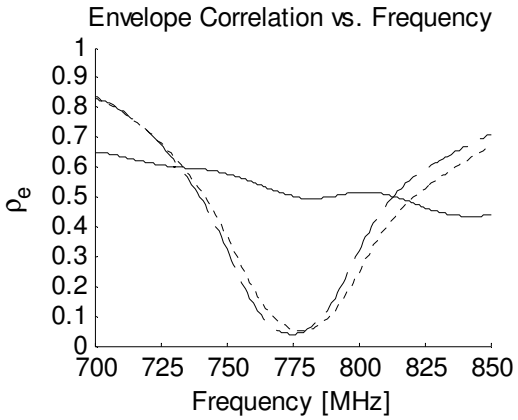

Fig. 4.15 Envelope correlation with and without compensating network.

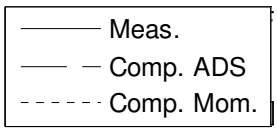

4.2.3 Network 3: Impedance Transformer with a Hybrid

In order to increase the number of degrees of freedom compared to the first network, an additional series piece of stripline was added together with a piece of 50 ohm line for the connectors. Furthermore two parallel sections were added at the two width steps. In other words the circuit resembles a coupler but with an extra stripline section, i.e. an impedance transformer followed by a hybrid coupler. Width and length of the two series sections, marked as 1 and 3 in Fig. 4.16, are optimized. Together with the widths of the two parallel pieces, 2 and 4 in the same figure gives six degrees of freedom in the optimization.

Table 4-5 displays widths and lengths of the individual lines, as in Fig. 4.16, after the optimization. Even though the network is quite large physically, 18.4 cm x 3 cm, it has excellent compensation properties. Both reflection and coupling S-parameters are higher than 9 - 10 dB at the frequency range of interest, see Fig. 4.17 and Fig. 4.18. Signal envelope correlation is approximately 0.17 at the same part of the spectrum, depicted in Fig. 4.20. An envelope correlation of 0.3 corresponds to a bandwidth of 60 MHz, 745 – 805 MHz. Fig. 4.19 displays antenna efficiency at port 1, where the desired value of higher than -1.5 dB is achieved. An interesting characteristic for all the graphs is the presence of two resonance tops, increasing the bandwidth significantly.

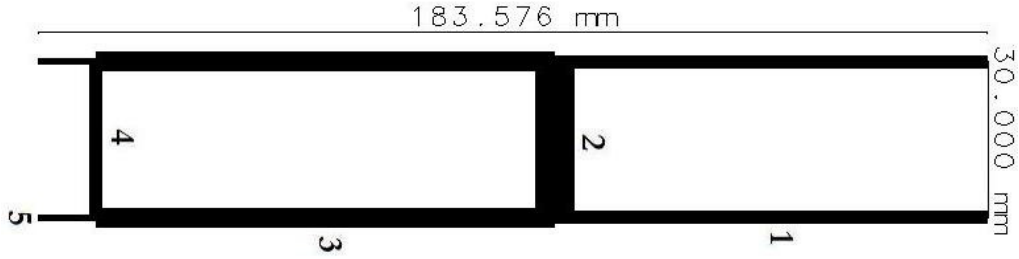

Fig. 4.16 Layout with outlined physical size of network 3. Numbering corresponds to different sections of stripline with different length and width, for more information check Table 4-5.

	Param.	Value	Optim.
1: Single stripline			
	Width	2.32 mm (27.6 Ω)	Yes
	Length	79.85 mm (128.7º)	Yes
2: Single stripline			
	Width	7.59 mm (10.2 Ω)	Yes
	Length	27.68 mm (44.6º)	No
3: Single stripline			
	Width	3.38 mm (20.5 Ω)	Yes
	Length	83.97 mm (135.4º)	Yes
4: Single stripline			
	Width	2.17 mm (29.1 Ω)	Yes
	Length	26.62 mm (42.9º)	No
5: Single stripline			
	Width	0.95 mm (50.0 Ω)	No
	Length	10.00 mm (16.1º)	No

Table 4-5 Optimization results for the impedance transformer with a hybrid.

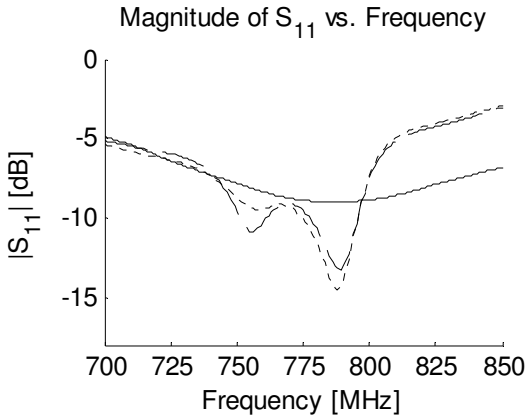

Fig. 4.17 Reflection with and without compensating network.

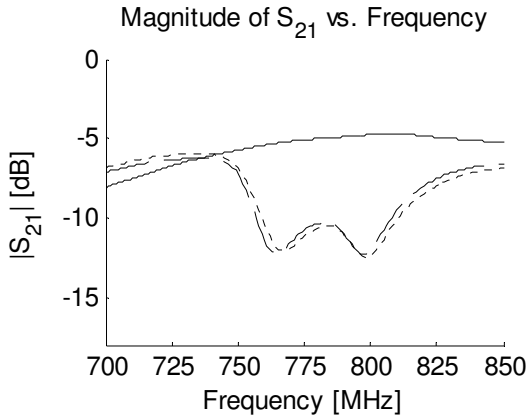

Fig. 4.18 Coupling with and without compensating network.

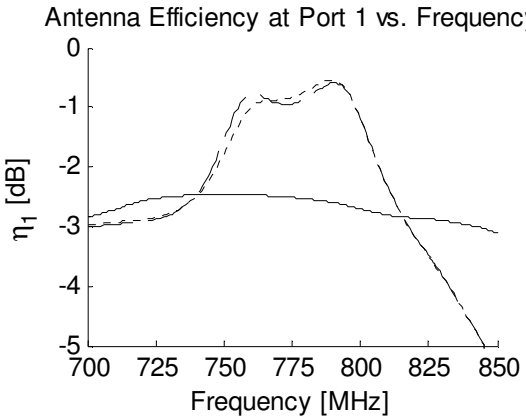

Fig. 4.19 Antenna efficiency at port 1 with and without compensating network.

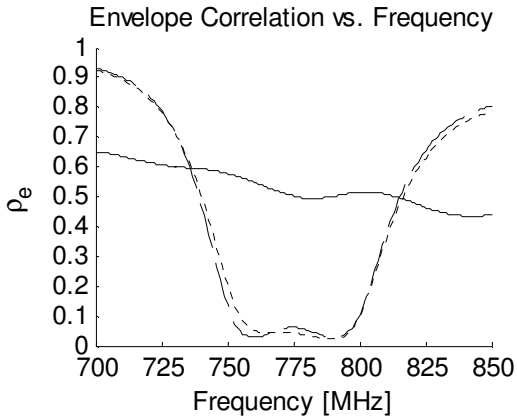

Fig. 4.20 Envelope correlation with and without compensating network.

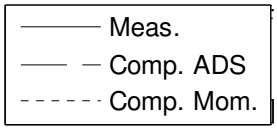

4.3 Network verification

4.3.1 Practical issues

Measurement verification of the designed compensation networks was somewhat delayed due to practical inexperience. Reviewing of the connector types was neglected in the design stage and following problems were encountered and solved through various improvisation.

4.3.1.1 Network connectors

Connectors frequently used for stripline solutions at the department were designed for approximately double substrate thickness compared to the one used for this project. Being both time-consuming and costly, ordering new connectors was early discarded. Instead, small pieces of the same substrate as used in the network design were cut out to fit connector dimensions. Pieces were “wrapped“ using copper tape to ensure connectivity between the connector and the ground plane. Connector solution, showing all the parts separate and mounted, is depicted in Fig. 4.21.

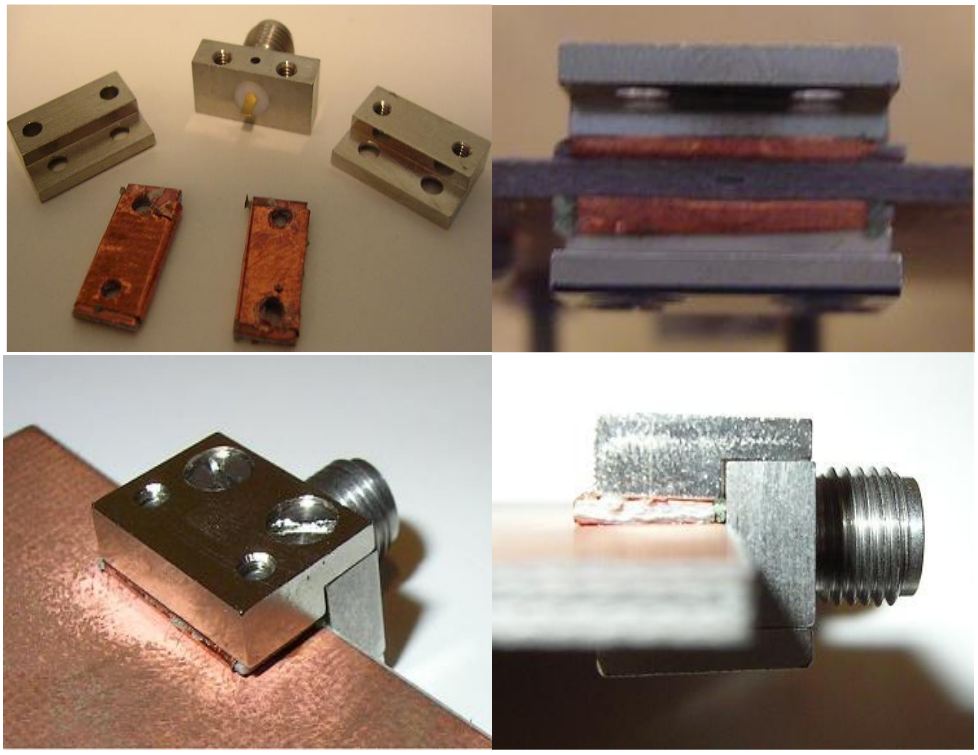

Fig. 4.21 Modified SMA connector used for the stripline compensation networks.

4.3.1.2 Antenna connectors

Another inconvenience was that SMA connectors for both the networks and the antennas were male. Antennas had to be remade with the new female connectors. Fig. 4.22 displays the new connectors together with the brass rod used, both separate and soldered together. White plastic clothing on the connector was pealed away and the inner conductor shortened to the same length as the previously used female connector.

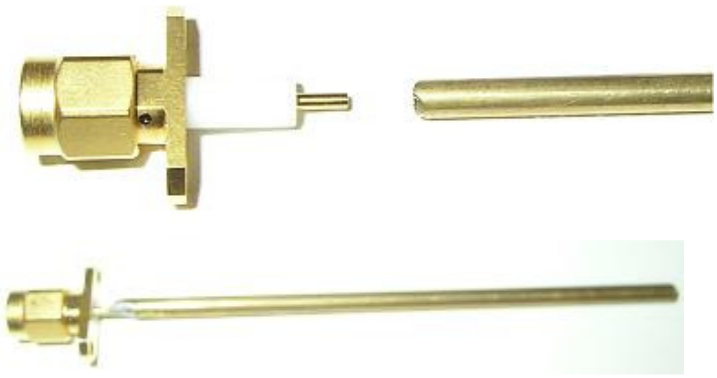

Fig. 4.22 Remaking of the monopole antennas using male SMA connectors.

In order to verify and ensure that the new antennas have the same performance and characteristics as the old ones, all 4 were measured, each separately, as a part of a single element monopole antenna. Reflection magnitude and phase are depicted and compared in Fig. 4.23. Both magnitude and phase of the new single monopoles corresponds well to the old antennas characteristics and levels. Phase for all of the four antennas is within 3.6º, and magnitude within 0.5 dB, at the center frequency.

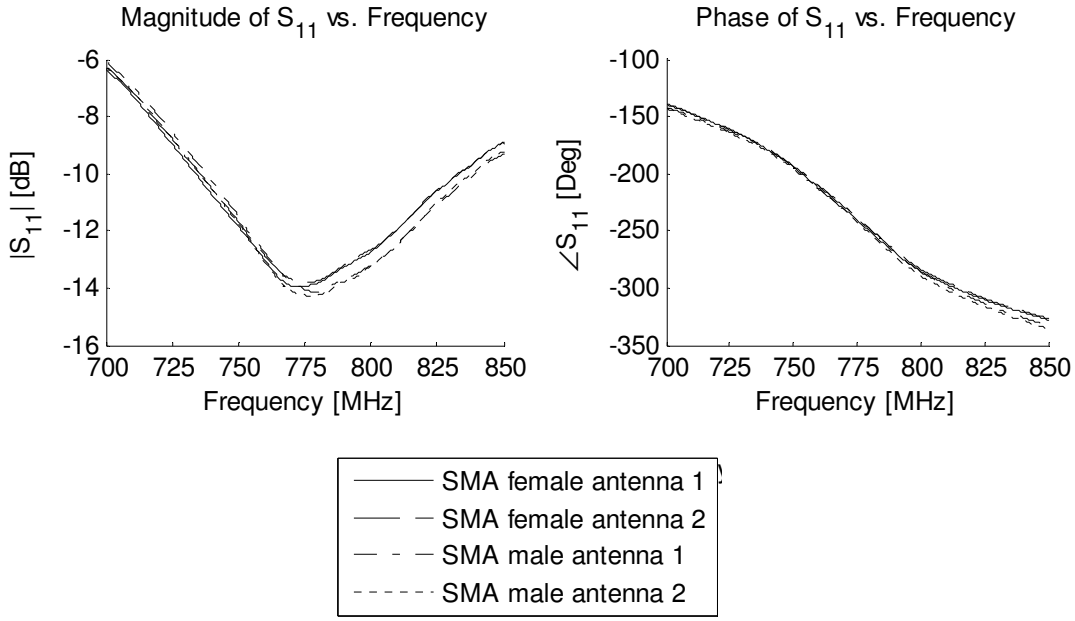

Fig. 4.23 Reflection magnitude and phase for the two antenna pairs, with two female and two male connectors.

4.3.2 Network verification

In this subchapter practical verification of the designed and manufactured compensation networks is presented. Measured reflection and coupling is compared to the designed performance in ADS and Momentum. The same procedure is applied for correlation and efficiency. This analysis is conducted without any consideration to losses due to losses not being accounted for during the design process in ADS and Momentum. Later, network efficiency, i.e. ohmic losses compared to the transferred power, is analyzed for each network and compared with the simulated values.

Network losses at port 1 are calculated using (4.1) and is defined as the power neither being reflected nor transmitted through the network.

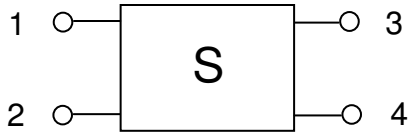

$$P_{loss} = 1 - \sum_{n=1}^{4} |S_{n1}|^2 \qquad (4.1)$$

In the end the performance of all the three networks is compared to one another by analyzing correlation and efficiency plots, both with and without the network efficiency included.

4.3.2.1 Network 1

The first network measured is the simple impedance transformer used for matching the input impedance of the 2-port to 50 Ω. A photo of the manufactured circuit is displayed in Fig. 4.24. Three, 3 mm in diameter, holes parallel to the x-axis are for drilled for equally many metallic screws and nuts. Despite the small physical size of the network, 30 mm x 30.25 mm, and four SMA connectors already keeping the two ground planes together, the screws are inserted in order to improve the mechanic stability. Furthermore their purpose is to short the two ground planes together in order to prevent the generation of spurious and parallel plate modes. The size of the ground plane is electrically large relative to the conducting strip, ensuring the electric field being confined entirely in the dielectric, and the mode propagated in the TEM mode.

Reflection and coupling are depicted in Fig. 4.25 and Fig. 4.26 respectively, and match the simulations in ADS and Momentum well. Same conclusions are drawn for antenna efficiency and envelope correlation, Fig. 4.27 and Fig. 4.28. Small differences can possibly be explained by the remade SMA connectors or/and not having a short piece of 50 Ω line at the antenna ports as well. Air pockets at the stripline-coaxial interface can lead to undesired mode excitations. Same thing applies for the lack of 50 Ω lines at the antenna ports.

A new quantity is introduced in this subchapter, *network efficiency*, being defined as 1- P_{loss} using (4.1) and is later used in 4.3.3 to adjust the antenna efficiency. Simulated and measured graphs are presented in Fig. 4.29. Losses are negligible and simulations and measurement correspond well to each other. Linear regression was used in order to fit the measured data due to a ripple in S_{31}, see appendix 0 for more details.

Fig. 4.24 Photo of the transmission lines in manufactured network 1. Antenna ports are on the upper side.

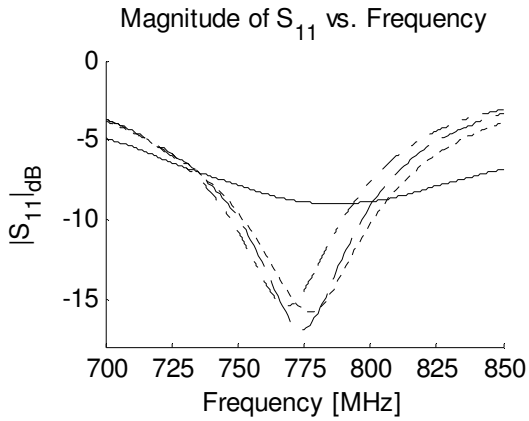

Fig. 4.25 Reflection with and without compensating network.

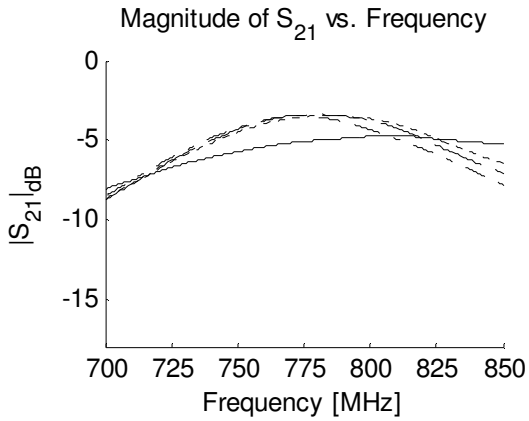

Fig. 4.26 Coupling with and without compensating network.

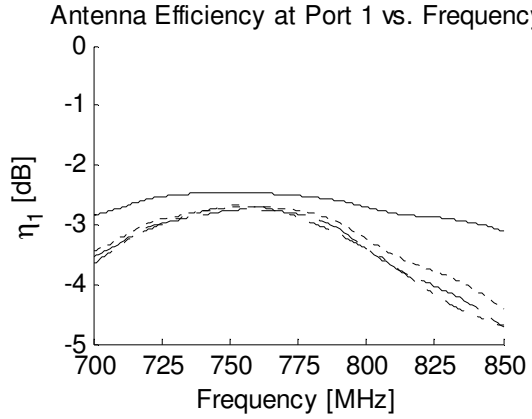

Fig. 4.27 Antenna efficiency at port 1 with and without compensating network.

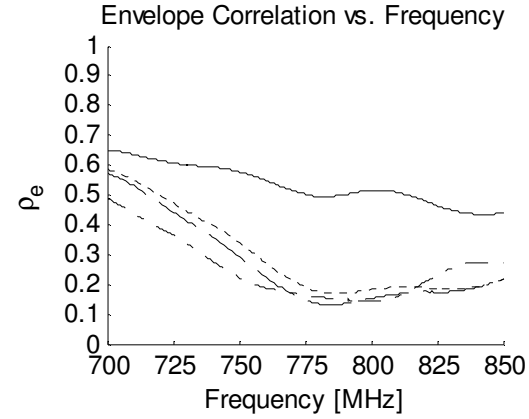

Fig. 4.28 Envelope correlation with and without compensating network.

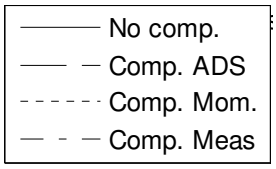

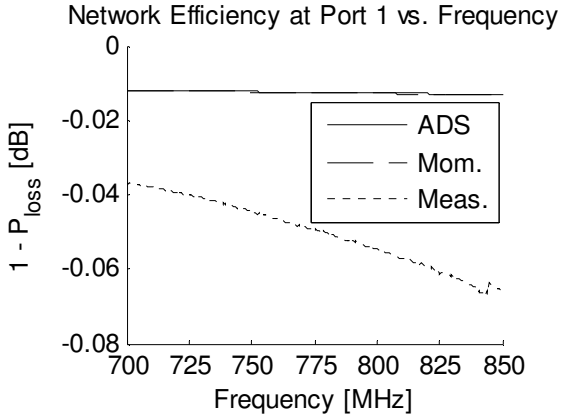

Fig. 4.29 Measured and simulated network efficiency.

4.3.2.2 Network 2

The second network is a combination of two impedance transformers and a pair of coupled lines, matching for both reflection and coupling at the same time. Metallic screws and nuts are inserted in this case as well, three on each side of the y-axis, see Fig. 4.30.

Fig. 4.31 and Fig. 4.32 show reflection and coupling with and without the compensating networks. Measured characteristics match the designed performance very well. The same is true for the antenna efficiency and envelope correlation, Fig. 4.33 and Fig. 4.34. Of all the three networks, performance of this network deviates the least compared to the simulations. This is believed to be a result of having 50 Ω lines at each port of the four-port.

Network efficiency is depicted in Fig. 4.35. Simulations and measurement differ around 0.1 dB on average over the measured frequency range. Linear regression was applied here also due to ripples in all of the transmission coefficients, see appendix 0 for more details.

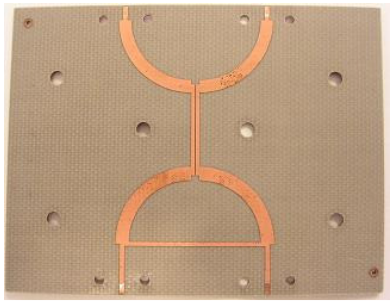

Fig. 4.30 Photo of the transmission lines in manufactured network 2. Antenna ports are on the upper side.

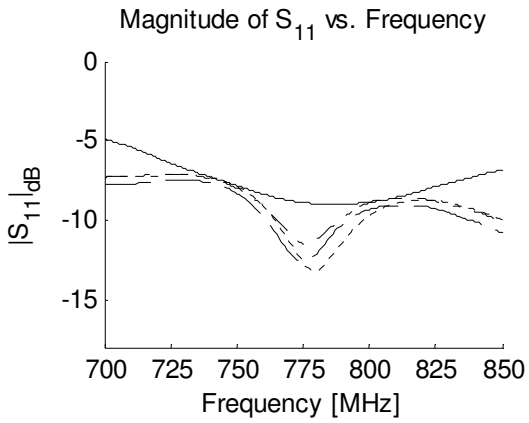

Fig. 4.31 Reflection with and without compensating network.

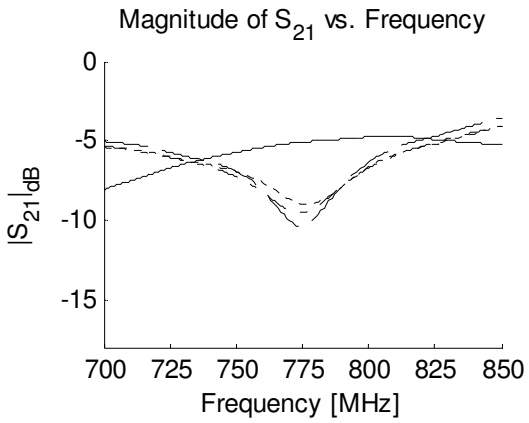

Fig. 4.32 Coupling with and without compensating network.

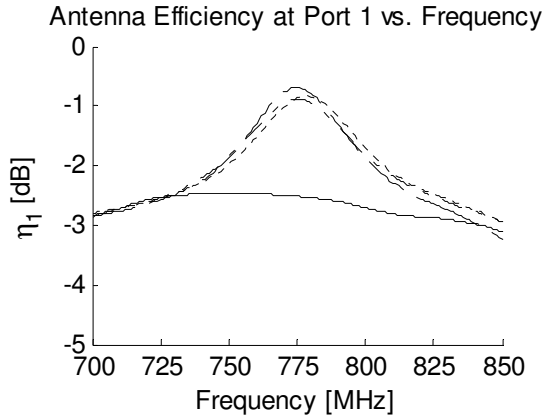

Fig. 4.33 Antenna efficiency at port 1 with and without compensating network.

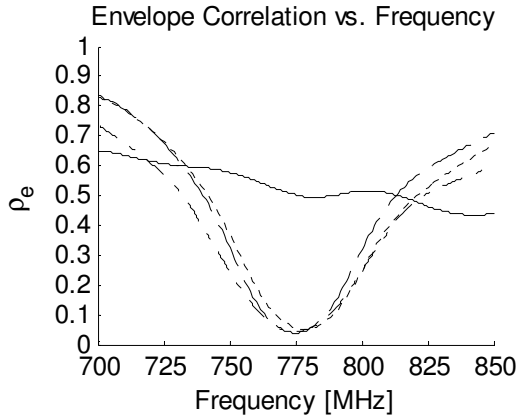

Fig. 4.34 Envelope correlation with and without compensating network.

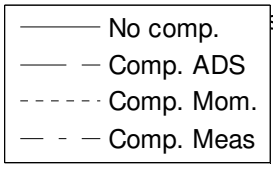

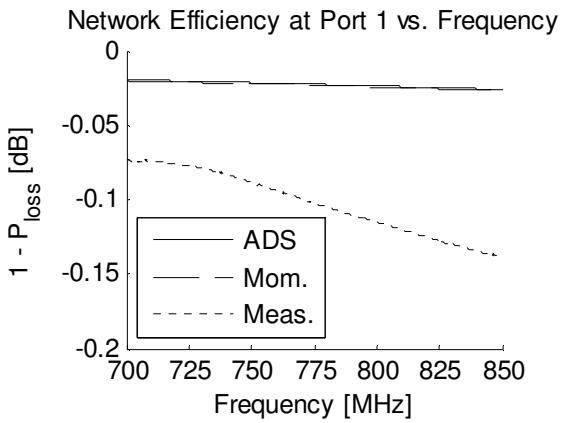

Fig. 4.35 Simulated and measured network efficiency.

4.3.2.3 Network 3

The last network presented is an impedance transformer followed by a hybrid coupler, allowing matching for both reflection and coupling with six degrees of freedom. For this layout ten metallic screws were used, see Fig. 4.36.

Reflection and coupling are displayed in Fig. 4.37 and Fig. 4.38, and antenna efficiency and envelope correlation in Fig. 4.39 and Fig. 4.40. All four quantities match designed characteristics well, with double resonance for larger bandwidth.

Measured network efficiency, Fig. 4.41, differs 0.31 – 0.55 dB compared to the simulations over the desired frequency band. This is believed to be a result of not using proper SMA connectors leading to air-pockets, or/and not enough amount of metallic screws, leading to air-pockets as well and therefore generation of parallel plate modes.

Fig. 4.36 Photo of the transmission lines in manufactured network 3. Antenna ports are to the right.

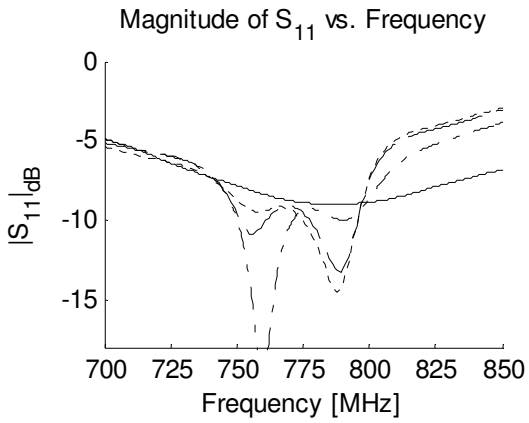

Fig. 4.37 Reflection with and without compensating network.

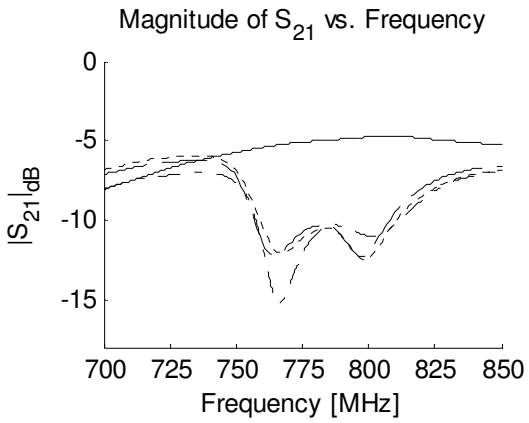

Fig. 4.38 Coupling with and without compensating network.

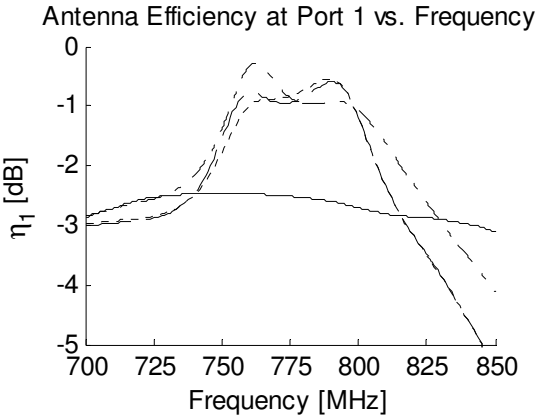

Fig. 4.39 Antenna efficiency at port 1 with and without compensating network.

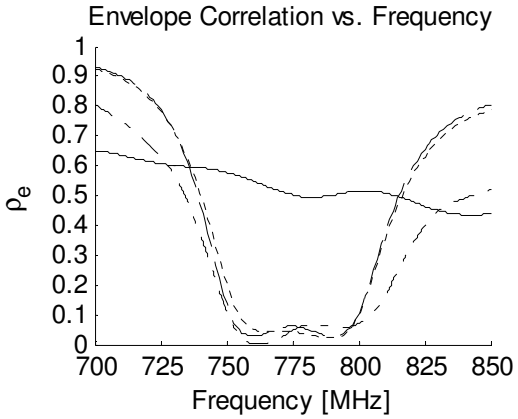

Fig. 4.40 Envelope correlation with and without compensating network.

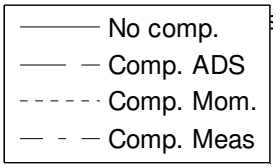

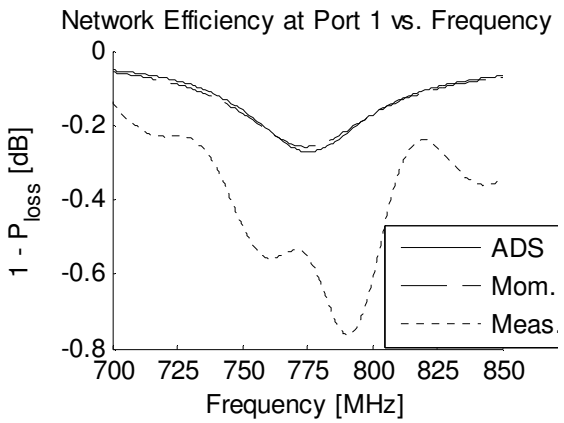

Fig. 4.41 Simulated and measured network efficiency.

4.3.3 Summary

Relevant measurement results are presented in this subsection. Figures of merit for 750, 775 and 800 MHz are summarized in Table 4-6.

Antenna efficiency is depicted in Fig. 4.42. Network 1 has clearly lowest efficiency, lower than without the network, ranging between -2.68 and -3.40 dB at 750 to 800 MHz. Networks 2 and 3 have approximately the same efficiency at center frequency, -0.86 dB, while network 3 has a larger bandwidth having better than -1.36 dB in the desired frequency band. Corresponding value for network 2 is -1.84 dB.

Fig. 4.43 shows the envelope correlation. All three networks fulfill the criteria of being bellow 0.3.

Overall, considering antenna efficiency and envelope correlation network 3 has the best performance. If size matters, then network 2 might be the best choice, which has the same mean efficiency as network 3 but slightly larger envelope correlation.

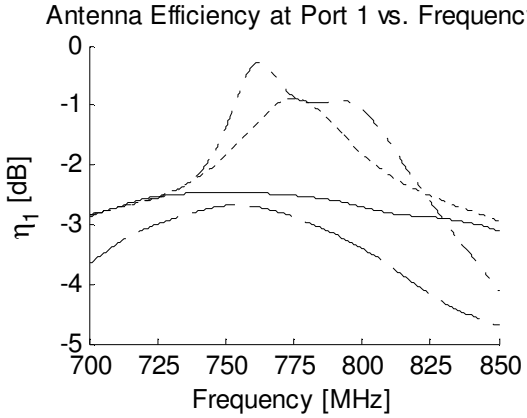

Fig. 4.42 Measured antenna efficiency with and without the compensating networks.

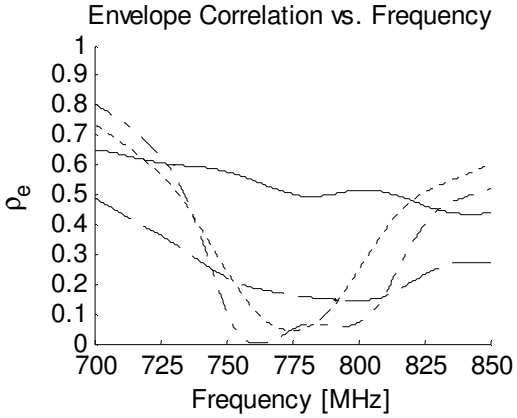

Fig. 4.43 Measured envelope correlation with and without the compensating networks.

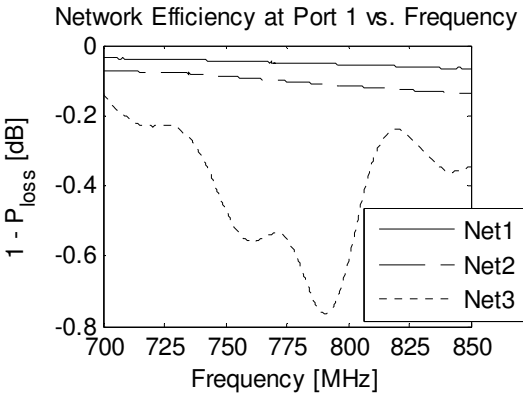

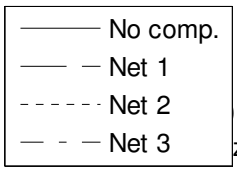

Fig. 4.44 Measured network efficiency for the compensating networks.

Summary	f [MHz]	No net	Net 1	Net 2	Net 3
Reflection					
[dB]	750	-7.8	-10.8	-8.0	-10.1
	775	-8.9	-14.5	-11.5	-9.4
	800	-8.9	-7.6	-8.9	-8.6
Mean	**750-800**	**-8.5**	**-11.0**	**-9.45**	**-9.3**
Coupling					
[dB]	750	-5.7	-4.2	-7.3	-7.7
	775	-5.1	-3.5	-9.6	-12.1
	800	-4.8	-4.3	-6.7	-11.0
Mean	**750-800**	**-5.2**	**-4.0**	**-7.85**	**-10.3**
Ant. Efficiency					
[dB]	750	-2.5	-2.7	-1.9	-1.8
	775	-2.5	-2.9	-1.0	-1.4
	800	-2.7	-3.5	-1.9	-1.7
Mean	**750-800**	**-2.6**	**-3.0**	**-1.6**	**-1.6**
Env. Corr.					
	750	0.58	0.22	0.24	0.11
	775	0.50	0.16	0.04	0.05
	800	0.51	0.15	0.25	0.07
Mean	**750-800**	**0.53**	**0.18**	**0.18**	**0.08**

Table 4-6. Measured quantities based on scattering parameters with and without network for 750, 775 and 800 MHz.

5 Performance

Antenna efficiency, diversity gain, complex correlation and ergodic Shannon capacity were measured in a reverberation chamber (1.93 x 2 x 1.39 m^2) from Bluetest, which simulates a uniform multipath environment. Radiation patterns were measured in a Stargate 64 anechoic chamber from Satimo at Sony Ericsson Mobile Communications in Lund. The results are presented together with the simulated values obtained from the HFSS simulations of the antenna array and the 4-port network S-parameters from ADS.

5.1 Radiation pattern

Embedded far-field patterns for the antennas with a network can be calculated from the S-parameters for the 4-port network and the antenna array and the embedded far-field patterns for the antenna array. If the generators are connected to port 1 and port 2 and the antennas are connected to port 3 and port 4, then the new far-field patterns are given by the following expression [20]

$$\mathbf{F} = \mathbf{F_0}(\mathbf{I} - \mathbf{S_{aa}}\mathbf{S}^A)^{-1}\mathbf{S_{ag}} \tag{5.1}$$

where $\mathbf{F_0}$ contains the far-field patterns without a network, $\mathbf{S}^A$ is the scattering matrix for the antenna array, $\mathbf{S_{aa}} = \begin{bmatrix} S_{33} & S_{34} \\ S_{43} & S_{44} \end{bmatrix}$, $\mathbf{S}_{ag} = \begin{bmatrix} S_{11} & S_{12} \\ S_{21} & S_{22} \end{bmatrix}$ and $\mathbf{I}$ is the identity matrix.

Radiation patterns for antenna 1 at the center frequency are given in Fig. 5.1 to Fig. 5.3. In Fig. 5.1 with network 1 the pattern is still very similar to the case without a network. Due to the network being a simple impedance transformer this comes as no surprise. The biggest difference is that the antennas are less omnidirectional in the ϕ-planes. With network 2 connected, see Fig. 5.2, the pattern is significantly more directive and most of the power from antenna 1 is radiated through the left half of the upper hemisphere. The maximum realized gain is about 5 dBi. Recalling that the second antenna's radiation pattern is mirrored about the yz-plane, it is evident that the overlap between the patterns has been reduced. For the third network in Fig. 5.3 it is not as clear that the correlation is significantly lower, and the low correlation is presumably a result of the phase difference between the antenna patterns.

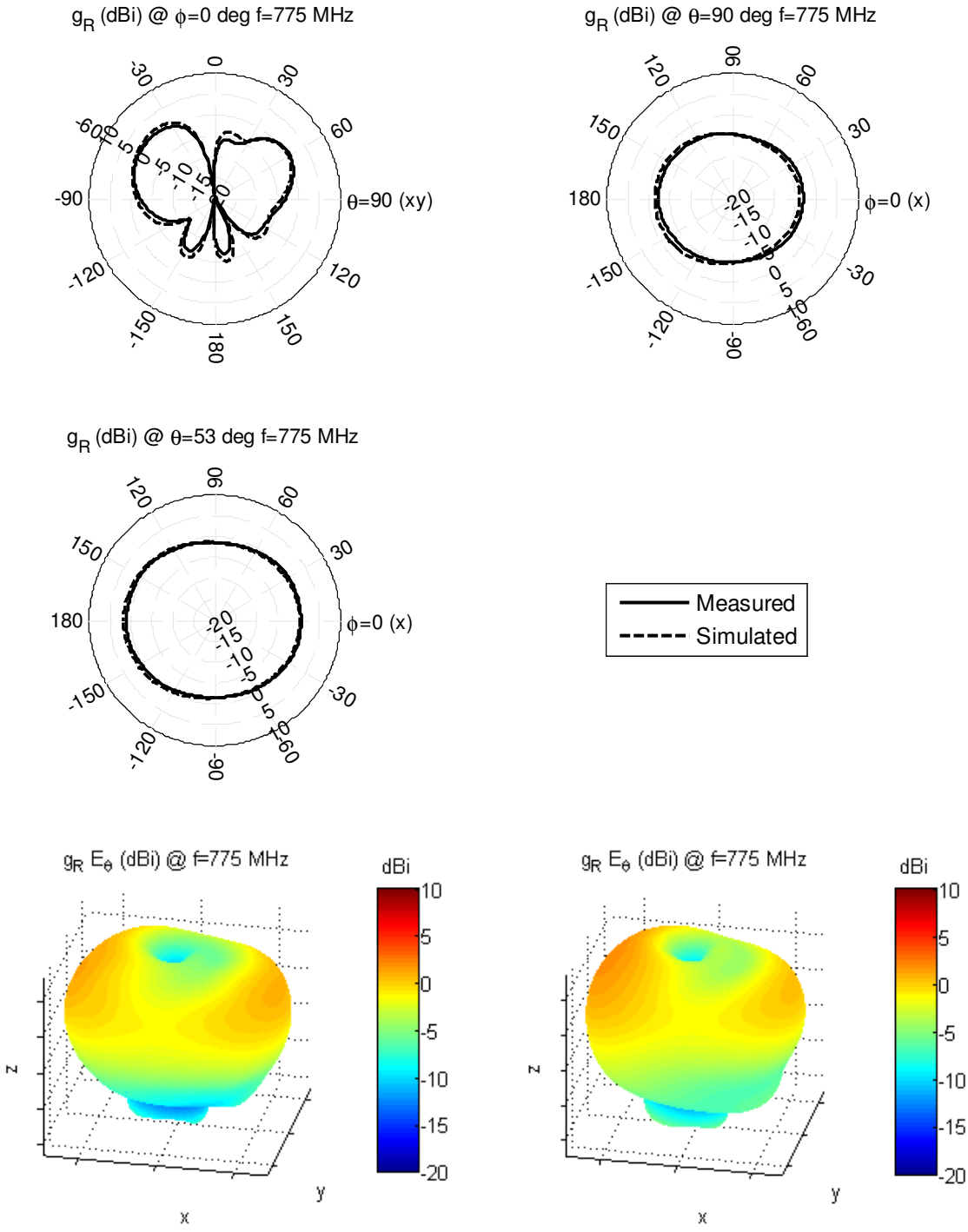

Fig. 5.1 Radiation patterns in partial realized gain for antenna 1 with network 1. The cross-section in $\theta = 53°$ contains the direction of maximum directivity.

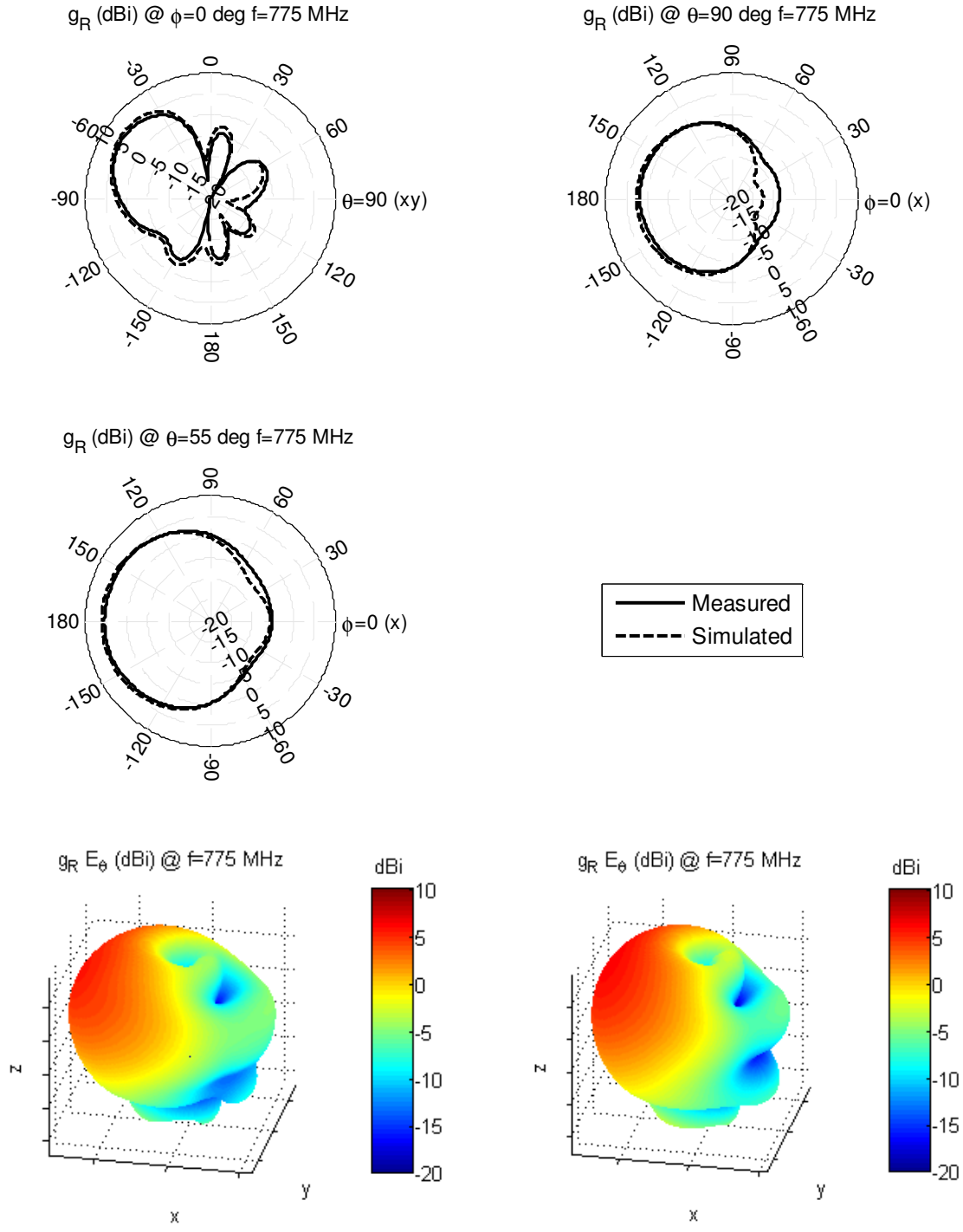

Fig. 5.2 Radiation patterns in partial realized gain for antenna 1 with network 2. The cross-section $\theta = 55$ contains the direction of maximum directivity.

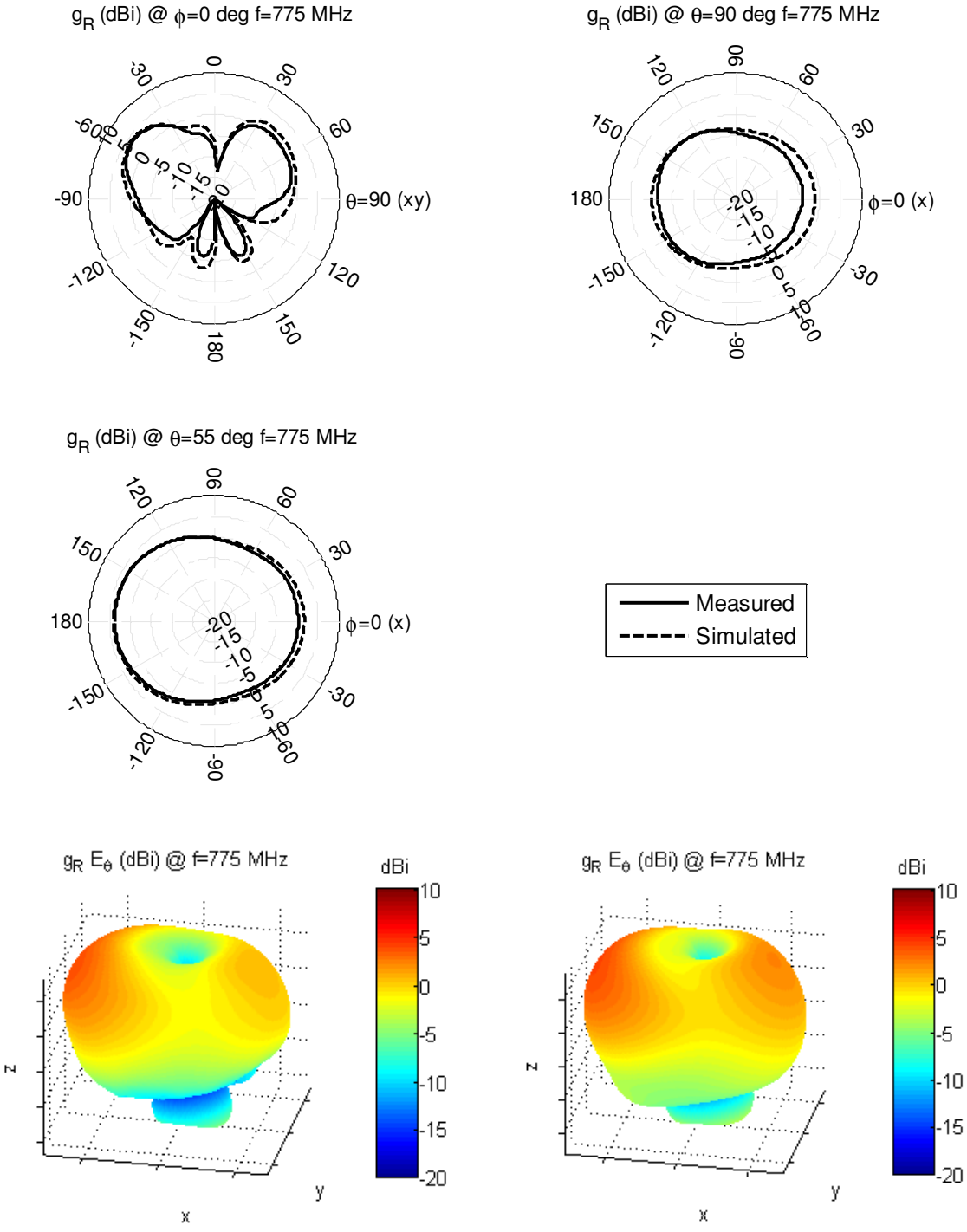

Fig. 5.3. Radiation patterns in partial realized gain for antenna 1 with network 3. The cross-section $\theta = 55$ contains the direction of maximum directivity.

5.2 Antenna efficiency

Efficiency measurements were done in a reverberation chamber from 750 MHz to 800 MHz and performed in 1 MHz steps. The accuracy of the measurement is improved by using frequency averaging, i.e., the efficiency at every frequency point is calculated by averaging over a range of neighboring frequencies. A total of 11 frequency points were used for each frequency. The theoretical efficiency was calculated from the realized embedded radiation patterns obtained with (5.1). In both cases the ohmic losses are included.

Measurements and simulations for the four cases are shown in Fig. 5.4. The measured efficiencies vary a lot more than the calculated efficiencies. This indicates that there is a lot of uncertainty in the measurements. One possible explanation is that the antenna is too large relative to the size of the chamber. Another reason could be that there are too few independent samples for every frequency point. The measured efficiency is, on average, slightly higher. Mean efficiencies are given in Table 5-1.

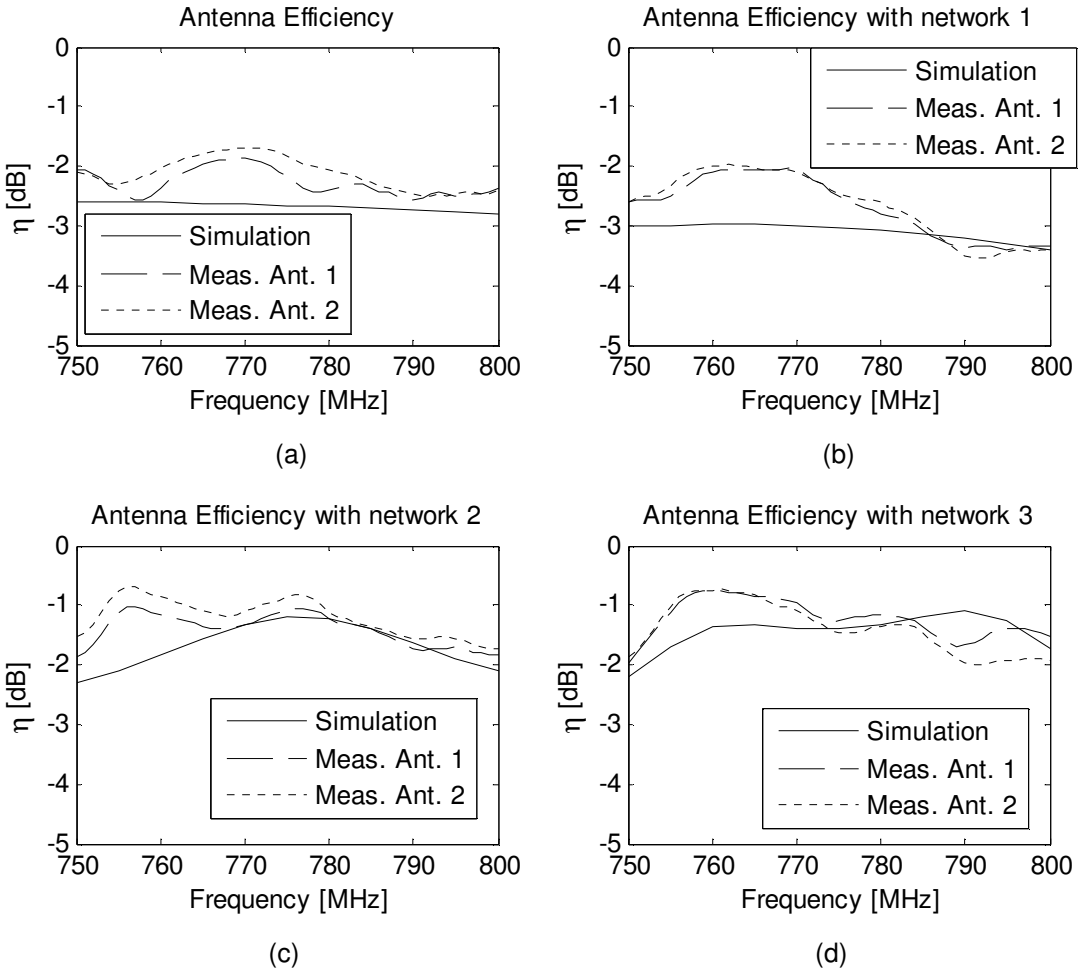

Fig. 5.4. Antenna efficiency for the antennas without a network in (a) and with (b) network 1, (c) network 2 and (d) network 3.

Mean efficiency [dB]	No network	Network 1	Network 2	Network 3
Simulated	-2.7	-3.1	-1.7	-1.4
Measured	-2.2	-2.6	-1.3	-1.3

Table 5-1 Mean efficiencies in the 750 MHz to 800 MHz band.

5.3 Correlation

The simulated correlation was calculated from the simulated far-field patterns with (2.15). When using the radiation patterns, ohmic losses are correctly accounted for, which is not the case when using S-parameters, although for small losses both methods will give similar values.

The envelope correlation between the measured voltages on the antenna ports and the simulated correlation for the four cases are given in Table 5-2 below. The agreement between measurement and simulation is very good for all cases except for network 3, where the measured envelope correlation is about 67 % higher, but it should be kept in mind that for low correlations the uncertainty is higher.

Envelope correlation	No network	Network 1	Network 2	Network 3
Simulated	0.58	0.25	0.19	0.12
Measured	0.59	0.23	0.23	0.20

Table 5-2 Mean envelope correlation in the 750 MHz to 800 MHz band.

5.4 Shannon capacity

The ergodic Shannon capacity in a simulated uniform Rayleigh fading environment was computed for the 2×2 MIMO system with uncorrelated transmitting antennas that use water filling, with and without a compensation network. Every receiving antenna was illuminated with independent rays, whose real and imaginary components have a Gaussian distribution and the angle of arrivals (AOA) are uniformly distributed. The channel matrix is equal to

$$\mathbf{H} = \begin{bmatrix} h_{11} & h_{12} \\ h_{21} & h_{22} \end{bmatrix} \tag{5.2}$$

where h_{mn} is the complex channel transfer function from antenna port m to n. Both the complex gain for the uniform Rayleigh fading channel and the embedded far-field pattern from the receiving antenna are included in the channel transfer function. The channel transfer function between two antennas is found by coherently adding the total complex gains for every ray, i.e.,

$$h_{mn} = \sum_{k=1}^{N_r} F_n(\hat{\mathbf{r}}_\mathbf{k}) a_{m,k} \tag{5.3}$$

where $a_{m,k}$ is the gain for ray k from antenna m , $F_n(\hat{\mathbf{r}}_\mathbf{k})$ is the realized embedded far-field at the arrival angle defined by $\hat{\mathbf{r}}_\mathbf{k}$ and N_r is the number of rays.

The channel is normalized such that $N_r \cdot E\left[a_{m,k} a_{m,k}^*\right] = 1$, where E is the expectation operator. The capacity for 10 000 different realizations of the channel with 20 rays was calculated according to (2.9). The ergodic capacity is found by averaging over all realizations. Because the capacity varies with frequency a more fair measure is obtained if the capacity is averaged over the frequency band of interest.

In Fig. 5.5 the simulated Shannon capacity is plotted vs. the SNR. There is clearly an improvement in the capacity when a network is used, although for network 1 the improvement is very small. Capacities at 20 dB SNR are given in Table 5-3. The improvement in capacity at 20 dB for network 3 is 17 %.

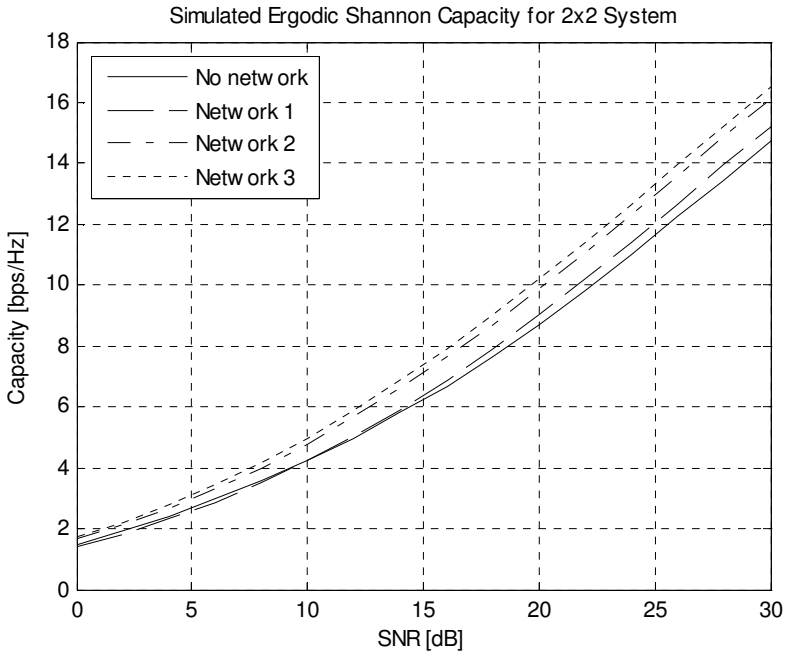

Fig. 5.5. Simulated ergodic Shannon capacity for the 2x2 system that uses water filling. The capacity is averaged for frequencies from 750 MHz to 800 MHZ, with 5 MHz spacing.

Shannon Capacity (bits/s/Hz)	**No network**	**Network 1**	**Network 2**	**Network 3**
Simulated (2 x 2)	8.7	9.0	9.9	10.2

Table 5-3 Mean Shannon capacity with water filling at 20 dB SNR.

5.5 Diversity

Diversity measurements for the antenna array with and without networks have been simulated and measured in the reverberation chamber.

The simulations were done with one transmit antenna and two receiving antennas in a uniform 3D Rayleigh fading channel. 10 000 different realizations of the channel with 20 rays were used together with the embedded far-field patterns. The power at receiving antenna n is calculated as

$$P_r = \left| \sum_{k=1}^{N_r} F_n(\hat{\mathbf{r}}_\mathbf{k}) \cdot a_k \right|^2 \tag{5.4}$$

Fig. 5.6 to Fig. 5.8 show the CDF of the received power for the antenna array with the different networks. For comparison, the case without a network is also shown in every figure. The received powers have been averaged over the frequency band (750 MHz – 800 MHz). Only MRC is used in the combining of the signals. In the case without a network the measured received power is slightly higher, both for the single branches and for the combined signals. This is due to the measured efficiency being slightly higher than the simulated efficiency. With MRC it can be seen that the diversity gain is higher when a network is connected to the antenna ports. Network 2 and network 3 gives the highest diversity gain improvements, while for network 1 the improvement is very small. Opposite to the case without a network, the simulations now give higher received powers. Most likely this is because the correlation between the simulated antenna ports is lower than the correlation between the measured ports. Effective diversity gains at 1% level are given in Table 5-4. The maximum improvement in diversity gain for simulations and measurements are 2.7 dB with network 3 and 1.3 dB with network 2, respectively.

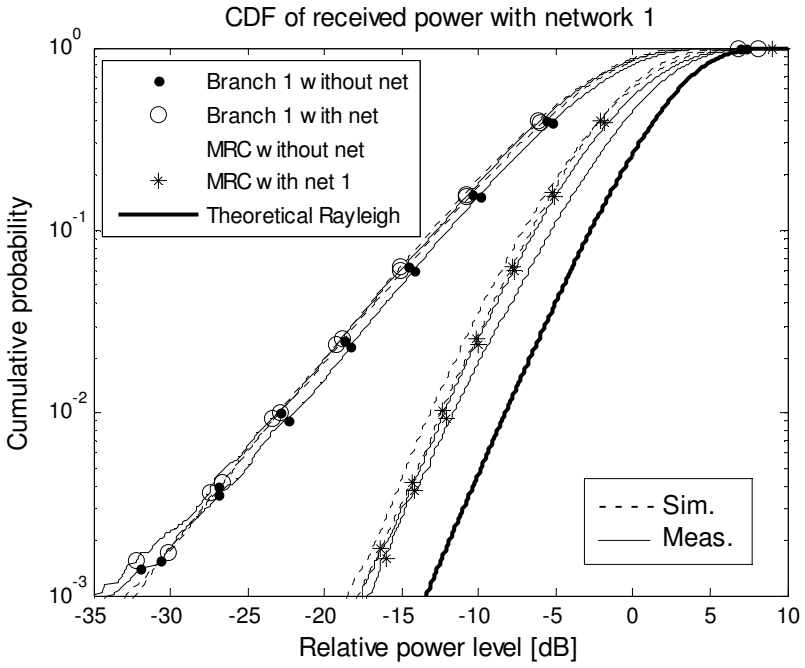

Fig. 5.6. CDF of received power with network 1 at 750 – 800 MHz. The solid lines are measurements, the dashed lines are simulations and the solid bold line corresponds to two uncorrelated ideal omnidirectional antennas with MRC in a Rayleigh channel.

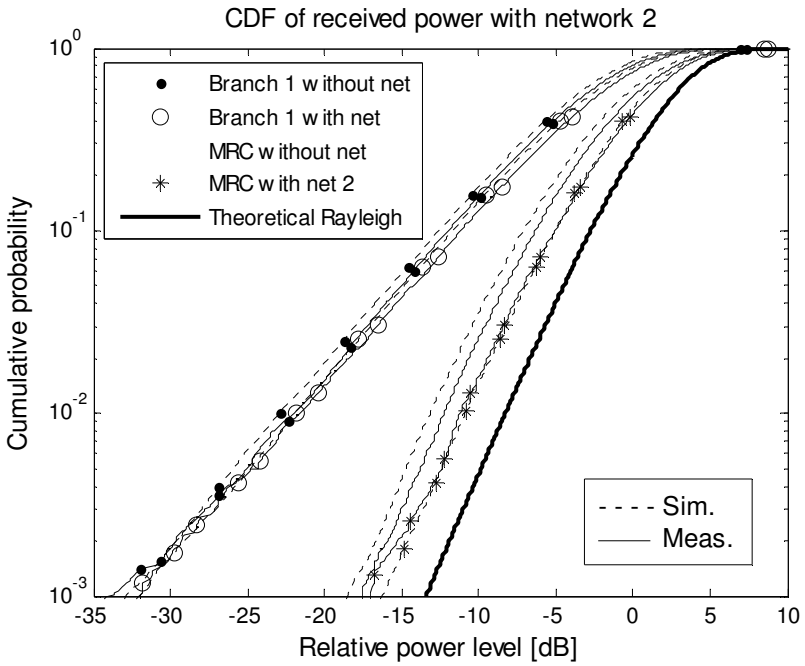

Fig. 5.7. CDF of received power with network 2 at 750 – 800 MHz. The solid lines are measurements, the dashed lines are simulations and the solid bold line corresponds to two uncorrelated ideal omnidirectional antennas with MRC in a Rayleigh channel.

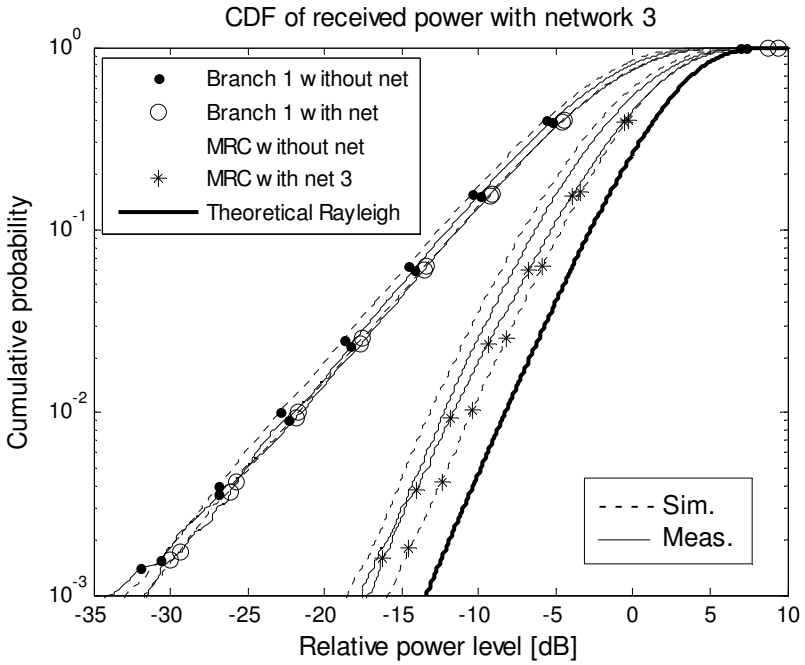

Fig. 5.8. CDF of received power with network 3 at 750 – 800 MHz. The solid lines are measurements, the dashed lines are simulations and the solid bold line corresponds to two uncorrelated ideal omnidirectional antennas with MRC in a Rayleigh channel.

Effective diversity gain at 1% (dB)	No network	Network 1	Network 2	Network 3
Simulated	7.1	7.8	9.4	9.8
Measured	7.7	8.1	9.0	8.5

Table 5-4 Mean effective diversity gain at 1% level with MRC.

5.6 Summary and conclusion

The measurements confirmed that the compensating networks increase the efficiency and decrease the correlation. It was also shown that the Shannon capacity and diversity gain are increased. Even though measurements and simulations were not always in perfect agreement, it is very clear that a performance improvement is obtained with the compensating networks. Mean values over frequency of the performance metrics are summarized in Table 5-5. The measured and simulated efficiency is improved with 0.95 dB and 1.25 dB, respectively. The envelope correlation is reduced from 0.59 to 0.20 and 0.59 to 0.12 for the measurements and simulations, respectively. The simulated Shannon capacity was increased with 17 %. In the simulations the maximum improvement in diversity gain was 2.7 dB. The results from the diversity measurement are surprising and somewhat confusing. Even though the correlation and efficiency for network 3 are better than for network 2, the diversity gain is lower. Any good explanation for this cannot be found. It may be a statistical anomaly or a measurement error.

Mean values	No network		Network 1		Network 2		Network 3	
	Sim.	Meas.	Sim.	Meas.	Sim.	Meas.	Sim.	Meas.
Efficiency (dB)	-2.7	-2.2	-3.1	-2.6	-1.7	-1.3	-1.4	-1.3
Envelope correlation	0.58	0.59	0.25	0.23	0.19	0.23	0.12	0.20
Shannon Capacity at 20 dB SNR (bits/s/Hz)	8.7	-	9.0	-	9.9	-	10.2	-
Effective MRC diversity gain at 1% (dB)	7.1	7.7	7.8	8.1	9.4	9.0	9.8	8.5

Table 5-5 Mean values over 750 MHz to 800 MHz of the performance metrics. Simulations are based on radiation patterns and measurements are performed in a reverberation chamber.

6 Dual-antenna mock-up

A more realistic case is being presented in this chapter. MIMO system for a possible real sized mobile telephone is designed and evaluated. First step consists of only antenna design where two different antenna types are analyzed. After the desired antenna type is selected and optimized in HFSS, the compensating network is designed using ADS. The entire setup, including both the antenna and the compensating network, is then evaluated in Ansoft HFSS. Furthermore the size of the setup versus the performance is analyzed and a possible solution example is presented.

6.1 Antenna design and optimization

6.1.1 Printed meander monopole antenna

A microstrip line fed meandered monopole antenna is the first solution for the dual-antenna mobile phone examined. Antenna characteristics and design considerations for a single antenna can be found in [21] and [22]. These articles are used when designing the symmetrical antenna array. The geometry of the antenna is shown in Fig. 6.1. Two meandered lines, which are fed with 50 ohm microstrip lines, are printed on a 0.8 mm thick Neltec 9300 substrate, see Fig. 6.1. The ground plane is removed on the opposite side of the substrate where the antennas are located, see dashed lines in Fig. 6.1. For simplicity the spacing between the microstrip lines is equal to the strip width *w*. An advantage with this antenna is the small physical size, which is a result of bending the lines. The total length of the antenna is still larger than a quarter wavelength, due to the corner effect of the meandered line [21].

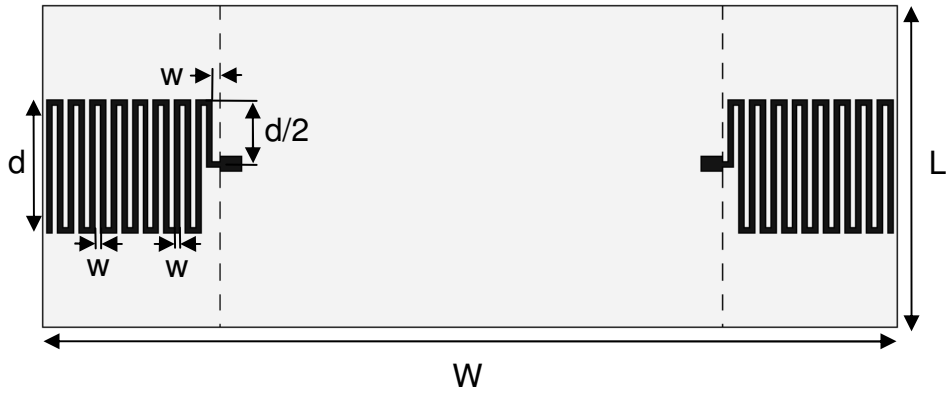

w = 0.75 mm
d = 18.8 mm
W = 125 mm
L = 45 mm

Fig. 6.1 Geometry of the meandered monopole antennas. The ground on the back of the substrate is marked with dashed lines.

6.1.1.1 Optimization for maximum return loss

In order to obtain maximum return loss at the center frequency the length d and width w of the antennas are tuned. The size of the substrate is fixed to *120 x 45 mm*^{2}. Calculated reflection and coupling are shown in Fig. 6.2. The antenna array is well matched: reflection is lower than -10.7 dB for the frequency band of interest (18.2 dB at center frequency). Coupling on the other hand is very high, higher in the range of -2.1 to -1.7 dB for the entire band and -1.7 dB at the center frequency. Antenna efficiency is depicted in Fig. 6.3. Even though the return loss is maximized at the center frequency, the impact of the coupling is dominating and the efficiency is very poor, lower than -4.6 dB for the entire frequency band and -5.2 dB at 775 MHz. The envelope correlation, Fig. 6.4, is higher than 0.5 bellow 760 MHz.

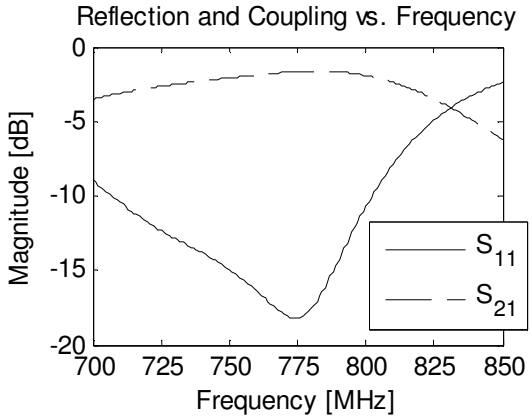

Fig. 6.2 Simulated reflection and coupling for the meandered antenna array, optimized for maximum return loss.

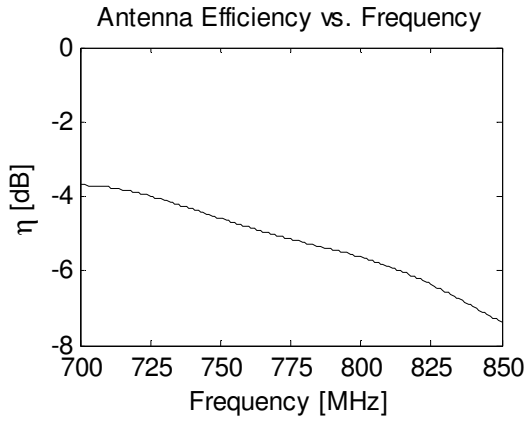

Fig. 6.3 Simulated antenna efficiency at port one and port two for the meandered antenna array, optimized for maximum return loss.

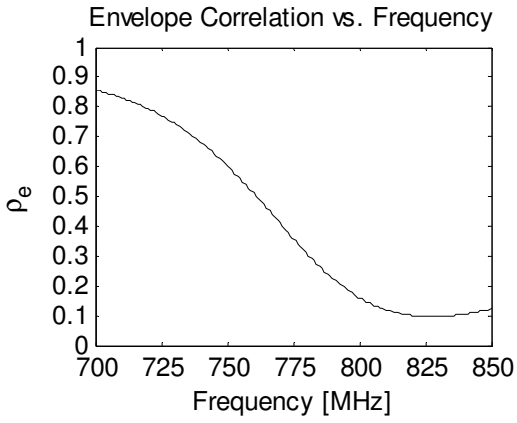

Fig. 6.4 Simulated envelope correlation for the meandered antenna array, optimized for maximum return loss.

6.1.1.2 Optimization for maximum antenna efficiency

In order to achieve maximum antenna efficiency at the center frequency the length of the line d is decreased. It is impossible to maximize return loss and minimize coupling at the same time, Fig. 6.5. Coupling is lower than -3.2 dB for the desired frequency band, -4.0 dB at 775 MHz, and reflection is lower than -5.7 dB for the same band, -8.3 dB at 775 MHz. Thus some compromise had to be made. A drawback of a higher efficiency is higher correlation, depicted in Fig. 6.6 and Fig. 6.7 respectively. Antenna efficiency is higher than -3.7 dB at 750 – 800 MHz, -3.4 dB at the center frequency. Envelope correlation is lower than 0.89 for frequencies higher than 750 MHz, 0.86 at 775 MHz.

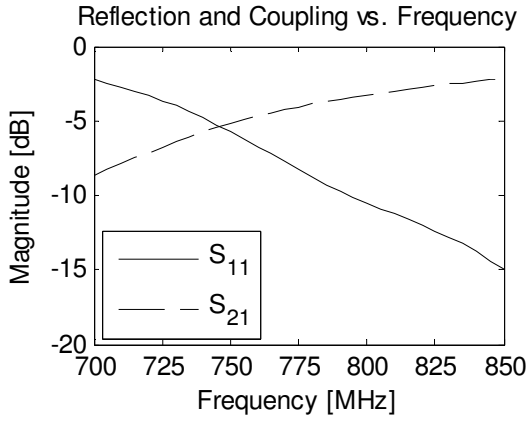

Fig. 6.5 Simulated reflection and coupling for the meandered antenna array, optimized for maximum antenna efficiency.

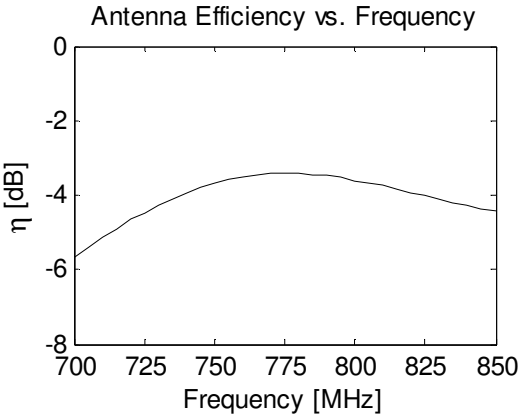

Fig. 6.6 Simulated antenna efficiency at port one and port two for the meandered antenna array, optimized for maximum antenna efficiency.

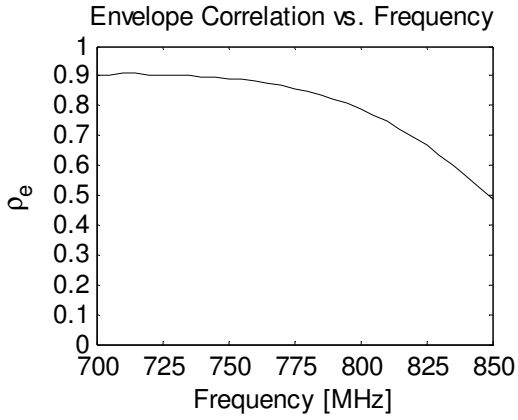

Fig. 6.7 Simulated envelope correlation for the meandered antenna array, optimized for maximum antenna efficiency.

6.1.1.3 Summary and Conclusion

All four figures of merit for the design and optimization of the meandered antenna array are presented in Table 6-1. When optimizing for either high return loss or high antenna efficiency the performance is not satisfactory.

In the first case high return loss and low envelope correlation are countered by very high coupling and very low antenna efficiency.

In the second case, by sacrificing return loss in order to decrease coupling, mean antenna efficiency over the frequency band is increased by 1.6 dB to -3.5 dB, which is still unacceptable. At the same time mean envelope correlation is increased from 0.37 to 0.85.

Furthermore, if considerations about a compensating network are taken into account the analyzed meander antenna becomes even less suitable as a possible mobile phone solution. If the compensating network is to be placed on the same card as the antennas there is an area of *71 x 45 mm*^{2} between the antenna ports where the network can be located, see Fig. 6.1, between the dashed lines. Considering that the frequency band of interest is 750 – 800 MHz and the work presented in chapter 4, one can easily conclude that a suitable network almost certainly will not fit into that small area.

Taking into account the low antenna efficiency of the antennas and a goal to achieve efficiency higher than -2 dB, a network resulting in a second order resonance is probably needed. Such a network would need to have several degrees of freedom during the optimization process and lengths up to a quarter-wavelength are to be expected.

For these reasons the meandered antenna array is discarded as the antenna solution for the intended MIMO system.

Summary	f [MHz]	Meander: RL Opt	Meander: η Opt.
Reflection			
[dB]	750	-14.9	-5.7
	775	-18.2	-8.3
	800	-10.7	-10.5
Mean	**750-800**	**-15.8**	**-8.2**
Coupling			
[dB]	750	-2.1	-5.2
	775	-1.7	-4.0
	800	-1.9	-3.2
Mean	**750-800**	**-1.8**	**-4.1**
Ant. Efficiency			
[dB]	750	-4.6	-3.7
	775	-5.2	-3.4
	800	-5.6	-3.6
Mean	**750-800**	**-5.1**	**-3.5**
Env. Corr.			
	750	0.60	0.89
	775	0.36	0.86
	800	0.16	0.79
Mean	**750-800**	**0.37**	**0.85**

Table 6-1 Simulated reflection, coupling, antenna efficiency and envelope correlation based on scattering parameters for both optimized return loss and antenna efficiency for 750 – 800 MHz.

6.1.2 Printed monopole slot antenna

In this section another approach is applied, and two printed monopole slot antennas, proposed in [23] are used. The geometry of the antenna is depicted in Fig. 6.8. A ground plane is printed on a 0.8 mm thick Neltec 9300 substrate, see Fig. 6.8, with dimensions of a modern mobile phone. An L-shaped slot is placed to the left and to the right on the same ground plane. Both antennas are fed with 50 Ω microstrip lines which are placed on the back of the substrate. The antenna was chosen primarily due to its small size, but also due to its simple structure. The small size increases the distance between the antennas, resulting in lower antenna coupling, and gives more space to the microstrip compensation network which is to be printed on the back of the same substrate.

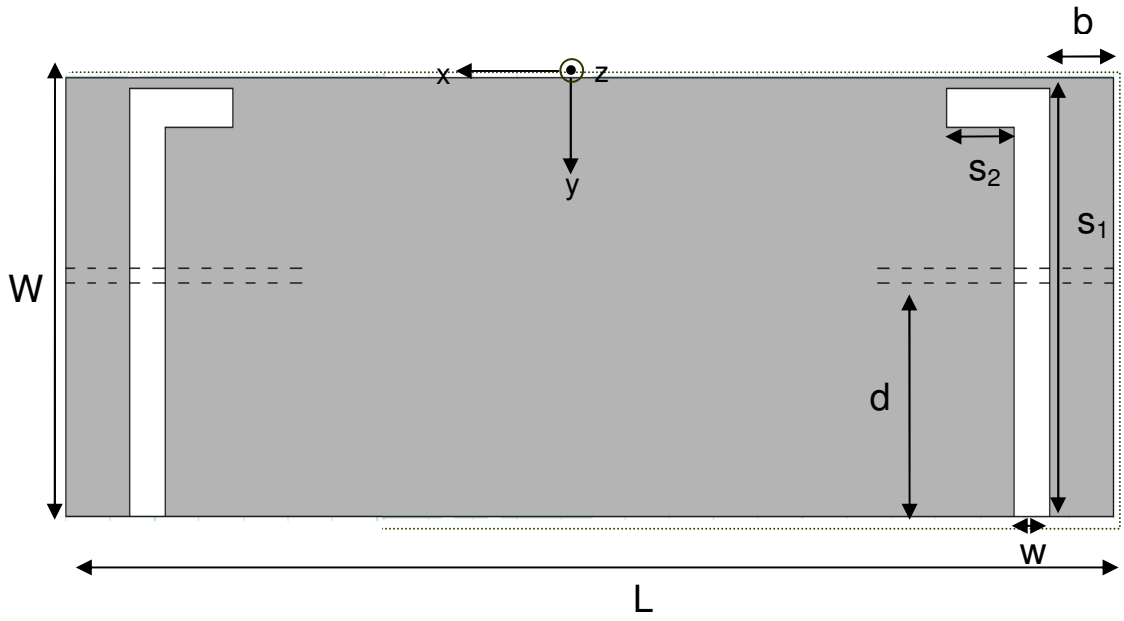

Fig. 6.8 Geometry of the two printed monopole slot antennas placed in a Cartesian coordinate system. The dashed lines are printed 50 ohm microstrip lines for excitation of the antennas.

The resonant frequency of the antenna can be adjusted by changing the total slot length, $s_1 + s_2$. Due to the presence of the substrate, where the waves are propagating, the length of the slot is shorter than one quarter of a free space wavelength [23]. The slot width w, the length of the top ground portion b and the conductor location d has large effects on the impedance matching for the single antenna [20]. Larger bandwidth and a slightly lower resonant frequency are usually obtained when the length of the top ground portion is increased. Increasing the width w can slightly increase the bandwidth. The conductor location d has a large effect on the bandwidth and a small effect on the resonant frequency. Choosing a proper length d is important in order to achieve a great bandwidth.

The antenna parameters were tuned to get either maximum return loss or maximum antenna efficiency at port 1. The conductor location d, slot width w and top ground plane length b were all swept using Ansoft HFSS. Two different substrates, Neltec 9300 and FR4 Epoxy, were under a trial. Substrate properties for both are presented in Table 6-2. Two different ground plane sizes were used for the Neltec 9300 while for the FR4 the ground plane size was fixed. An advantage with a larger ground plane is lower mutual coupling between the antennas and a larger space for the compensating network. Having a substrate with a higher relative permittivity can have the same effect if most of the coupling is due to the currents in the ground plane, due to ground plane being electrically larger. The side effect of a larger relative permittivity is higher losses in both the antenna and the network. Simulation results for the two different cases are presented below.

Parameters	**Neltec 9300**	**FR 4 Epoxy**
Relative permittivity	3.0±0.04	4.4
Loss tangent	0.0023	0.02
Conductor to ground plane distance	0.8 mm	0.8 mm
Conductor thickness	34 µm	34 µm

Table 6-2 Microstrip parameters for the two substrates used for the design of the printed monopole slot antenna.

6.1.2.1 First case: Neltec 9300

Only two ground plane sizes are considered here, *120 x 45 mm^2* and *145 x 50 mm^2*. The length of the ground plane was increased by *5 mm* steps from *120* to *160* mm using a width of *50 mm*. The design parameters were tuned until the maximum return loss was in the frequency band of interest, see appendix 0 for more details. Dimensions for the considered cases are given in Table 6-3. S-parameters for the optimized antennas were imported in ADS where compensating networks without any geometrical restrictions were optimized to get an overall picture of what is possible to achieve ideally. For that purpose layout depicted in Fig. 4.16 was used. The main idea was to get an insight in how large the mobile telephone needed to be for this frequency band in order to achieve acceptable performance. For the lengths larger than *145 mm* the performance incorporating ideal compensating networks do not vary significantly. Considering the trade-off to physical size the compromise is made at *145 x 50 mm^2*.

Dimensions [mm]	L x W = 120 x 45 mm^2	L x W = 145 x 50 mm^2
s_1	43.4(42.5)	46.4(46.5)
s_2	10.5	10.5
d	26	26
b	7.3	7.3
w	5	5

Table 6-3 Dimension for the printed monopole slot antenna. Values in parenthesis are dimension for maximum efficiency optimization.

The size of the ground plane does not have any larger impact on the return loss, see Fig. 6.9. Highest value for the smaller ground plane size is -6.5 dB, -12.3 dB at centre frequency, while the corresponding value for the larger one is -7.3, -13.1 dB at 775 MHz. Coupling is lower than -3.2 dB and -3.9 dB for the smaller and larger ground plane size respectively, both values for the center frequency. It is lower for the larger ground plane, which is to be expected as it decreases with increasing distance between the antennas. Consequently the antenna efficiency is higher and the correlation is lower, Fig. 6.10 and Fig. 6.11 respectively. If maximum efficiency is desired then the efficiency is not peaking at the correct frequency for the smallest ground plane, but is very close to optimal for the larger ground plane. Mean antenna efficiency for 750 – 800 MHz is -3.4 and -2.8 dB for the ground plane sizes, first being for the smaller one. Mean envelope correlation is 0.47 and 0.36 respectively.

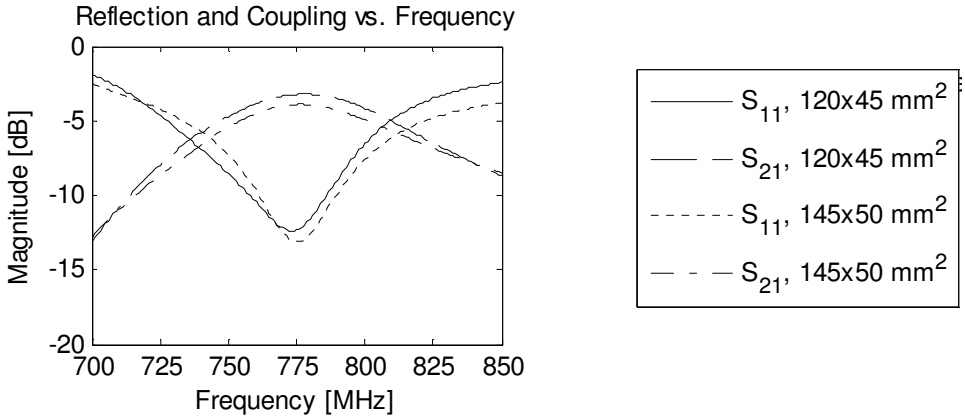

Fig. 6.9 Simulated reflection and coupling for two different ground plane sizes, optimized for maximum return loss.

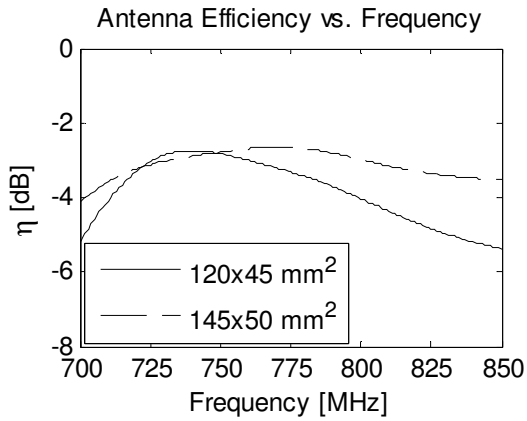

Fig. 6.10 Simulated antenna efficiency for two different ground plane sizes, optimized for maximum return loss.

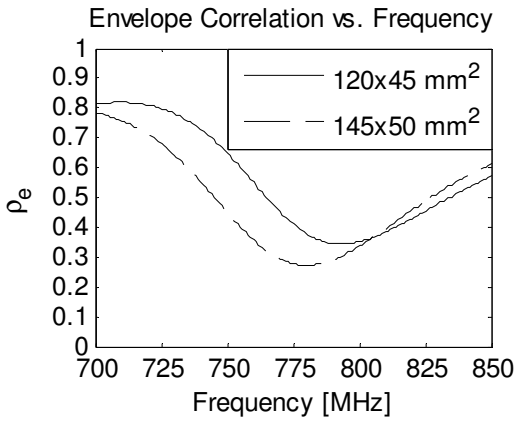

Fig. 6.11 Simulated envelope correlation for two different ground plane sizes, optimized for maximum return loss.

In Fig. 6.12 to Fig. 6.14, the design parameters were tuned with respect to efficiency. As in the previous optimization the correlation is lower and the efficiency is higher for larger ground planes, but now the peak has been moved to the correct frequency. Compensating networks give a slightly better performance for the return losses optimized antennas are therefore chosen as the antenna solution.

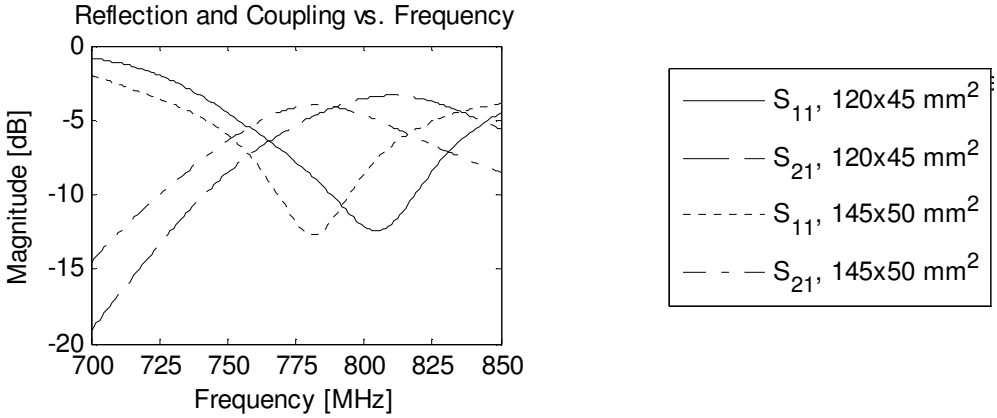

Fig. 6.12 Simulated reflection and coupling for two different ground plane sizes for the slot antenna array, optimized for maximum antenna efficiency.

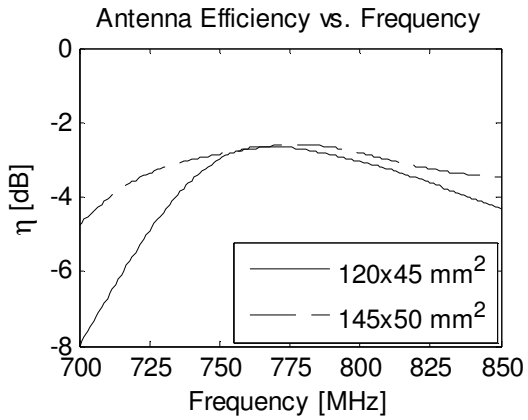

Fig. 6.13 Simulated antenna efficiency at port one and port two for the two different ground plane sizes for the slot antenna array, optimized for maximum antenna efficiency.

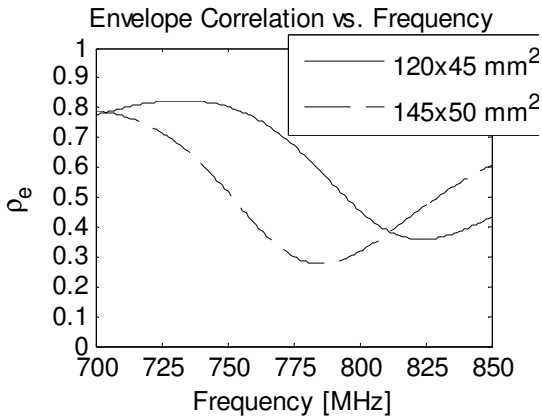

Fig. 6.14 Simulated envelope correlation for two different ground plane sizes for the slot antenna array, optimized for maximum antenna efficiency.

6.1.2.2 Second case: FR4 Epoxy

The simulations and optimizations for the second case were only made for a ground plane size of *120 x 45 mm²*. The same procedure as for the Neltec 9300 substrate was carried out, first optimizing the antenna for maximum return loss for the frequency band of interest, and later optimizing an ideal network in order to evaluate the possible performance. This approach was soon abandoned due to large ohmic losses in both the antenna and the compensating network. Attenuation for FR4 Epoxy is 2.36 dB/m while the corresponding value for the Neltec 9300 is just 0.19 dB/m, both for a characteristic impedance of 50 Ω. By taking into consideration the distance between the antenna ports of *89.4 mm* for both substrates, a single piece of a 50 Ω line connecting the ports result in 0.21 dB and 0.02 dB for the FR4 and the Neltec 9300 respectively.

Hence a design with the second substrate was abandoned. The results are plotted in Fig. 6.15 to Fig. 6.17. The coupling, efficiency and correlation are significantly lower compared to a design with Neltec 9300. The distance between the antennas in wavelengths for the FR4 substrate for this design is approximately equal to a ground plane length of 150 mm when using Neltec 9300. Despite this the coupling is 3.1 dB lower using FR4. An explanation for this could be that the coupling currents are much lower due to larger losses in the ground plane.

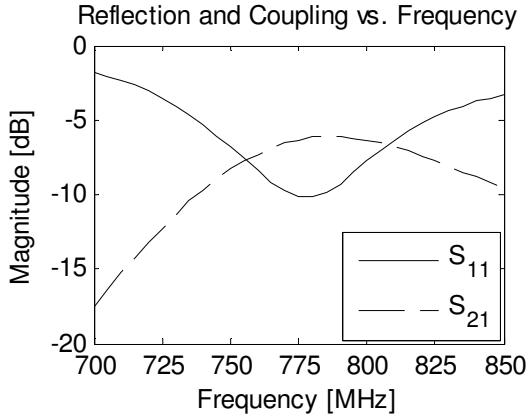

Fig. 6.15 Simulated reflection and coupling for the printed monopole slot antenna array using FR4 Epoxy substrate, optimized for maximum return loss.

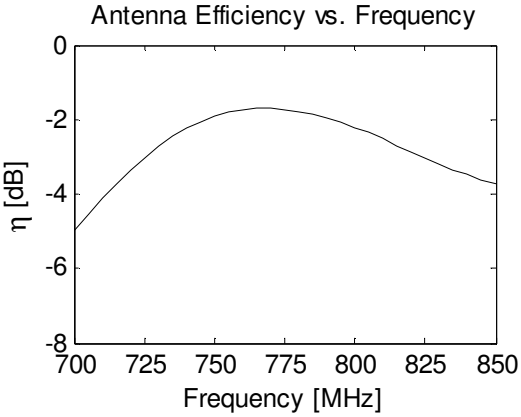

Fig. 6.16 Simulated antenna efficiency for the printed monopole slot antenna array using FR4 Epoxy substrate, optimized for maximum return loss.

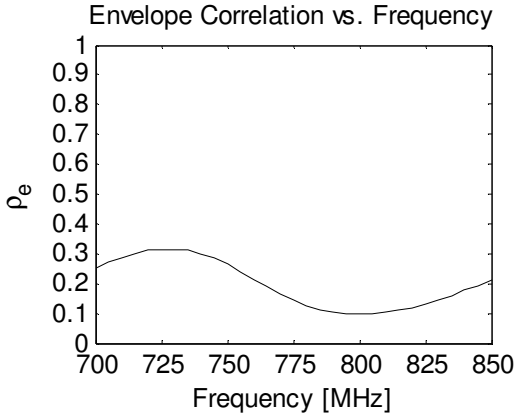

Fig. 6.17 Simulated envelope correlation for the printed monopole slot antenna array using FR4 Epoxy substrate, optimized for maximum return loss.

In order to get an idea of the amount of loss in a compensating network a layout depicted in Fig. 6.19 was optimized in ADS, and the network efficiency using (4.1) is shown in Fig. 6.18. Mean is at -1.44 dB for 750 – 800 MHz. This is totally unacceptable taking into account that optimization for maximum antenna efficiency is in the order of 1 dB. Furthermore an even larger loss is to be expected in practice.

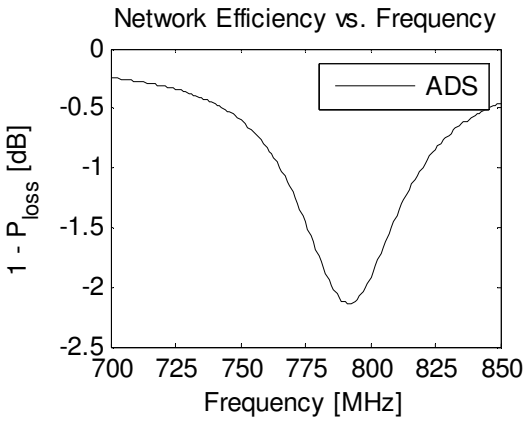

Fig. 6.18 Simulated network efficiency for a possible network solution in FR4.

6.2 Antenna design summary

Simulation results for the printed slot antenna array, using Neltec 9300,for the two ground plane sizes optimized for the maximum return loss are presented in Table 6-4. Meandered antenna is also presented for easier comparison.

Summary	f [MHz]	Meander 120 x 45	Slot 120 x 45	Slot 145 x 50
Reflection				
[dB]	750	-14.9	-8.5	-7.3
	775	-18.2	-12.3	-13.1
	800	-10.7	-6.5	-7.6
Mean	**750-800**	**-15.8**	**-9.1**	**-9.3**
Coupling				
[dB]	750	-2.1	-4.7	-4.9
	775	-1.7	-3.2	-3.9
	800	-1.9	-4.2	-4.9
Mean	**750-800**	**-1.8**	**-4.0**	**-4.6**
Ant. Eff.				
[dB]	750	-4.6	-2.8	-2.8
	775	-5.2	-3.3	-2.7
	800	-5.6	-4.0	-3.0
Mean	**750-800**	**-5.1**	**-3.4**	**-2.8**
Env. Corr.				
	750	0.60	0.65	0.45
	775	0.36	0.41	0.28
	800	0.16	0.35	0.34
Mean	**750-800**	**0.37**	**0.47**	**0.36**

Table 6-4 Simulated reflection, coupling, antenna efficiency and envelope correlation based on scattering parameters for optimized return loss for 750 – 800 MHz using 0.8 mm Neltec 9300 substrate.

6.3 Network design

In this subchapter two compensating networks are presented: one for each of the two printed monopole slot antennas optimized for maximum return loss presented in 6.1.2.1. Substrate used in both cases is Neltec 9300. S-parameters for the optimized 2-element antenna array, obtained during the design and optimization process in the Ansoft HFSS, were imported in Agilent ADS where compensating networks were optimized. Default values were used and 600 iterations were performed. When the layout was finished a Momentum simulation was carried out as well to get a more realistic look at the performance.

6.3.1 Network 1 – ground plane dimensions 120 x 45 mm^2

Approach used in the design process of the layout was to modify the impedance transformers/coupler network depicted in Fig. 4.16. As mentioned earlier the distance between the antenna ports is 89.4 mm. In order to fit the proposed network in the area of *120 x 45 mm^2*, bending of lines is necessary in order to keep the same number of degrees of freedom and thereby achieve second order resonance. The proposed layout solution including the antennas is shown in Fig. 6.19.

Optimization goals are presented in Table 6-5. Due to the geometrical restrictions of the compensating network the envelope correlation is not allowed above 0.5, as stated in the Introduction. Recalling the results for only the antennas, Fig. 6.11, the envelope correlation is above the maximum value for frequencies up to 765 MHz. The goal for the optimization of the antenna efficiency was changed manually until an optimum value of -2.2 dB was found.

Expression	Min	Max	Frequency Range
$\rho_e = \frac{\left\lvert S_{11}^* S_{12} + S_{21}^* S_{22} \right\rvert^2}{(1-\lvert S_{11}\rvert^2 - \lvert S_{21}\rvert^2)(1-\lvert S_{12}\rvert^2 - \lvert S_{22}\rvert^2)}$	-	0.5	750 – 800 MHz
$\eta_{dB} = 10 \cdot \log_{10}(1-\lvert S_{11}\rvert^2 - \lvert S_{21}\rvert^2)$	-2.2 dB	-	750 – 800 MHz

Table 6-5 Optimization goals for the *120 x 45 mm^2* mock-up.

Table 6-6 displays optimized lengths and widths for the compensating network.

	Param.	Value	Optim.
1: Microstrip line			
	Width	5.99 mm (22.4 Ω)	Yes
	Length	10.00 mm (14.8º)	Yes
2: Microstrip line			
	Width	0.97 mm (74.3 Ω)	Yes
	Length	14.80 mm (21.9º)	No
3: Microstrip line			
	Width	0.29 mm (119.7 Ω)	Yes
3.1			
	Length	25.47 mm (37.3º)	Yes
3.2			
	Length	68.97 mm (102.1º)	Yes
4: Microstrip line			
	Width	3.70 mm (32.5 Ω)	Yes
4.1			
	Length	12.77 mm (18.9º)	Yes
4.2			
	Length	33.39 mm (19.4º)	Yes
5: Microstrip line			
	Width	5.68 mm (23.3 Ω)	Yes
5.1			
	Length	8.94 mm (13.2º)	Yes
5.2			
	Length	10.72 mm (15.9º)	Yes
6: Microstrip line			
	Width	1.97 mm (50.0 Ω)	No
	Length	*6.00 mm (8.7º)*	*No*

Table 6-6 Optimization results for the network.

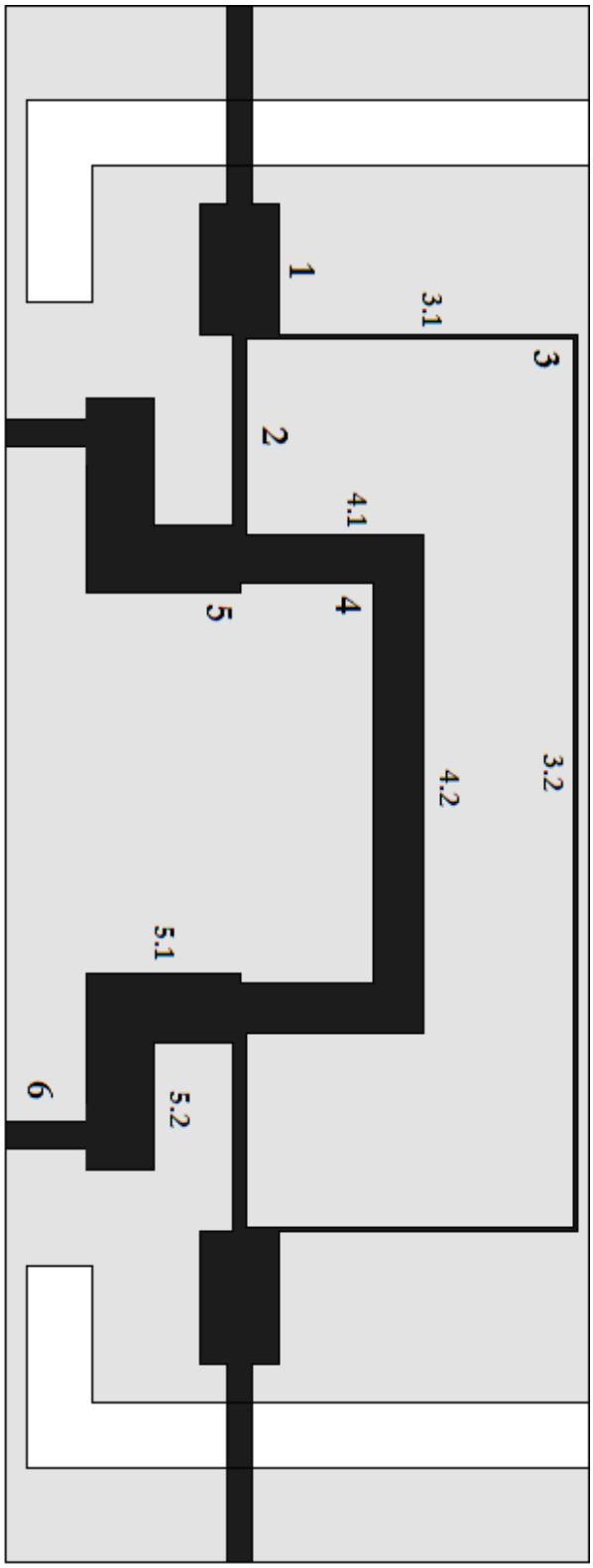

Fig. 6.19. Layout for the compensating network for the *120 x 45 mm*^{2} solution. Numbering corresponds to different sections of microstrip lines with different length and width, for more information check Table 6-6.

Due to matching for reduced reflection and coupling while also emphasizing bandwidth is not possible a compromise had to be made, Fig. 6.20 and Fig. 6.21. Mean return loss over the desired bandwidth has increased by 0.4 dB (9.1 dB to 9.5 dB), while the mean coupling has been reduced by approximately 2 dB (-4.0 dB to -6.2 dB). Antenna efficiency is depicted in Fig. 6.22. Mean value without the network connected and with is -3.4 dB and –2.3 dB respectively. Mean envelope correlation has decreased from 0.47 to 0.31, see Fig. 6.23. Values for 750 MHz, 775 MHz and 800 MHz are presented in Table 6-10.

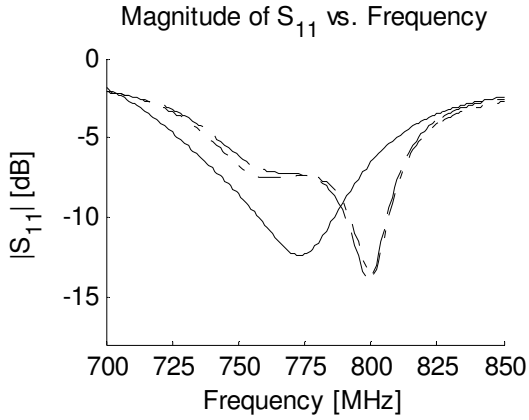

Fig. 6.20 Simulated reflection with and without compensating network.

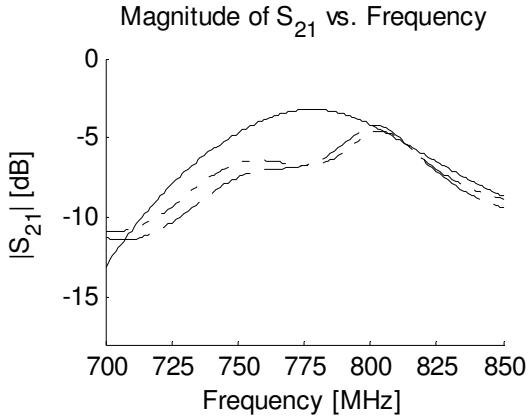

Fig. 6.21 Simulated coupling with and without compensating network.

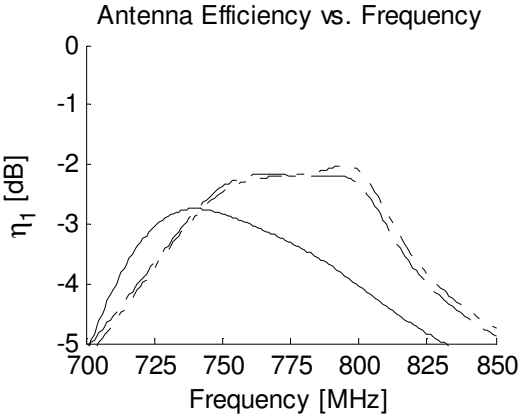

Fig. 6.22 Simulated antenna efficiency at port 1 with and without compensating network.

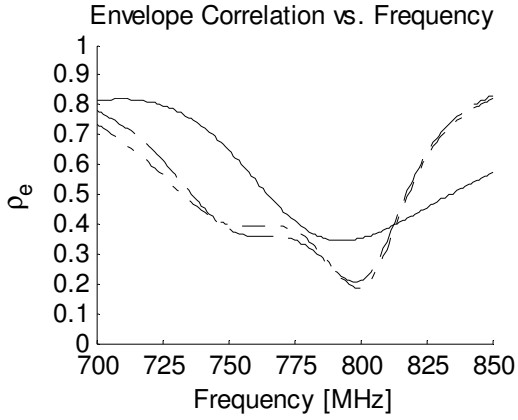

Fig. 6.23 Simulated envelope correlation with and without compensating network.

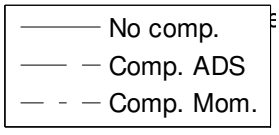

6.3.2 Network 2 – ground plane dimensions 145 x 50 mm^2

In this case the ground plane size was increased until both the performance of the antennas alone, see section 6.1.2.1, and with compensating network was improved. Using a length of 145 mm, the distance between the antenna ports is increased by 25 mm to 114.4 mm compared to the previous case with a smaller ground plane. Therefore, the layout of the impedance transformers/coupler network depicted in Fig. 4.16, could be used unmodified. The proposed layout solution is shown in Fig. 6.24.

Optimization goal is presented in Table 6-7. Note that a correlation goal is missing compared to the goals for the first compensating network, see Table 6-5. This is a result of the correlation already having acceptable values after the antenna design, see section 6.1.2.1. The goal for the optimization of the antenna efficiency was changed manually until an optimum value of -1.6 dB was found.

Expression	**Min**	**Max**	**Frequency Range**
$\eta_{dB} = 10 \cdot \log_{10}(1 - \lvert S_{11} \rvert^2 - \lvert S_{21} \rvert^2)$	-1.6 dB	-	750 – 800 MHz

Table 6-7 Optimization goals for the *145 x 50 mm^2* mock-up.

Table 6-7 displays optimized lengths and widths for the compensating network.

	Param.	**Value**	**Optim.**
1: Microstrip line			
	Width	2.80 mm (39.6 Ω)	Yes
	Length	10.42 mm (14.4º)	Yes
2: Microstrip line			
	Width	0.81 mm (80.9 Ω)	Yes
	Length	108.80 mm (150.2º)	No
3: Microstrip line			
	Width	0.20 mm (134.2 Ω)	Yes
	Length	10.66 mm (14.7º)	Yes
4: Microstrip line			
	Width	0.55 mm (95.9 Ω)	Yes
	Length	109.76 mm (151.5º)	No
5: Microstrip line			
	Width	1.97 mm (50.0 Ω)	No
	Length	6.00 mm (8.7º)	No

Table 6-8 Optimization results for the network.

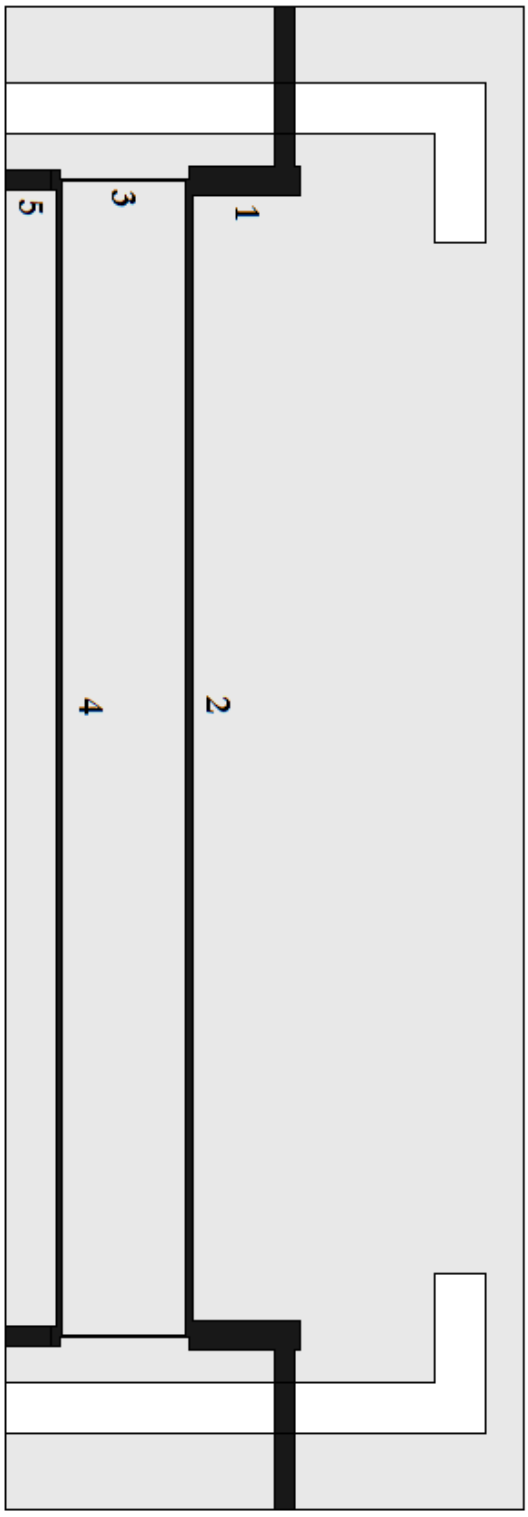

Fig. 6.24 Layout for the compensating network for the *120 x 45 mm*^{2} solution. Numbering corresponds to different sections of microstrip lines with different length and width, for more information check Table 6-8.

Reflection and coupling are displayed in Fig. 6.25 and Fig. 6.26 respectively. While the mean reflection over the desired frequency range has increased by 1.8 dB (-9.3 dB to -7.6 dB), the coupling has decreased by around 3 dB (-4.8 dB to -7.8 dB). Mean antenna efficiency has been increased by 1.1 dB (-2.8 to -1.7 dB), see Fig. 6.27. Envelope correlation is depicted in Fig. 6.28. Mean value has decreased from 0.36 to 0.22, a reduction by 0.14. Values for 750 MHz, 775 MHz and 800 MHz are presented in Table 6-10.

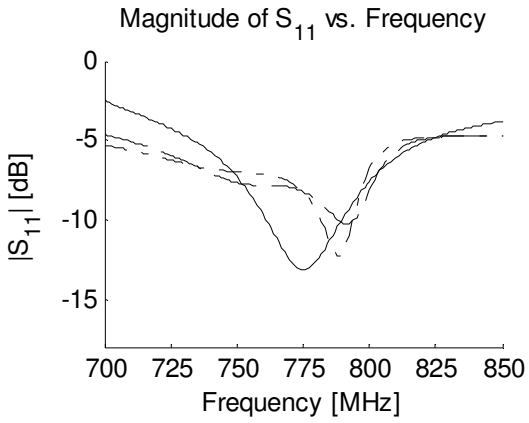

Fig. 6.25 Simulated reflection with and without compensating network.

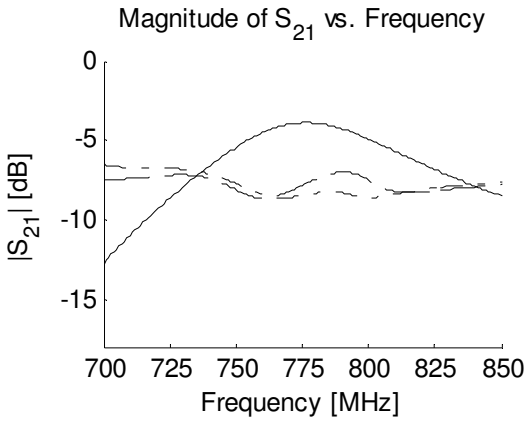

Fig. 6.26 Simulated coupling with and without compensating network.

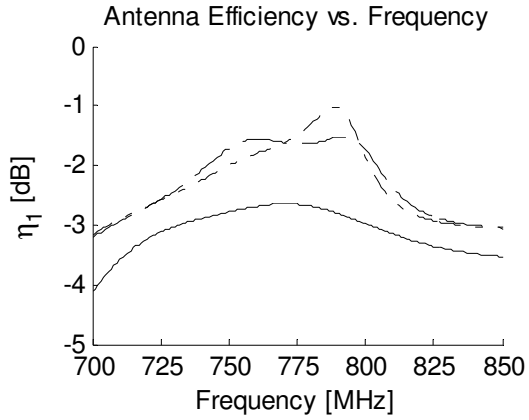

Fig. 6.27 Simulated antenna efficiency at port 1 with and without compensating network.

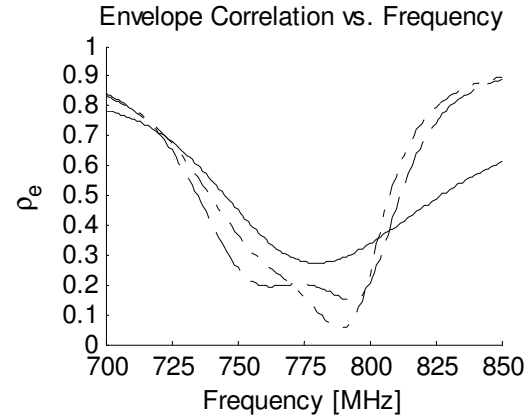

Fig. 6.28 Simulated envelope correlation with and without compensating network.

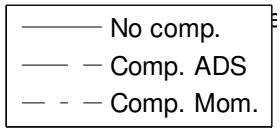

6.3.3 Summary and Conclusion

Two mobile phone mock-ups, consisting of a dual slot antenna and a compensating network, have been designed and analyzed. All four figures of merit for the design and optimization are displayed in Table 6-10.

Comparing the results it is easily concluded that in order to obtain acceptable performance for this frequency band, focusing primarily on antenna efficiency and envelope correlation, the mobile phone size needs to be increased by approximately 20 % compared to the phones on the market. Increasing the size results in decreased correlation due to reduced coupling, and thus increasing the performance of the antenna array. Furthermore, a realization of a larger compensating network is possible using more complex layouts with larger electrical lengths, which is of special importance for wavelengths this large.

Network efficiencies for the both networks are depicted in Fig. 6.29 and Fig. 6.30 respectively, and the results are summarized in Table 6-9.

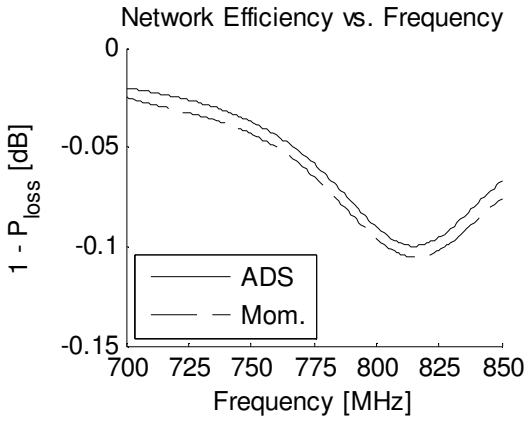

Fig. 6.29 Simulated network efficiency for *120 x 45 mm²*

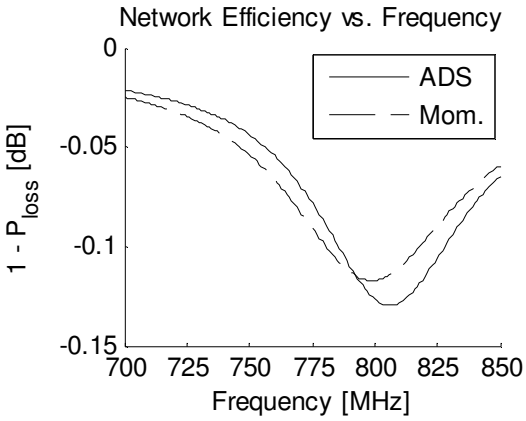

Fig. 6.30 Simulated network efficiency for *145 x 50 mm²*

Mean network efficiency for the frequency band of interest is bellow 0.1 dB for both networks. Furthermore the larger network has only 0.02 dB more losses compared to the smaller one.

1-P_{Loss} [dB]	**750 MHz**	**775 MHz**	**800 MHz**	**Mean: 750 – 800 MHz**
120 x 45 mm²	-0.04	-0.06	-0.09	-0.06
145 x 50 mm²	-0.04	-0.08	-0.013	-0.08

Table 6-9 Simulated network efficiencies for the two designed compensating networks without the antennas.

Summary	f [MHz]	No net	Net	No net	Net
		145 x 50 mm^2		*120 x 45 mm^2*	
Reflection					
[dB]	750	-7.3	-7.7	-8.5	-6.2
	775	-13.1	-8.3	-12.3	-8.4
	800	-7.6	-6.8	-6.5	-13.9
Mean	**750-800**	**-9.3**	**-7.6**	**-9.1**	**-9.5**
Coupling					
[dB]	750	-5.4	-8.1	-4.7	-7.5
	775	-3.9	-7.8	-3.2	-6.8
	800	-4.9	-7.5	-4.2	-4.3
Mean	**750-800**	**-4.8**	**-7.8**	**-4.0**	**-6.2**
Ant. Eff.					
[dB]	750	-2. 8	-1.7	-2.8	-2.3
	775	-2.7	-1.6	-3.3	-2.2
	800	-3.0	-1.7	-4.0	-2.3
Mean	**750-800**	**-2.8**	**-1.7**	**-3.4**	**-2.3**
Env. Corr.					
	750	0.45	0.26	0.65	0.38
	775	0.28	0.16	0.41	0.35
	800	0.34	0.23	0.35	0.21
Mean	**750-800**	**0.36**	**0.22**	**0.47**	**0.31**

Table 6-10 Reflection, coupling, antenna efficiency and envelope correlation based on scattering parameters for optimized return loss for 750 – 800 MHz for both solutions.

6.4 Performance

Both antenna arrays including networks with SMA-connectors at the ports were modeled and simulated in HFSS. The efficiency, correlation, Shannon capacity and diversity gain were then simulated or calculated from the radiation patterns in the same way as in chapter 5. S-parameters from HFSS for both cases are shown in Fig. 6.31 and Fig. 6.32, and they are in good agreement with the parameters obtained from ADS.

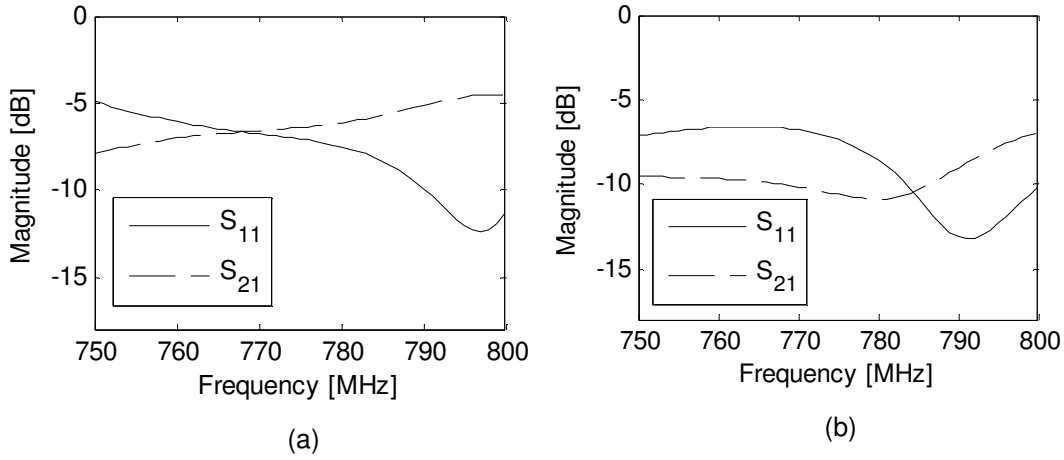

Fig. 6.31 S-parameters for HFSS simulated antenna array with network for size (a) 120 x 45 mm^2 and (b) 145 x 50 mm^2.

6.4.1 Radiation patterns

The radiation patterns as a power sum of both polarization components for both antennas for the 120 x 45 mm^2 and 145 x 50 mm^2 arrays are given in Fig. 6.32 and Fig. 6.33, respectively. The ϕ-component of the field is dominating in the ϕ = 0 – plane, while the θ-component of the field is dominating in the ϕ = 90 – plane. For both antenna arrays the patterns are very similar with and without a network and it does not seem like the correlation has been reduced much. This will be explained more in section 7.4.3.

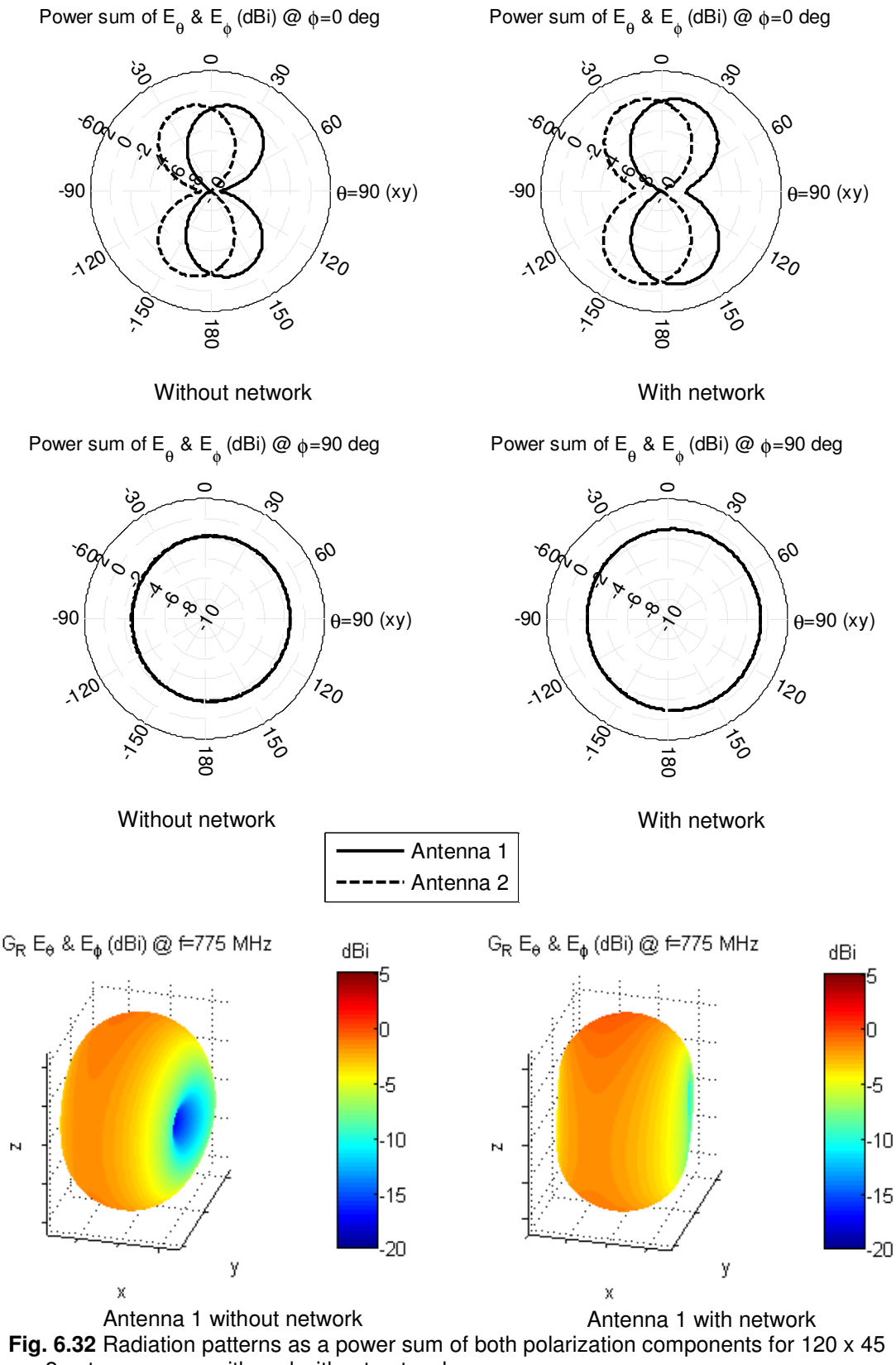

Fig. 6.32 Radiation patterns as a power sum of both polarization components for 120 x 45 mm2 antenna array, with and without network.

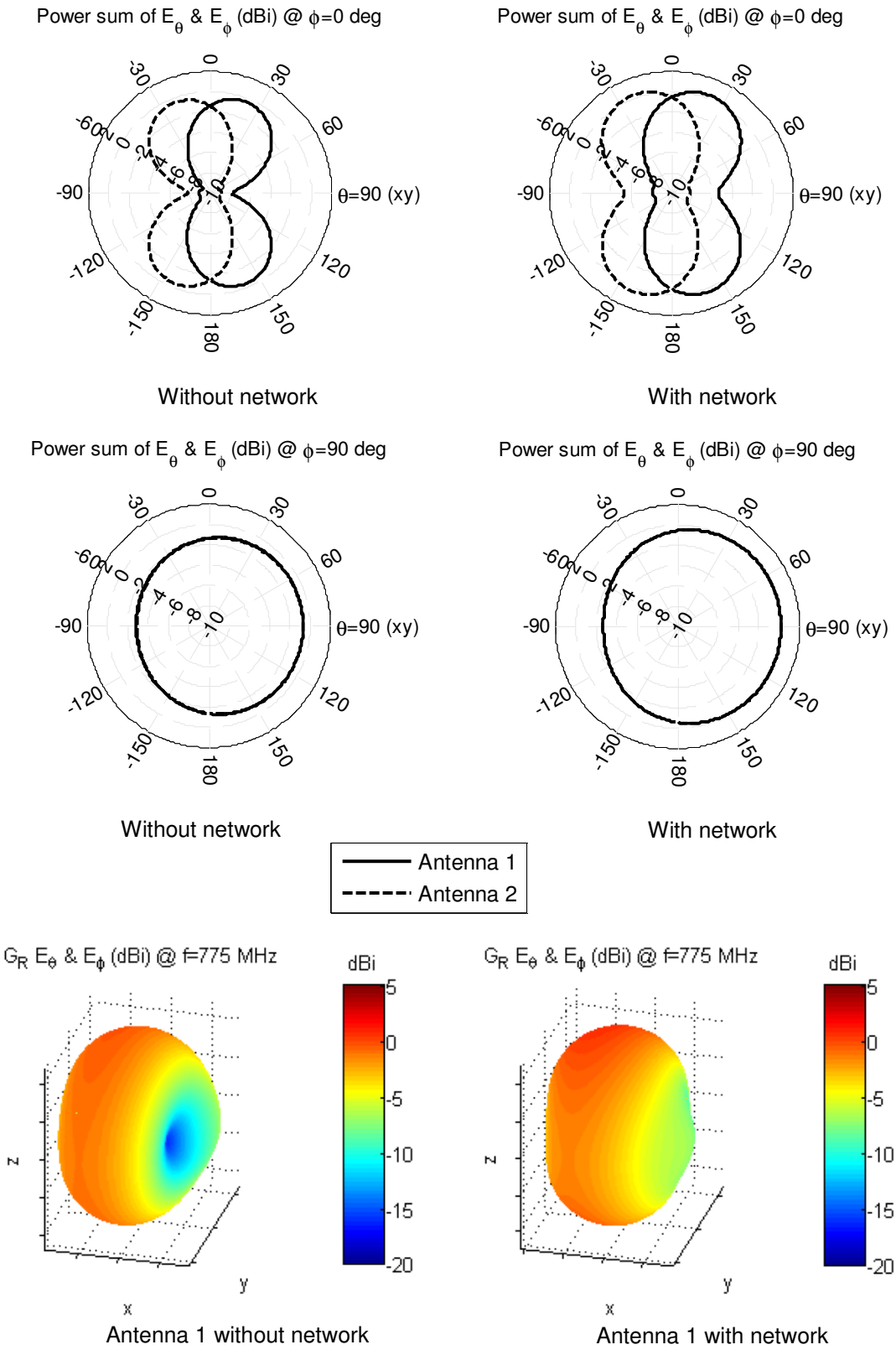

Fig. 6.33 Radiation patterns as a power sum of both polarization components for 145 x 50 mm2 antenna array, with and without network.

6.4.2 Antenna efficiency

The antenna efficiencies including radiation efficiencies, with and without a network, shown in Fig. 6.34, follow the same characteristic as the efficiencies obtained from ADS, but due to losses now being included the efficiencies are reduced. The average efficiency with network 1 and network 2 is still 0.7 dB and 0.8 dB higher than in the case without a network, respectively.

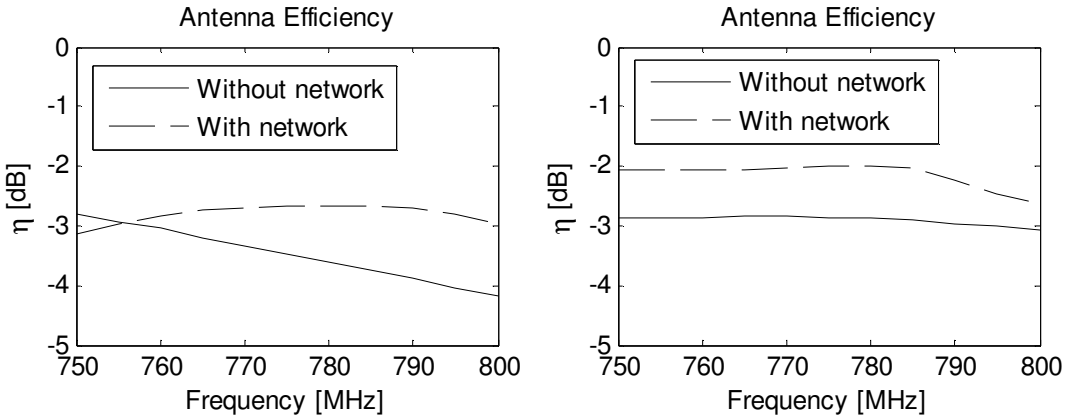

Fig. 6.34 Antenna efficiency including radiation efficiency for antenna array with network for size (a) 120 x 45 mm^2 and (b) 145 x 50 mm^2.

Mean efficiency [dB]	Without network	With network
120 x 45 mm^2	-3.5	-2.8
145 x 50 mm^2	-2.9	-2.1

Table 6-11 Mean antenna efficiency over 750 MHz to 800 MHz.

6.4.3 Correlation

Far-field radiation patterns were used to calculate the correlation between the antennas, which is shown in Fig. 6.35. Mean values over 750 MHz to 800 MHz are given in Table 6-12.

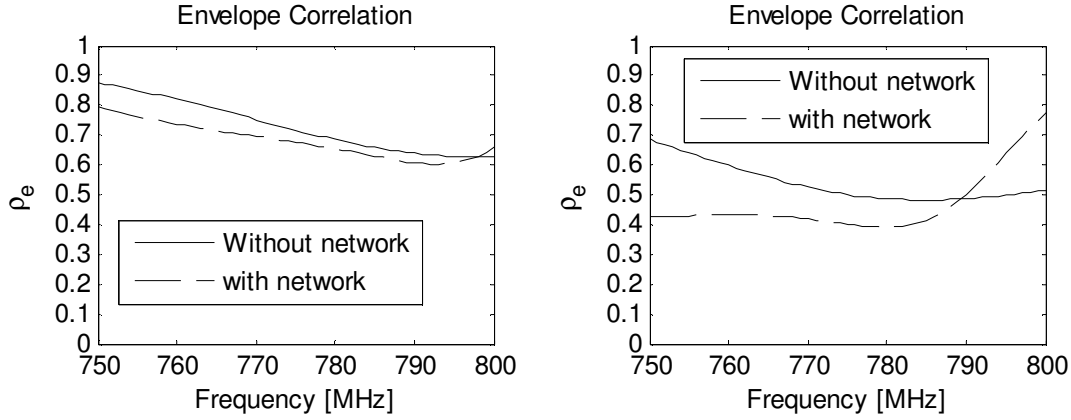

Fig. 6.35 Envelope correlation from radiation patterns for antenna array with network for size (a) 120 x 45 mm^2 and (b) 145 x 50 mm^2.

Mean envelope correlation	Without network	With network
120 x 45 mm^2	0.73	0.68
145 x 50 mm^2	0.54	0.47

Table 6-12 Mean envelope correlation over 750 MHz to 800 MHz.

Surprisingly, the correlation is much higher than earlier calculated with the S-parameters. The reason is that the radiation efficiency should also be considered, and when the radiation efficiency is not close to 100% there are large uncertainties in the values calculated from S-parameters [24]. The correlation with respect to both S-parameters and radiation efficiencies is given by [24]

$$\rho = \frac{-(S_{11}^* S_{12} + S_{21}^* S_{22})}{\sqrt{(1-|S_{11}|^2-|S_{21}|^2)(1-|S_{12}|^2-|S_{22}|^2)\eta_{rad,1}\eta_{rad,2}}} - \rho_{loss}\sqrt{(1/\eta_{rad,1}-1)(1/\eta_{rad,2}-1)} \quad (6.1)$$

where ρ_{loss} is the complex correlation between the losses, which is often unknown. Minimum and maximum values can still be obtained from (6.1) and they are plotted in Fig. 6.36. The upper bound ($\rho_{e,\max}$) on the envelope correlation is now very close to the one calculated from radiation patterns.

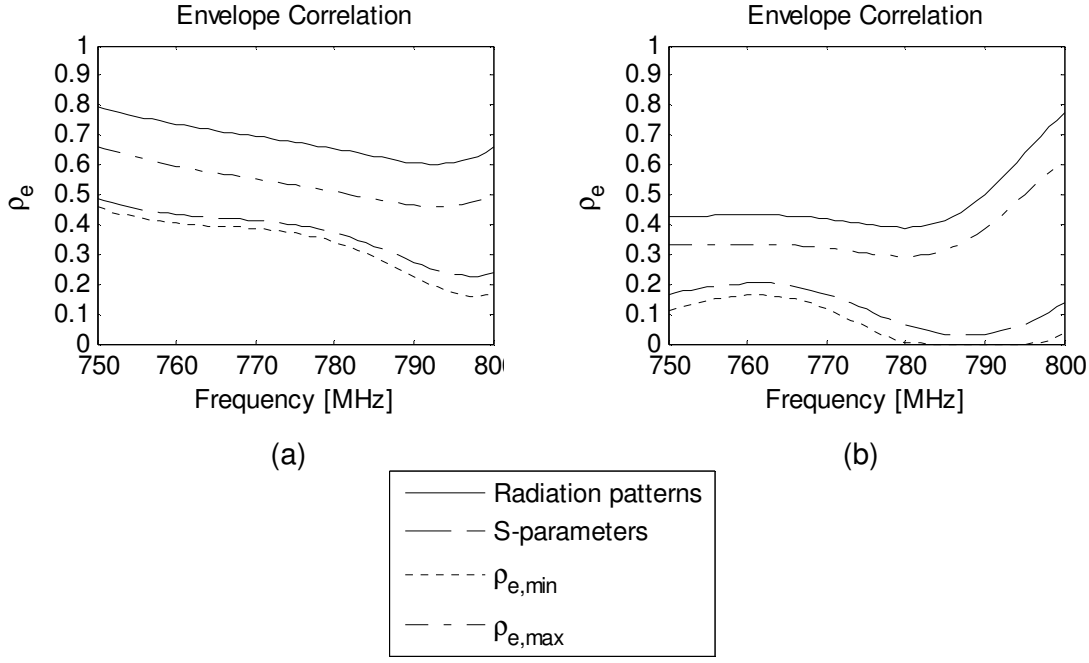

Fig. 6.36 Envelope correlation for (a) 120 x 45 mm^2 and (b) 145 x 50 mm^2 antenna arrays with network, calculated with both radiation patterns and S-parameters. The upper and lower bound obtained from the S-parameters and radiation efficiencies are also included.

6.4.4 Shannon capacity

Ergodic Shannon capacities with and without a network are compared in Fig. 6.37. Mean values at 20 dB SNR are given in Table 6-13. For both sizes the capacity is improved with about 6% compared to the case without a network.

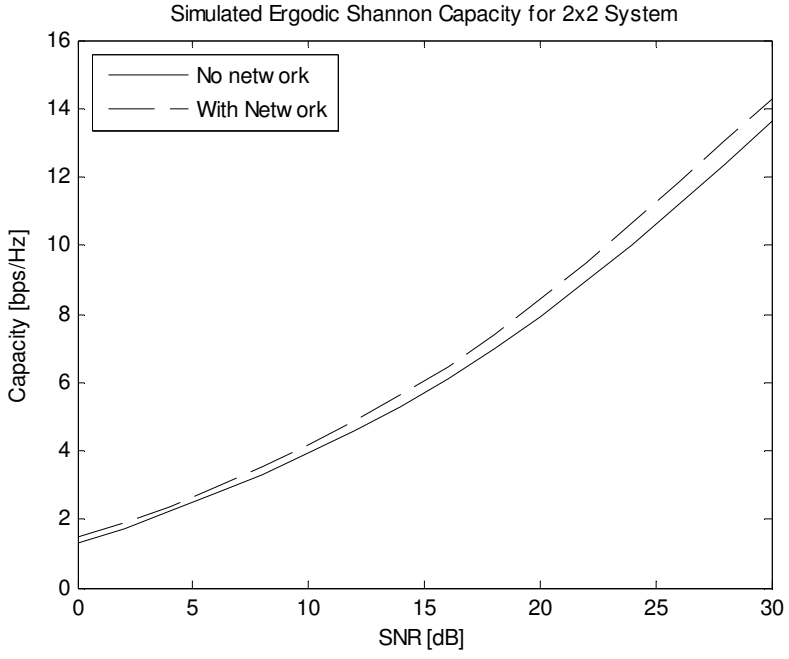

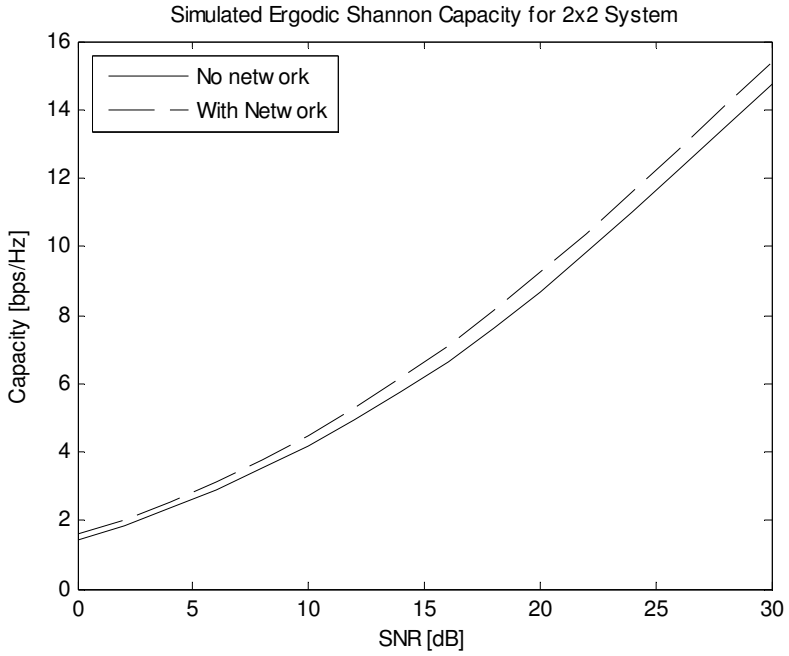

(b)

Fig. 6.37 Ergodic Shannon capacity averaged over 750 MHz to 800 MHz for a 2 x 2 MIMO system with water-filling. (a) 120 x 45 mm^2 . (b) 145 x 50 mm^2.

Shannon Capacity [bps/Hz]	Without network	With network
120 x 45 mm^2	7.9	8.4
145 x 50 mm^2	8.7	9.2

Table 6-13 Ergodic Shannon capacity at 20 dB SNR with water filling averaged over 750 MHz to 800 MHz.

6.4.5 Diversity gain

The simulated CDF's of the normalized power, with and without a network for both a single branch and MRC, are given in Fig. 6.38 (a) for the smaller ground plane and in Fig. 6.38 (b) for the larger ground plane. Effective diversity gains at 1 % level are given in Table 6-14. The improvement with network 1 is 1.4 dB and with network 2 the improvement is 0.9 dB. Despite that the efficiency improvement is slightly smaller in the case with a smaller ground plane and the correlation improvement is about the same, the diversity gain is improved with about 0.5 dB more. Apparently, the diversity is more sensitive to the envelope correlation coefficient at higher correlations, which is in agreement with the theory in [16].

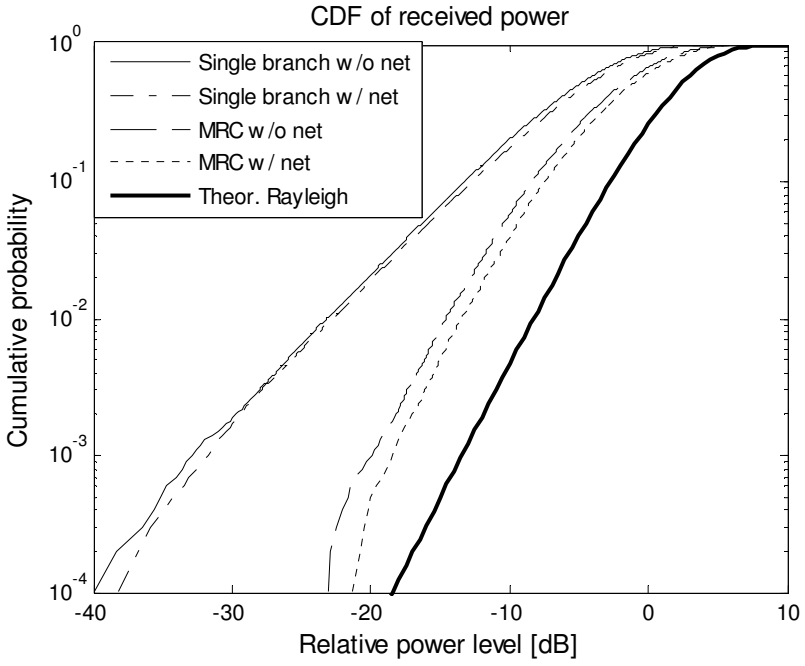

Fig. 6.38 CDF of the received power for (a) 120 x 45 mm^2 and (b) 145 x 50 mm^2 antenna arrays with network. The solid bold line corresponds to two uncorrelated ideal omnidirectional antennas using MRC in a Rayleigh channel.

Effective diversity gain [dB]	Without network	With network
120 x 45 mm^2	5.1	6.5
145 x 50 mm^2	7.1	8.0

Table 6-14 Effective diversity gain with MRC averaged over 750 MHz to 800 MHz.

6.4.1 Summary and conclusion

Mean values over frequency of the performance metrics are summarized in Table 6-15.

The simulations showed that the performance of the antennas were not as good as predicted during the design stages, but reasonable improvement on all performance metrics was still achieved. The goal was to obtain an antenna efficiency below -2 dB and, but this wasn't done with neither network. For the larger antenna array the efficiency was just slightly below -2 dB and this can be considered as acceptable. A mean envelope correlation below 0.5 was only obtained with the larger antenna array.

The main reason for the poorer performance is that the radiation efficiencies were higher than predicted and that the method of calculating correlation coefficients from S-parameters was very inaccurate and gave too low values.

Mean values	120 x 45 mm^2 No network	120 x 45 mm^2 Network	145 x 50 mm^2 No network	145 x 50 mm^2 Network
Efficiency (dB)	-3.5	-2.8	-2.9	-2.1
Envelope correlation	0.73	0.68	0.54	0.47
Shannon Capacity at 20 dB SNR (bits/s/Hz)	7.9	8.4	8.7	9.2
Effective MRC diversity gain at 1% (dB)	5.1	6.5	7.1	8.0

Table 6-15 Simulated mean values based on radiation patterns over 750 to 800 MHz of all the performance metrics.

7 Discussion

One theme throughout the first part of the project has been the issue of connectors. Making the design for the correct kind and later improvising using another solution. As mentioned earlier, connectors for the antennas had to be replaced in order to fit the network connectors, both having the same gender in the beginning. Furthermore the network connectors were made for double substrate thickness, leading to improvisation using pieces of substrate and copper tape. This could have resulted in air-pockets and therefore generation of higher order modes.

In addition to the wrong connectors, the networks did not have an extra section of 50 Ohm line at each port in order to make the transition from stripline and coaxial cable, and vice versa, as smooth as possible.

Network 2, see section 5.3.2.2, had the necessary pieces of extra line at all ports and the difference between simulated and measured figures of merit is the smallest compared to the other networks. So an important insight is the importance of more focus on transitions and connectors from one technology to another.

8 Conclusions

It has been shown that the performance in terms of efficiency, correlation, Shannon capacity and diversity gain of closely spaced antennas can be improved with a simple compensating transmission line network. Excellent performance improvement is obtained with the networks for the monopoles on the circular ground plane, but to be able to fit these into a hand-held device they need to be reduced in size. To show that the concept can be implemented into a mobile phone operating at the lower frequencies, two different sized antenna arrays with similar networks were printed on a substrate, which represents the circuit board of a mobile phone. It is clearly shown that the network improves the performance, but if improved performance is to be obtained the size of the phone should be slightly larger than current standards. Alternatively, more emphasis could be put into designing antennas with lower coupling before integrating them with a compensating network.

9 Future work

This section will focus only on the design of the mobile phone dual antenna mock-up.

Making the design of the antenna array a larger priority, using more complex antenna layouts and harder requirements during the optimization process, would improve overall performance of the MIMO system.

Compensating network design would also benefit from this, making it possible to design physically smaller networks and therefore saving precious space.

If a similar work is to be repeated for a higher frequency band, using a substrate with a higher permittivity should definitely be looked into further, resulting in lower coupling. Another positive consequence of this is smaller physical size. On the downside, higher frequencies result in a higher loss but our estimation is that reduction in physical size would result in a higher loss reduction than the amount of increased loss due to this, resulting in less total loss.

Making an estimation model of the losses and incorporating it into the optimization process of both the antennas and the networks, would offer a more realistic insight in the total performance of the system. When calculating the correlation for lossy antennas from S-parameters it is recommended to check the validity of the results with the radiation patterns. It seems like the larger the losses are, the more the S-parameter method underestimates the correlation. Hence, if losses are expected it is also recommended to design for a lower correlation than desired.

If the emphasis is strictly on physical size, considering that the technology of choice is microstrip, a possible approach for the compensating networks is using lumped components. Parasitics that often follow with higher frequencies would not be of a major concern when designing for the 750-800 MHz band. Furthermore, more complex circuits having more degrees of freedom could be realized, resulting in a higher order resonance.

The project can be taken even further by including the chassis and electronics of the phone, which might result in an even lower efficiency.

10 References

[1] E. Biglieri, R. Calderbank, A. Constantinides, A. Goldsmith, A. Paulraj and H. V. Poor, *Mimo Wireless Communications*, Cambridge university press, 2007.

[2] D. Tse and P. Viswanath, *Fundamentals of Wireless Communications,* Cambrdige university press, 2005.

[3] A. Stjernman, "Antenna Mutual Coupling Effects on Correlation, Efficiency and Shannon Capacity", Proc. *EuCAP 2006,* Nice, France, p.6 pp., Nov 2006.

[4] S. Chen, Y. Wang and S. Chung, "A Decoupling Technique for Increasing the Port Isolation Between Two Strongly Coupled Antennas", *IEEE Trans. Antennas Propag*., vol 56, no 12, pp. 3650 - 3658, Dec 2008.

[5] A. Diallo, C. Luxey, P. L. Thuc, R. Staraj, and G. Kossiavas, "Study and reduction of the mutual coupling between two mobile phone PIFAs operating in the DCS1800and UMTS bands," *IEEE Trans. Antennas Propag*., vol. 54, no. 11, pp. 3063–3073, Nov. 2006.

[6] S. Ranvier, C. Luxey, P. Suvikunnas, R. Staraj, and P. Vainikainen, "Capacity enhancement by increasing both mutual coupling and efficiency: A novel approach," 2007 IEEE *Antennas and Propagation Society International Symposium*, p 3632-5, Jun. 2007.

[7] C. Y. Chiu, C. H. Cheng, R. D. Murch, and C. R. Rowell, "Reduction of mutual coupling between closely-packed antenna elements*," IEEE Trans. Antennas Propag*., vol. 55, no. 6, pp. 1732–1738, Jun 2007.

[8] D. A. Sánchez-Hernández, *Multiband Integrated Antennas for 4G Terminals,* Artec House, 2008.

[9] D. Gesbert and J. Akhtar, Breaking the barriers of Shannon's capacity: An overview of MIMO wireless systems, *Telektronikk Telenor Journal*. Jan. 2002.

[10] T. Svantesson and A. Ranheim, "Mutual coupling effects on the capacity of multielement antenna systems", *Proc. IEEE CASSP'2001,* vol. 4, Salt Lake City, UT, May 7---11, 2001, pp. 2485---2488.

[11] J. L. Allen and B. L. Diamond, "Mutual Coupling in Array Antennas", Technical report EDS-66-442, Lincoln Lab., MIT, Oct 1966

[12] P.-S. Kildal, *Foundations of Antennas a Unified Approach*, Studentlitteratur, 2000

[13] G. J. Foschini and M. J. Gans, "On the limits of wireless communications in a fading environment when using multiple antennas", *Wireless Personal Communications,* (6), pp. 331-335, 1998

[14] A. Goldsmith, *Wireless Communications,* Cambridge university press, New York, 2005

[15] R. G. Vaughan and J. Bach Andersen. *Channels, Propagation and Antennas for Mobile Communications*, volume no. 50 of IEEE Electromagnetic Waves Series. The Institution of Electrical Engineers, London, United Kingdom, 2003.

[16] R.G. Vaughan and J. Bach Andersen, "Antenna diversity in mobile communication", *IEEE Transactions of Vehicular Journal of Technology,* Vol. 36, pp. 149-172, 1987.

[17] A. Stjernman, “Relationship between radiation pattern correlation and scattering matrix of lossless and lossy antennas”, *IEE Electron. Lett.*, vol 41, no 12, pp. 1106, June 2005

[18] M. M. Weinder, S. P. Cruze, C. Li and W. J. Wilson, *Monopole Elements on Circular Ground Planes,* Artec House, 1987.

[19] C. A. Balanis, *Antenna Theory Analysis and Design,* Wiley, 3rd ed, 2005.

[20] J. W. Wallace and M. A. Jensen, “Mutual Coupling in MIMO Wireless Systems: A Rigorous Network Theory Analysis”, *IEEE Transactions on Wireless Communications*, Vol. 3, no. 4, pp. 1317-1325, July 2004

[21] N. T. Pham, G.-A. Lee and F. D. Flaviis, “Minimized Dual-Band Coupled Line Meander Antenna for system-In-a-Package Applications”, *IEEE Antennas and Propagation Society International Symposium,* Vol 2, pp. 1451 - 1454, June 2004

[22] H.-D Chen, “Compact CPW-fed dual-frequency monopole antenna”, *IEE Electron. Lett.*, Vol 38, no 25, pp. 1622-1624, Dec 2002

[23] C.-I. Lin and K.-L- Wong, “Printed Monopole Slot Antenna for Internal Multiband Mobile Phone Antenna”, *IEEE Trans. Antennas Propag.*, Vol 55, no 12, pp. 3690 - 3697, Dec 2007

[24] P. Hallbjörner, “The Significance of Radiation Efficiencies When Using S-parameters to Calculate the Received Signal Correlation From Two Antennas”, *IEEE Antennas and Wireless Propagation Letters*, Vol 4, n 11, p 97-9, 2005

Appendix

A Ripple in the transmission coefficients

Due to ripples in the measured transmission coefficients for the first two compensating networks, see 4.3.2.1 and 4.3.2.2, interpolation was carried out when calculating network efficiency. Simple first order linear regression was used and the results with and without the regression can be viewed in the figures bellow.

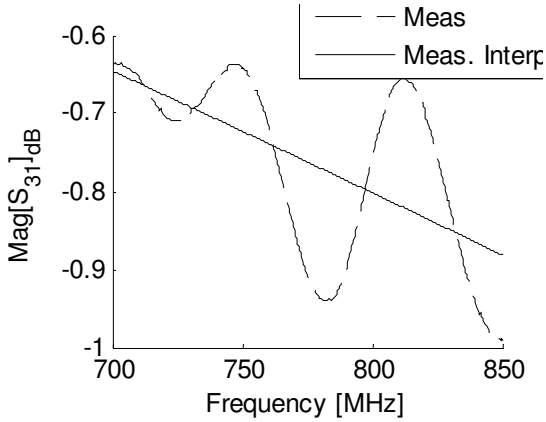

Measured S_{31} for network 1 with interpolation

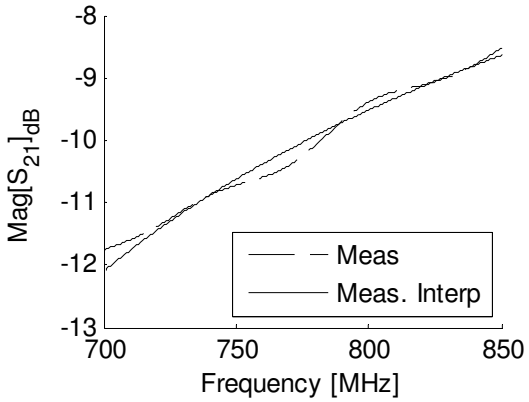

Measured S_{21} for network 2 with interpolation

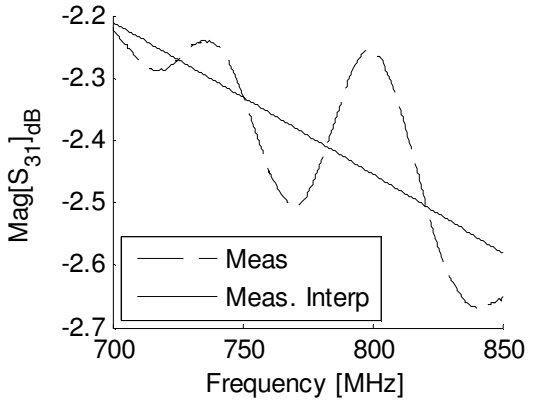

Measured S_{31} for network 2 with interpolation

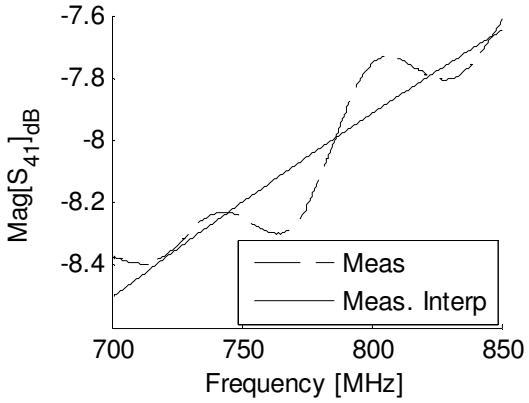

Measured S_{41} for network 2 with interpolation

B Ground plane size variation

As stated in 6.1.2.1, 5 ground plane sizes were tested and tuned until a compromise was made between size and performance. As one can easily conclude, reflection and coupling are marginally better for *160 x 45 mm²* compared to the *160 x 45 mm²*. Little larger difference can be seen for antenna efficiency and envelope correlation but considering the size a choice for a smaller ground plane is obvious.

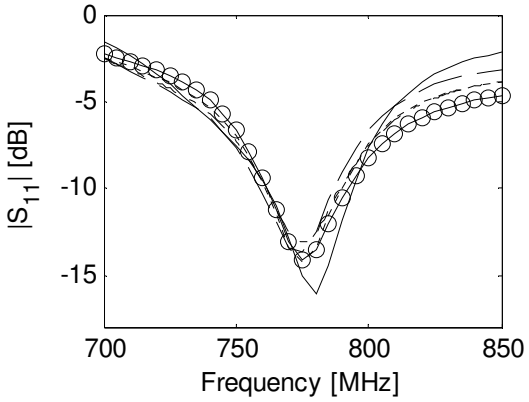

Reflection for varying ground plane size

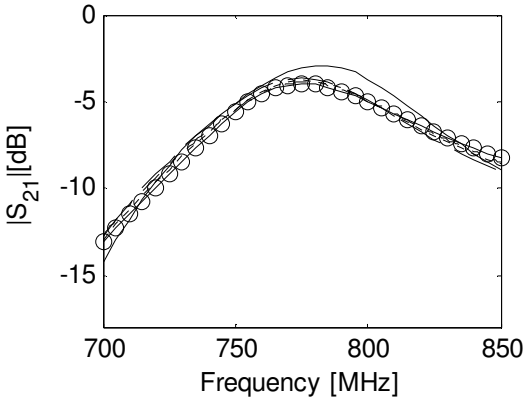

Coupling for varying ground plane size

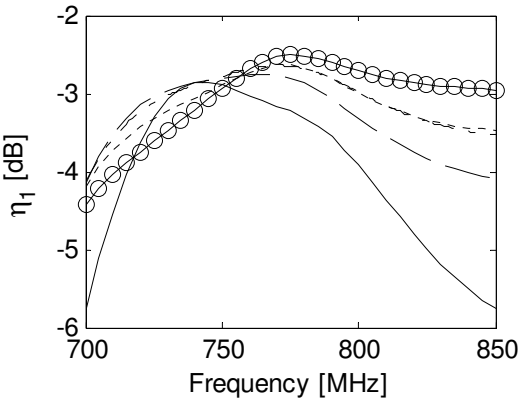

Antenna efficiency for varying ground plane size

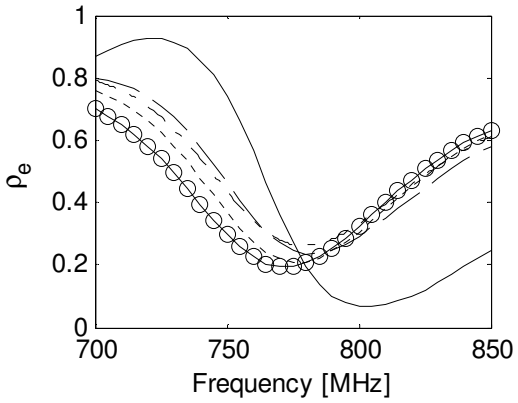

Envelope correlation for varying ground plane size